PREPARATION AND CHARACTERIZATION OF NICKEL (II) PHTHALOCYANINE TETRASULFONIC ACID TETRASODIUM SALT FOR ORGANIC SOLAR CELLS

MUHAMAD SAIPUL BIN FAKIR

FACULTY OF SCIENCE
UNIVERSITY OF MALAYA
KUALA LUMPUR

2013

PREPARATION AND CHARACTERIZATION OF NICKEL (II) PHTHALOCYANINE TETRASULFONIC ACID TETRASODIUM SALT FOR ORGANIC SOLAR CELLS

MUHAMAD SAIPUL BIN FAKIR

DISSERTATION SUBMITTED IN FULLFILLMENT OF THE REQUIREMENT FOR THE DEGREE OF MASTER OF SCIENCE

DEPARTMENT OF PHYSICS
FACULTY OF SCIENCE
UNIVERSITY OF MALAYA
KUALA LUMPUR

2013

UNIVERSITI MALAYA
ORIGINAL LITERARY WORK DECLARATION

Name of Candidate: **Muhamad Saipul bin Fakir** (I.C/Passport No: **870724-43-5683**)

Registration/Matric No: **SGR100006**

Name of Degree: **Master of Science (Dissertation)**

Title of Dissertation ("this Work"):
PREPARATION AND CHARACTERIZATION OF NICKEL (II) PHTHALOCYANINE TETRASULFONIC ACID TETRASODIUM SALT FOR ORGANIC SOLAR CELLS

Field of Study: Organic Electronics

I do solemnly and sincerely declare that:

(1) I am the sole author/writer of this Work;
(2) This Work is original;
(3) Any use of any work in which copyright exists was done by way of fair dealing and for permitted purposes and any excerpt or extract from, or reference to or reproduction of any copyright work has been disclosed expressly and sufficiently and the title of the Work and its authorship have been acknowledged in this Work;
(4) I do not have any actual knowledge nor do I ought reasonably to know that the making of this work constitutes an infringement of any copyright work;
(5) I hereby assign all and every rights in the copyright to this Work to the University of Malaya ("UM"), who henceforth shall be owner of the copyright in this Work and that any reproduction or use in any form or by any means whatsoever is prohibited without the written consent of UM having been first had and obtained;
(6) I am fully aware that if in the course of making this Work I have infringed any copyright whether intentionally or otherwise, I may be subject to legal action or any other action as may be determined by UM.

Candidate's Signature Date:

Subscribed and solemnly declared before,

Witness's Signature Date:
Name: **Dr. Khaulah Sulaiman**
Designation: **Senior Lecturer**

ABSTRACT

Organic solar cells (OSCs) referred to as third-generation solar photovoltaics, after crystalline silicon and thin-film solar technologies. There are two categories of OSCs: large molecules (polymer-based) and small molecules (oligomer-based). Herein, however only small molecules are used due to its lower cost compared to polymeric materials. Nickel (II) phthalocyanine tetrasulfonic acid tetrasodium salt (NiTsPc) and tris(8-hydroxyquinolinato) aluminium (Alq3) are utilized as donor layer and acceptor layer, respectively. The main focus of this study is to modify the donor layer via a solvent treatment in order to enhance the ability of the charge carrier transport at the donor/acceptor interface hence leading to the improvement in the OSC performance. Initially, NiTsPc thin films are deposited on the cleaned glass substrate using spin-coating technique at constant rotation speed to produce 120nm film. Surface modification was done by immersing the NiTsPc films in the selected low solubility solvents of chloroform and toluene. Morphology of the solvent treated NiTsPc films has shown some different features compared to the untreated film, as viewed by Atomic Force Microscopy (AFM) images. The treated film forms a smaller granular structure as a result of the etching process by the solvent. Prior to the next stage of solvent treatment, the NiTsPc films are thermally treated at 140°C. Formation of nano fibers can be clearly observed in the Field Effect Scanning Electron Microscopy (FESEM) images, as a result of thermal treatment. Then the influence of immersion time at 0, 40, 80 and 120 minutes on the nanofibers diameter size was examined by observing the FESEM images, for the NiTsPc films being soaked in the selected solvent. The number of small nanofibers increases upon immersing the NiTsPc films, compared to the untreated film. Further measurement via absorption spectroscopy has shown NiTsPc films possess two distinct regions in the B-band and the Q-band. There is an increase approximately 30% in light absorption intensity upon the immersion time of 60 minutes, compared to the untreated film. Furthermore, the optical

energy gaps in these B and Q bands are calculated using a Tauc plot, to be in the range of 2.70 to 2.85 eV and 1.43 to 1.50 eV, respectively. The drop of 5% in the fundamental energy gap has been obtained for the film being treated 60 minutes in chloroform. The drop in the NiTsPc energy gap can be explained in terms of defects formation (density of states of energy level) upon solvent treatment. The presence of these defects is further supported by the results obtained from the Raman spectra. The intensity ratio between the D and G peak (I_D/I_G) in the Raman spectra is deviated from unity, indicating the defects formation in NiTsPc molecule due to the solvent treatment. In the final part of this study, the acceptor layer of Alq3 is brought into contact with the treated NiTsPc donor layer, which then sandwiched between two electrodes of indium tin oxide (ITO) and aluminium. The current density-voltage *(J-V)* curves present that the double value of short-circuit-current density, J_{sc} has been obtained in the device consists of treated NiTsPc. This result confirms the enhanced charge carrier transport at donor/acceptor interface which agrees with PL quenching phenomena. Therefore, the performance of OSC can be improved to some extent via thin film surface modification by soaking in a suitable solvent at an optimum time.

ABSTRAK

Sel suria organik (OSC) yang disebut sebagai fotovoltaik solar generasi ketiga, selepas silikon kristal dan teknologi solar filem nipis. Terdapat dua kategori OSC: molekul besar (berasaskan polimer) dan molekul kecil (berdasarkan oligomer). Di sini, hanya molekul kecil digunakan kerana kosnya yang lebih rendah berbanding dengan bahan polimer.Nikel (II) phthalocyanine tetrasulfonic asid tetrasodium garam (NiTsPc) dan tris (8-hydroxyquinolinato) aluminium (Alq3) digunakan sebagai lapisan penderma dan lapisan penerima. Fokus utama kajian ini adalah untuk mengubah suai lapisan penderma melalui rawatan pelarut dalam usaha untuk meningkatkan keupayaan pengangkutan pembawa caj di antara muka penderma/penerima lalu membawa kepada peningkatan dalam prestasi OSC. Pada mulanya, filem nipis NiTsPc didepositkan pada substrat kaca dibersihkan menggunakan teknik salutan putaran pada kelajuan putaran yang malar untuk menghasilkan filem 120nm. Pengubahsuaian permukaan telah dilakukan dengan merendam filem NiTsPc dalam perlarut yang mempunyai keterlarutan rendah iaitu klorofom dan toluena.Morfologi filem NiTsPc yang dirawat pelarut telah menunjukkan beberapa ciri-ciri yang berbeza berbanding dengan filem yang tidak dirawat, seperti yang dilihat oleh imej Mikroskop Daya Atom (AFM). Filem yang dirawat membentuk struktur berbutir kecil sebagai hasil daripada proses punaran oleh pelarut. Sebelum ke peringkat seterusnya untuk rawatan pelarut, filem NiTsPc dirawat dengan haba pada suhu 140 ° C. Pembentukan gentian nano boleh jelas diperhatikan dalam Mikroskopi Elektron Daya Imbasan (FESEM), sebagai hasil rawatan haba. Kemudian, pengaruh masa rendaman pada 0, 40, 80 dan 120 minit pada saiz diameter nanofibers diperiksa dengan memerhatikan imej FESEM, untuk filem NiTsPc yang direndam di dalam pelarut dipilih. Bilangan nanofibers kecil meningkat apabila filem NiTsPc yang direndam, berbanding dengan filem yang tidak dirawat. Pengukuran lanjut melalui spektroskopi penyerapan telah menunjukkan filem-filem NiTsPc mempunyai dua kawasan yang berbeza dalam B-band dan Q-band. Terdapat

peningkatan kira-kira 30% dalam keamatan penyerapan cahaya apabila masa rendaman 60 minit, berbanding dengan filem yang tidak dirawat. Tambahan pula, jurang tenaga optik di B dan Q band dikira menggunakan plot Tauc, berada dalam julat 2.70-2.85 eV dan 1.43-1.50 eV, masing-masing. Penurunan sebanyak 5% dalam jurang tenaga asas telah diperolehi untuk filem itu sedang dirawat 60 minit dalam kloroform.Penurunan dalam jurang tenaga NiTsPc boleh dijelaskan dari segi pembentukan kecacatan (ketumpatan negeri tahap tenaga) akibat rawatan pelarut. Kehadiran kecacatan ini turut disokong oleh keputusan yang diperolehi daripada spektra Raman. Nisbah keamatan antara puncak D dan G (I_D/I_G) dalam spektra Raman menyisih daripada nilai satu, menunjukkan pembentukan kecacatan dalam molekul NiTsPc disebabkan rawatan pelarut. Dalam bahagian akhir kajian ini ini, lapisan penerima Alq3 dibawa ke dalam hubungan dengan lapisan penderma yang dirawat NiTsPc, yang kemudian diapit di antara dua elektrod indium timah oksida (ITO) dan aluminium. Graf ketumpatan arus-voltan (*J-V*) menunjukkan bahawa nilai kepadatan litar pintas semasa, J_{SC} sebanyak dua kali ganda telah diperolehi dalam peranti terdiri daripada NiTsPc yang dirawat. Keputusan ini mengesahkan pembawa caj pengangkutan dipertingkatkan pada antara muka penderma/penerima yang mana bersetuju dengan fenomena pelindap kejutan PL. Oleh itu, prestasi OSC boleh diperbaiki sedikit melalui pengubahsuaian permukaan filem nipis dengan rendaman dalam pelarut yang sesuai pada masa yang optimum.

ACKNOWLEDGEMENT

First and foremost I would like to thank God “the almighty Allah” for blessing me with sufficient time and health to get my goals. I would like to thank my parents, Hj Fakir Hj Noor and Hjh Rezaiyah Hj Othman and all my siblings for their patient, all the love and support they have given me throughout my life.

I would like to acknowledge my supervisors, Dr. Khaulah Sulaiman for her continuous support and encouragement to conduct research in a scientific area, which had fascinated me for a long time since my undergraduate studies. Thanks for all the invaluable help, feedbacks, constructive comments and suggestions throughout the research.

I am greatly indebted to my group mates especially Dr. Zubair, Lim Lih Wei, Mohd Nizam, Ali Imran, Muhammad Fahmi Fariq, Toong Way Yun, Zurianti, Shahino Mah, Fadilah and Mohd Nazry for their assistance and support throughout the process.

Here in Low Dimensional Materials Research Center (LDMRC), I would like to thank all lecturers and postdoctoral in LDMRC for great collaboration and valuable inputs and also to Mr Mohamad and Mrs Norlela for the technical assistance. More thanks go to all my colleagues especially Rehana, Nur Khairiah, Mohd Arif, Maisara, Nur Maisarah, Hamizah, Siti Hajar, Ragib and all LDMRC members for all the support and help.

Last but not least, I would like to thank University of Malaya (UM) for providing the research grant PS342/2010B to support my research works and participate in conference. Besides, special thanks to UM for awarding Skim Biasiswa Universiti Malaya (SBUM) to me for two years.

I hope with this project, I was able to make a contribution towards the big dream of human kind to exploit the sun’s enormous energy potential to realize a sustainable future energy supply.

RESEARCH PAPERS AND CONFERENCES

A. Published Full Papers (ISI-cited)

1. Muhamad Saipul Fakir, Zubair Ahmad, and Khaulah Sulaiman (2012). Modification of Optical Band Gap and Surface Morphology of NiTsPc Thin Films. *Chinese Physics Letters*, 29(12), 126802.

2. Khaulah Sulaiman, Zubair Ahmad, Muhamad Saipul Fakir, Fadilah Abd Wahab, Shahino Mah Abdullah and Zurianti Abd. Rahman. (2013). Organic Semiconductors: Applications in Solar Photovoltaic and Sensor Devices, *Materials Science Forum*, 737 126.

3. Khaulah Sulaiman and Muhamad Saipul Fakir (2011). Electrical Conduction and Photovoltaic Effects of TPA-Derivative Solar Cells, *Thin Solid Films*, 519, 5219-5222.

4. Y.L. Kong, M.S. Fakir, S.V. Muniandy, and K. Sulaiman. (2013). Morphological Image Interpretation of Phthalocyanine Tetrasulfonic Acid Tetrasodium (TsNiPc) Thin Film Using Fractal Analysis, *Advanced Materials Research* (submitted)

B. Conference Papers (Non-ISI cited)

1. Muhamad Saipul Fakir& Khaulah Sulaiman., "Organic photovoltaic devices based on solution processablephthalocyanine". Paper presented at International Thin Films Conference in Kenting, Taiwan.

TABLE OF CONTENTS

Original Literary Work Declaration …….…… ii

Abstract ……..……..... iii

Abstrak …….…… v

Acknowledgement ……..…….. vii

Research Paper and Conference .....……... viii

Table of Contents …..…… ix

List of Figures ..……. xi

List of Tables ..…….. xiv

List of Abbreviation …….. xv

CHAPTER 1: INTRODUCTION

1.1 Project Background and History of Solar Cells ……..... 1

1.2 Motivation …… 4

1.3 Research Objectives …… 5

1.4 Thesis Outline ……. 6

CHAPTER 2: LITERATURE REVIEW

2.1 Chapter Overview …… 8

2.2 Working Principle of Organic Solar Cells ……... 8

2.3 Device Structure …….. 10

2.4 Factors Govern the Performance of organic solar cells ……... 13

2.4.1 Selection of Materials …….. 13

2.4.2 Charge Carrier Transport Properties …… 20

2.5 Electrical Analysis ……... 22

CHAPTER 3: EXPERIMENTAL METHODS

3.1 Chapter Overview …… 27

3.2 Substrate Preparation …….. 27

3.3 Material and Preparation of Solution …….. 29

3.4 Deposition of Thin Film …….. 29

3.4.1 Drop Casting Solution ……. 29

3.4.2 Spin Coating Technique ……... 30

3.5 Solvent Treatment …… 31

3.6 Device Fabrication …….. 32

3.7 Thickness Measurement ……. 34
3.8 X-ray Diffraction (XRD) ……. 35
3.9 Atomic Force Microscopy (AFM) …….. 35
3.10 Field Effect Scanning Electron Microscopy (FESEM) ……... 36
3.11 Ultraviolet-Visible-Near Infrared (UV-Vis-NIR) Spectroscopy …… 37
3.12 Raman Spectroscopy …… 40
3.13 Photoluminescence Spectroscopy …… 41
3.14 Electrical Measurement ……... 42

CHAPTER 4: RESULTS AND DISCUSSIONS

4.1 Chapter Overview …… 44
4.2 Part I: Selection of parameters …… 45
4.2.1 Concentration of NiTsPc solution …… 45
4.2.2 Optimum Temperature in Thermal Treatment process…… 47
4.2.3 Selection of poor solvent for film surface treatment …… 50
4.3 Part II: Effects of solvent treatment time to morphological, structural, optical and electrical properties …… 57
4.3.1 Morphological properties …… 57
4.3.2 Structural properties …… 63
4.3.3 Optical properties …… 69
4.3.4 Electrical properties ……. 76

CHAPTER 5: CONCLUSIONS AND FUTURE WORKS

5.1 Conclusions ……. 10
5.2 Closing Remarks ……. 85
5.2 Future Works …… 86

REFERENCES…….. 87

LIST OF FIGURES

Figure 1.1:	The development of photovoltaic technologies provided by National Renewable Energy Laboratory (NREL), United States of America …….	3
Figure 2.1:	(a) Different levels of HOMO and LUMO represent an energy gap, (b) A step potential at the well adapted energy profiles of the two dissimilar materials……	9
Figure 2.2:	(a) Simple structure of single layer device (b) Schematic diagram of the electron flow in a single layer device…….	11
Figure 2.3:	(a) Structure of a bilayer device (b) Schematic diagram of the electron flow in a bilayer device……	12
Figure 2.4:	(a) Structure of a bulk hetero-junction device (b) Schematic diagram of a bulk hetero-junction device……..	13
Figure 2.5:	The schematic diagrams of charge transport: (a) A high potential at the acceptor of the active layer, (b) a well-adapted energy profile for easier charge transport. ……	17
Figure 2.6:	Absorption of P3HT, CdS and mixture of P3HT and CdS……	18
Figure 2.7:	(a) Metal free phthalocyanine Pc, (b) Nickel (II) phthalocyanine, NiPc (c) Nickel (II) phthalocyaninetertrasulfonic acid tetrasodium salt, NiTsPc (d) Copper (II) 1,2,3,4,8,9,10,11,15,16,17,18,22,23,24,25-hexadecafluoro-29H,31H-phthalocyanine, $CuF_{16}Pc$……	19
Figure 2.8:	3D atomic force microscopy images of P3HT:PCBM blend films dissolved in (a) pure DCB solvent, (b) CH solvent, and (c) DCB:CH co-solvent yield surface mean roughness 11.062 nm, 12.623 nm and 14.2777 nm respectively……	21
Figure 2.9:	Comparison of AFM images of the surface of the P3HT: PCBM active layer (A) fast-thermal-annealing and (B) slow-solvent-vapor-treatment…….	21
Figure 2.10:	Typical *J-V* graph for organic solar cells……..	22
Figure 2.11:	The value of shifted to a bigger value when the PCBM incorporated with another material which has different energy level……	23
Figure 2.12:	Variation of J_{sc} caused by solvent treatment …….	25
Figure 2.13:	A double-log graph constructed from a linear *J-V* graph……	26
Figure 3.1:	(a) Patterned ITO using spray paint. (b) Substrate after etching process……	28
Figure 3.2:	Deposition process using spin coating technique…….	31
Figure 3.3:	(a) Inside view of home built thermal evaporator. (b) Auto Edward 306 deposition system……..	33
Figure 3.4	Schematic diagram of photovoltaic device with arrangement of ITO/treated NiTsPc/n-type material/Al…….	34

Figure 3.5:	Printed screen shot of the surface profilometer, indicates the difference in the height profile of film surface and the substrate to give the film thickness…….	34
Figure 3.6:	Schematic diagram of working principle of AFM…….	36
Figure 3.7:	Picture of FEI Quanta 200 field emission scanning electron microscope (FESEM)……	37
Figure 3.8:	Photograph of Jasco V-570 UV/VIS/NIR Spectroscopy…….	39
Figure 3.9:	Schematic diagram of working principle of UV-Vis-NIR Spectroscopy……	39
Figure 3.10:	Possible electronic transition of electron……	39
Figure 3.11:	The electronic transition of Rayleigh scattering (a), (b) and (c) Raman scattering…….	40
Figure 3.12:	Electronic transitions in PL……	41
Figure 3.13:	The top view of photovoltaic device where effective area is shown…….	43
Figure 4.1:	The effect of NiTsPc solution concentration on the absorption spectra of the respective film ……..	47
Figure 4.2:	(a) The absorption spectra of NiTsPc,(b) Magnification of the absorption spectra at the B band (UV region) and (c) Magnification of the absorption spectra at the Q band (visible region)……	49
Figure 4.3:	AFM images of NiTsPc films in 3-D (on the left) and in 2-D (on the right) for (a) the untreated, (b) treated with chloroform, and (c) treated with toluene…….	51
Figure 4.4:	The chemical structure of chloroform (left) and toluene (right)…	52
Figure 4.5:	Influence of NiTsPc film being treated with different solvent on the current density – voltage (*J-V*) characteristics of the ITO/treated NiTsPc/PTCDA/Al devices. The devices were tested in air under light illumination 100 mW/cm^2…….	53
Figure 4.6:	The energy level diagrams; (a) NiTsPc film incorporated with PTCDA and (b) NiTsPc film incorporated with Alq3……..	55
Figure 4.7:	The current density – voltage (J-V) characteristics of ITO/NiTsPc/Alq3/Al and ITO/treated NiTsPc/Alq3/Al devices. The devices were tested in air under light illumination 100 mW/cm^2……	56
Figure 4.8:	The FESEM images of the NiTsPc thin film (a) before thermal annealing with 10k magnification (b) before thermal annealing with 30k magnification (c) after thermal annealing with 20k magnification……	58
Figure 4.9:	FESEM images comparing the morphology of NiTsPc films upon different treatment times. (a) untreated, (b) 40 minutes, (c) 80 minutes and (d) 120 minutes……	60
Figure 4.10:	AFM images comparing the morphology of NiTsPc films upon different treatment times. (a) Untreated, (b) 40 minutes, (c) 80 minutes and (d) 120 minutes……	61
Figure 4.11:	XRD diffraction pattern for the NiTsPc film with different treatment time……..	64

Figure 4.12: Chemical structure of NiTsPc (left) and Alq3 (right) ……. 64
Figure 4.13: Raman Spectra for the untreated NiTsPc film…….. 65
Figure 4.14: Stacks of Raman spectra for the untreated and treated NiTsPc films with different immersion time in a suitable solvent…… 67
Figure 4.15: The D and G peak of Raman Spectra around 1350 and 1580 cm^{-1} (The plot is magnified from Figure 4.14)…….. 67
Figure 4.16: Intensity ratio of D and G peak for different treatment time….. 68
Figure 4.17: Absorption properties of NiTsPc, Alq3 and NiTsPc/Alq3 double layer films……. 69
Figure 4.18: (a) The absorption spectra for untreated and treated NiTsPc with chloroform (b) Magnification of the absorption intensity at B band (c) Magnification of the absorption intensity at Q band….. 72
Figure 4.19: (a) The Tauc's Plot of the untreated and treated NiTsPc films with different treatment time, (b) Enlargement of the fundamental energy gap region, and (c) Enlargement of the onset energy gap region. Optical energy gap was obtained by extrapolating line from 1.7 and 3.5 eV…… 74
Figure 4.20: Photoluminescence spectra of untreated and treated NiTsPc films…….. 76
Figure 4.21: The current density – voltage (J-V) characteristics of the Photovoltaic devices consist of untreated and treated NiTsPc film for different immersion time. The devices were tested in air under light illumination 100 mW/cm^2……. 78
Figure 4.22: The short-circuit current density (Jsc) of the photovoltaic device……. 78

LIST OF TABLES

Table 1.1: The brief history of the development of organic solar cells as reported by researchers……. 2

Table 2.1: The energy level of the organic semiconductor materials and its suitable solvent…….. 14

Table 2.2: The energy level, energy gap and V_{oc}…… 23

Table 3.1: Parameter for the Atomic Force Microscope (AFM) measurement…… 36

Table 3.2: Set up parameter for Raman spectroscopy…….. 41

Table 3.3: Set up parameter for PL measurement…… 42

Table 4.1: Variation of thickness and the corresponding photographs of NiTsPc films, produced from different solution concentrations…. 46

Table 4.2: The rms roughness value of solvent treated thin films, obtained from the AFM images…… 62

Table 4.3: Tentative band assignment of Raman active modes of NiTsPc film.. 66

Table 4.4: List of the optical energy gaps for the untreated and treated NiTsPc films with different treatment time…….. 75

Table 4.5: The value of P_{max}, J_{sc}, V_{oc} and fill factor (FF)…….. 80

LIST OF ABBREVIATION

OSC	…	Organic Solar Cells
SCLC	…	Space Charge Limited Current
SSVT	…	Slow Solvent Vapor Treatment
HOMO	…	Highest Occupied Molecular Orbital
LUMO	…	Lowest Unoccupied Molecular Orbital
ITO	…	Indium Tin Oxide
HCL	…	Hydrochloric acid
rpm	…	Revolution per Minute
FWHM	…	Full Width at Half Maximum
SMU	…	Source Measuring Unit
D/A	…	Donor-Acceptor
V_{oc}	…	Open-circuit voltage
V_{max}	…	Maximum voltage
J_{sc}	…	Short-circuit –current density
J_{max}	…	Maximum-current density
FF	…	Fill Factor
AFM	…	Atomic Force Microscopy
FESEM	…	Field Effect Scanning Electron Microscopy
XRD	…	X-ray Diffraction
PL	…	Photoluminescence
XPS	…	X-ray photoemission
UPS	…	Ultraviolet photoemission
P3HT	…	Poly(3-hexylthiophene-2,5-diyl)
P3OT	…	Poly(3-octylthiophene-2,5-diyl)
PCBM	…	6,6]-phenyl-C61-butyric acid methyl ester.
DH6T	…	5,5′′′′-Dihexyl-2,2′:5′,2″:5″,2‴:5‴,2⁗:5⁗,2′′′′′-sexithiophene
PDHF-BT	…	Poly[{9,9-dihexylfluorene-alt-{4-(3,4-ethylenedioxythiesnyl)-2,1,3-benzothiadiazole]
Alq3	…	Tris(8-hydroxyquinolinato)aluminium
PTCDA	…	Perylene-3,4,9,10-tetracarboxylic dianhydride
Pc	…	Phthalocyanine
NiPc	…	Nickel (II) phthalocyanine
CuPc	…	Copper (II) phthalocyanine
$CuF_{16}Pc$	…	Copper (II) 1,2,3,4,8,9,10,11,15,16,17,18,22,23,24,25-hexadecafluoro-29H,31H-phthalocyanine.
NiTsPc	…	Nickel (II) phthalocyanine tetrasulfonic acid tetrasodium salt
CuTsPc	…	Copper (II) phthalocyanine tetrasulfonic acid tetrasodium salt

CHAPTER 1

INTRODUCTION

1.1 PROJECT BACKGROUND AND HISTORY OF SOLAR CELLS

The world today is highly dependent on energy from the earth's resources. The study to find new sources of energy as the early precaution setup to replace existing energy is developing. Natural resources such as petroleum are expected to decrease in the 10 to 20 years due to high consumption of energy nowadays. Organic solar cells are a promising alternative way for the energy production.

Research in solar energy started in 1954 at Bell Laboratory, with the discovery of silicon based inorganic solar cells (Spanggaard *et al.,* 2004). After a few years of research, the efficiency of the photovoltaic cells rise to 24% from initially 6% (Martin A. Green *et al.*, 2003). After that period, intensive research on inorganic solar cells was made. Inorganic solar cell really promises a great efficiency nevertheless a huge drawback comes from its high production cost. Therefore, there is a need to find other alternatives to reduce the production cost of solar cells, and organic-based devices turn out to be one of the best solutions to solve such problem.

At the initial period of research activities on organic-based solar cells, small organic compounds which also known as oligomers were used as an active layer such as anthracene. This anthracene was the first oligomer, used active layer in solar device by Alfredo Pochettino and Max Volmer in the early of the 20^{th} century (Spanggaard *et al.*, 2004). Besides, chlorophyll and organic dyes were also used to be incorporated into organic solar cells (Spanggaard *et al.,* 2004). In 1986, Ching W. Tang discovered a high molecular weight material known as conjugated polymer, which can behave as a semi-conducting material (Tang, 1986). He found this conjugated polymer can conduct electricity and produced a photovoltaic effect.

Extension of the work was made by Niyazi Serdar Saricifti (Sariciftci *et al.*, 1993). He fabricated the first polymer/fullerene based solar cells in 1993 and known as the best organic photovoltaic device until the polymer/polymer based solar cells were introduced by Yu and Hall in 1995 (Frederik C, 2009; Spanggaard *et al.*, 2004). After that, there were intensive research studies have been performed on the modification of material structures, improvement of device architectures, surface modifications and fabrication processes.

Despite of all the efforts throughout these years, the device efficiency only about 6% was reported in 2009 (Chen *et al.*, 2009; S. H. Park *et al.*, 2009). Recently, efficiency of 10.6 % recorded by You *et al.* using device with tandem structure. The history of the development of organic solar cells is summarized in Table 1.1. In addition, Figure 1.0 shows the development of photovoltaic technologies provided by National Renewable Energy Laboratory (NREL), United States of America.

Table 1.1: The development of organic solar cells as reported by researchers.

Year	**Achievement**	**Reference**
1839	Discovery of photovoltaic effect by Becquerel.	(Martin A, 2002)
1873	Photoconductivity in selenium observed by Willoughby Smith.	(Smith, 1873)
1906	Photoconductivity in anthracene by Alfedro Pochettino was observed.	(Spanggaard *et al.*, 2004)
1950s	Investigation of organic dye, chlorophyll and related compounds in photovoltaic devices.	(Spanggaard *et al.*, 2004)
1958	Kearns and Calvin *et al.* successfully measured open circuit voltage of 200mV in their MgPc based device.	(Kearns *et al.*, 1958)
1986	Bilayer heterojunction organic photovoltaic cell invented by Ching W. Tang with power conversion efficiency of 1%.	(Tang, 1986)

Year	Achievement	Reference
1991	Power conversion efficiency reached 0.7% when Hiramoto and his co-researchers fabricated the first dye/dye based device.	(Hiramoto *et al.*, 1991)
1997	Polymer/perylene based solar cells yield power conversion efficiency of 1% discovered by Yu and Hall.	(Spanggaard *et al.*, 2004)
2005	Tandem arrangement of photovoltaic device was reported by Kuwat Triyana and researchers with 1.38% efficiency.	(Triyana *et al.*, 2005)
2009	Kwanghee Lee and Alan J. Heeger *et al.* reported fullerence based organic solar cell, with power conversion efficiency of 6.1% and near 100% internal quantum efficiency.	(S. H. Park *et al.*, 2009)
2012	Highest power conversion efficiency so far at 10.6% for device with tandem structure, reported by You *et al.*	(You *et al.*, 2013)

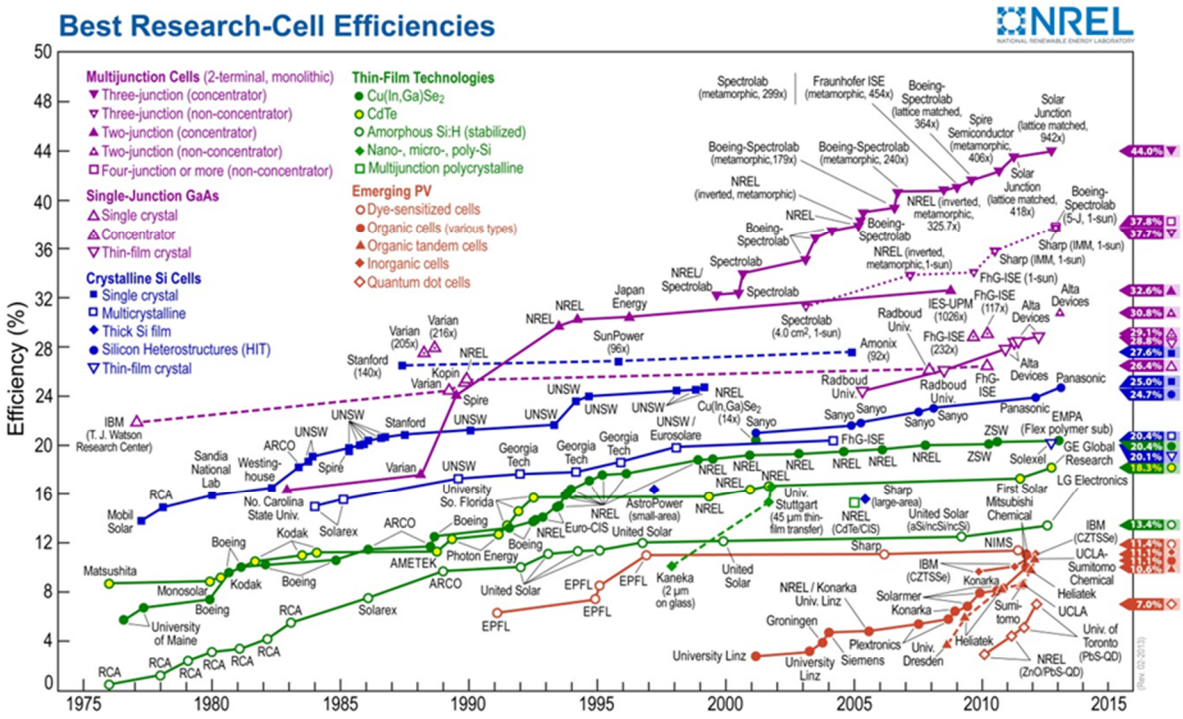

Figure 1.1: The development of photovoltaic technologies provided by National Renewable Energy Laboratory (NREL), United States of America.

1.2 MOTIVATION

Research on organic semiconductor materials for solar cells application becomes one of the hot topics around the world. At early stage of research, organic solar cells utilizing small compounds (oligomers), the deposition process of the active layer was done by a dry processing method of thermal evaporation technique. However, this evaporation method is an intricate, a lot of material being wasted and high cost production which is contrary to the objective of introducing organic solar cells for cost effective. Therefore, a wet processing method of spin-coating is applied to replace the conventional dry processing technique. This spin-coating method can provide a simpler way to deposit the active layer, small material consumption as well as cheaper end-product (Kodigala, 2010).

Among many organic semiconductor small compound materials, phthalocyanine is one of the materials that being extensively investigated since it is known to have the promising properties to be used in optoelectronics device. Phthalocyanine has high symmetry, planarity, physical properties and good electron delocalization (Günes *et al.*, 2007). It has a good chemical stability and excellent film growth. Most of phthalocyanine acts as hole conducting material that exhibit an intense absorption in the both ultraviolet and visible region (Aziz *et al.*, 2012).

In this work, metal-phthalocyanine is used as one of the thin films in the active layer of organic solar cell. In general, the conventional evaporation method is employed to deposit metal-phthalocyanine films due to constrain of material insolubility in any organic solvent. A lot of studies were reported by chemists by modifying the material molecular structure, in order to produce soluble phthalocyanine (Liu *et al.*, 2001; Ribeiro *et al.*, 2006; Šebera *et al.*, 2009). Besides, very few reports can be found on the utilization of soluble phthalocyanine in the fabrication of organic solar cells (Chunder *et al.*, 2010; Schumann *et al.*, 2011). Some examples of soluble phthalocyanines in organic solar cells will be discussed in Chapter 2.

Solvent treatment is a common way to modify the surface of the organic thin film. Previous work reported that the modification of surface resulting a better charge carrier on transport behaviour (Schmidt-Mende *et al.*, 2001). Besides, the surface of polymer thin film was modified via a so-called "slow-solvent-vapor treatment" to enhance the performance of the organic solar device (Y. Zhao *et al.*, 2007), in which the film was exposed to the chosen concentrated solvent vapor in a covered container. However, in this work, the investigation is performed on the physical properties of a soluble phthalocyanine thin film by immersing the film in the selected solvents.

1.3 RESEARCH OBJECTIVES

Besides the investigation of the new organic materials to be used in the solar photovoltaic device, surface modification of the active layer may improve the device performance. Herein, a soluble phthalocyanine of nickel (II) phthalocyaninetetrasulfonic acid tetrasodium salt (NiTsPc) is used as the donor material while tris(8-hydroxyquinolinato)aluminium (Alq3) as the acceptor for active layer in the device.

The first objective of the work is to investigate and find the optimum the parameters such as the material concentration, spin rate and annealing temperature in order to form the homogenous NiPsPc thin film with good physical characteristics. The NiTsPc thin film is deposited on the solid substrates using spin-coating of wet processing method. The spin-coated NiTsPc thin films will be analysed in terms of absorption behaviour and morphological properties. Secondly, the study is focused to investigate the effect of surface modification on the morphology and optical properties of the NiTsPc films. The modification process of NiTsPc films surface will be done by immersing the films in the selected solvents. Besides, the variation in physical properties with different immersion time in the solvent, will be investigated.

The final objective is to fabricate and study the electrical properties of the photovoltaic devices containing the solvent treated NiTsPc film as a donor layer and Alq3

as an acceptor layer. Correlation between the surface modification of NiTsPc and the performance of photovoltaic devices will be explored.

Hence the objectives of this study can be summarized as listed below:

i. To investigate the parameters in forming the homogenous NiTsPc thin film with good physical characteristics using spin-coating method.
ii. To investigate the effect of surface modification via solvent immersion on the morphology and optical properties of the NiTsPc films.
iii. To fabricate and study the electrical properties of the photovoltaic devices utilizing the solvent treated NiTsPc.

1.4 THESIS OUTLINE

This thesis consists of five chapters. In Chapter One, an introduction and a brief historical development of the organic solar cells research are mentioned. Furthermore, this first chapter describes the motivation to perform the research, followed by the objectives of the research also mention in this chapter.

Chapter Two reports the fundamental issues in organic solar cells including the working principle of organic solar cells and the basic device architecture. In addition, two major challenges are reviewed in this chapter; how to make a proper selection of material for organic solar cell and charge carriers transport properties. The solubility of materials, energy levels and a material (phthalocyanine) are also reviewed. Besides, this chapter explains the effect of solvent treatment on the charge carrier transport properties in organic solar cells. Finally, a description on the electrical analysis of the organic solar device is also presented.

The experimental details are presented in Chapter Three. All the experimental steps, starting from the preparation of substrate, preparation of solution, deposition process until the device fabrication are presented in great details. In addition, the principles of the physical instrumentations used in this study, are also briefly described.

Chapter Four is divided into two parts of the experimental results and discussion. The first part explains the selection of parameter such as suitable concentration, optimum temperature and selection of solvent in treating the organic film. Correlation between the solvent treatment time on the morphology, structural, optical and electrical of solar device are presented in the second part.

The conclusions as well as closing remark based on the results obtained from the experimental studies are presented in Chapter Five. Finally, suggestions of possible future studies in enhancing the performance of organic solar cells are described.

CHAPTER 2

LITERATURE REVIEW

2.1 CHAPTER OVERVIEW

Several topics regarding the organic solar cells are described in this chapter. Besides, the previous works reported by other researchers on organic solar cells are also reviewed. This chapter begins with explanations of the basic working principles of the organic photovoltaic device. In order to build the device, the materials selection for active layer is one the prime importance, hence this aspect will be discussed in great detail. The organic photovoltaic device architecture comprised of the active layers that sandwiched between two dissimilar electrodes. The surface modification of the organic active layer is utilized in order to enhance the performance of the device either via increment in light absorption or charge transport. Therefore, different approaches being utilized in the modification of the organic thin films are reviewed in this chapter. Finally, the electrical conduction of the device after being modified is reviewed and discussed.

2.2 WORKING PRINCIPLE OF ORGANIC SOLAR CELLS

An organic material consist of two energy levels which called the Highest Occupied Molecular Orbital (HOMO) and Lowest Unoccupied Molecular Orbital (LUMO) (Nunzi, 2002). These energy levels are also known as the ionization energy or the valence band and electron affinity or the conduction band. The different between these energy levels correspond to the energy gap of a material. A well-adapted energy level is formed when two materials incorporated and forming energy level as shown in Figure 2.1(b). The LUMO and HOMO level of the materials are form a step potential and make the electrons and holes easier to transport to the respective electrodes.

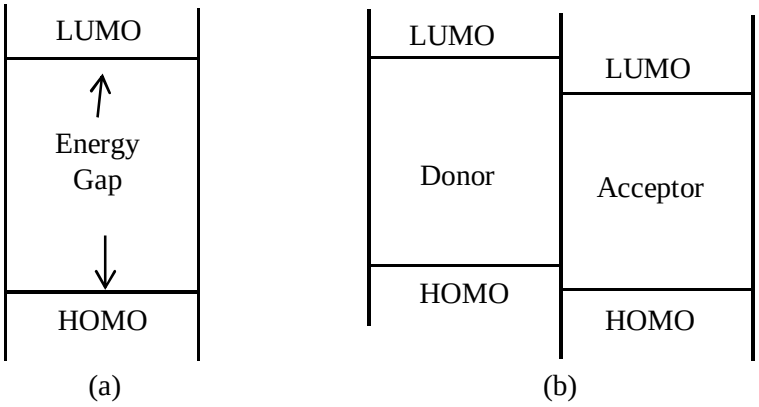

Figure 2.1: (a) Different levels of HOMO and LUMO represent an energy gap, (b) A step potential at the well adapted energy profiles of the two dissimilar materials.

Generally, the working principle of the organic solar cells depends on five important factors:

a. Absorption of light and generation of exciton

b. Diffusion of excitons to interface

c. Charge separation

d. Charge transport

e. Charge collection

The operation of organic solar cells starts with the absorption of light. Instead of free carriers formation (for the case of inorganic material), light absorption by organic film results primarily in the production of excitons (bound state of electron and hole pair). In order to produce free charge carriers, the photogenerated excitons must diffuse to an interface where they dissociate into an electron in one phase and a hole in the other. However, the excitons diffusion length in organic film was reported to be in the range of 5 to 15 nm only (Dennler *et al.*, 2005; Skompska, 2010), which is much smaller compared to the thickness of active layer (around 100 nm). In general, an organic solar cell consists of a donor and an acceptor as active layer, which then sandwiched between two electrodes with different work functions. The built-in electric field is produced from the different work functions of the electrodes and plays an important role to dissociate and separate the

excitons into free charge carriers of electrons and holes at the donor/acceptor interface (Peumans *et al.*, 2004). Then, the produced electron and holes are transported and collected at the respective electrodes before flowing out to the external circuit. However, some portion of produced electrons and holes may recombination geminately and will not contribute to the photocurrent. The generated photocurrent is measured as the current produced by the organic solar cells device. Therefore, the electrical conduction of the free charge carriers is an important role for a better photovoltaic device performance.

2.3 DEVICE STRUCTURE

The design of the photovoltaic device is developed in order to fabricate a better photovoltaic device. The designs of photovoltaic device include homo-junction and hetero-junction. Homo-junction photovoltaic device or single layer is shown in Figure 2.2(a) which depicted the active layer sandwiched between two electrodes with different work functions. This arrangement is also known as the Schottky type device since the charge separation take place at one of the electrodes. After absorption of light, the exciton is dissociated into free charge carrier and transport to its respective electrode. Further discussion of this process is done by referring the diagram in Figure 2.2(b). The contact of one of the electrodes and organic layer cause the band bending at the interface within the depletion region. The generated exciton is dissociated in this region before travel to its respective electrode. However, the dissociation process only occurred at the depletion region. Therefore, the recombination loses are high as the free charge carrier travel in the thin photoactive layer and results in low power conversion efficiency (Huang *et al.*, 1997; Shrotriya, 2010).

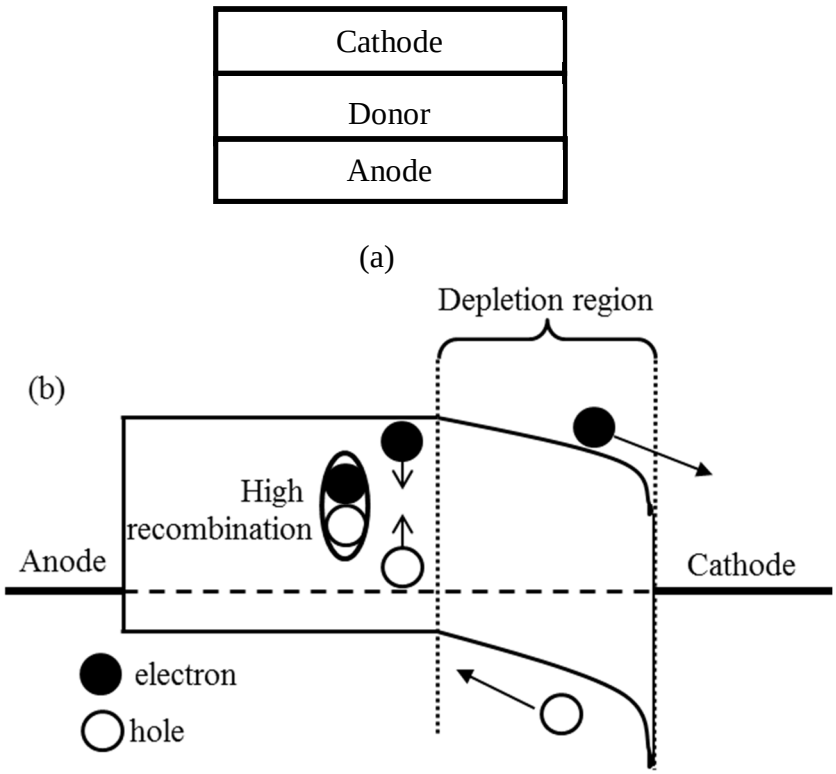

Figure 2.2: (a) Simple structure of single layer device (b) Schematic diagram of the electron flow in a single layer device.

Taking into account the recombination problem in a single layer device, the hetero-junction photovoltaic device is then introduced. Two layers consist of p-type and n-type material are stacked between two different electrodes to form a hetero-junction photovoltaic device or also known as the bilayer device. Figure 2.3(a) shows the diagram of the hetero-junction device. The HOMO-LUMO level of the stacked material must be well matched in order to create an efficient exciton separation process. During the absorption of photon, exciton is created very near to donor/acceptor interface, within approximately 10-20 nm from the interface to allow exciton diffusion process (Winder *et al.*, 2004). By comparing to the single layer device, this double layer arrangement enables the dissociation process occurs at the interface between donor and acceptor since it creates a large potential drop between them as shown in Figure 2.3(b).

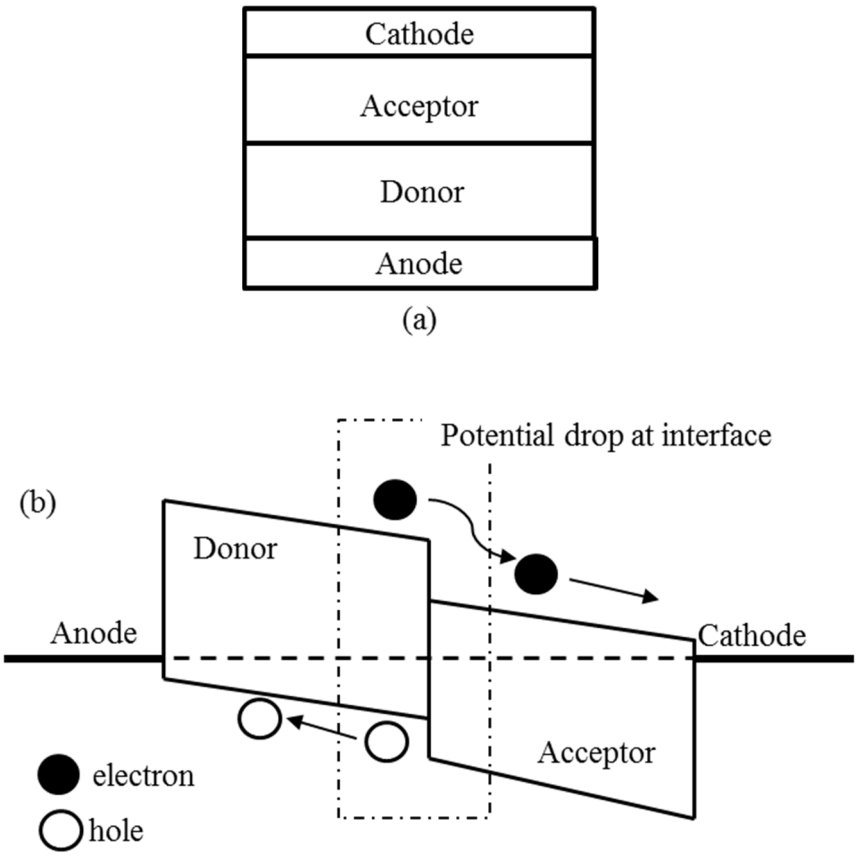

Figure 2.3: (a) Structure of a bilayer device (b) Schematic diagram of the electron flow in a bilayer device.

Using the same principle as the bilayer junction, a bulk hetero-junction device can be fabricated by introducing a mixture of donor and acceptor creating a three-dimensional (3-D) inter-penetrating network (D. W. Zhao *et al.,* 2010) instead of stacked them together as shown in Figure 2.4(a). Compared to the bilayer structure device, the exciton can be dissociated throughout the active layer in the bulk hetero-junction device, as the donor and acceptor are well blended. Moreover, this device provides a good contact between donor and acceptor and provides a charge percolation path for the free charge carriers produced. The recombination loses is reduced since most of the free charge successively collected at its respective electrode and not recombined with its counterpart. As a result, the photocurrent value is increased drastically the performance of the bulk hetero-junction photovoltaic device (Dennler *et al.*, 2005).

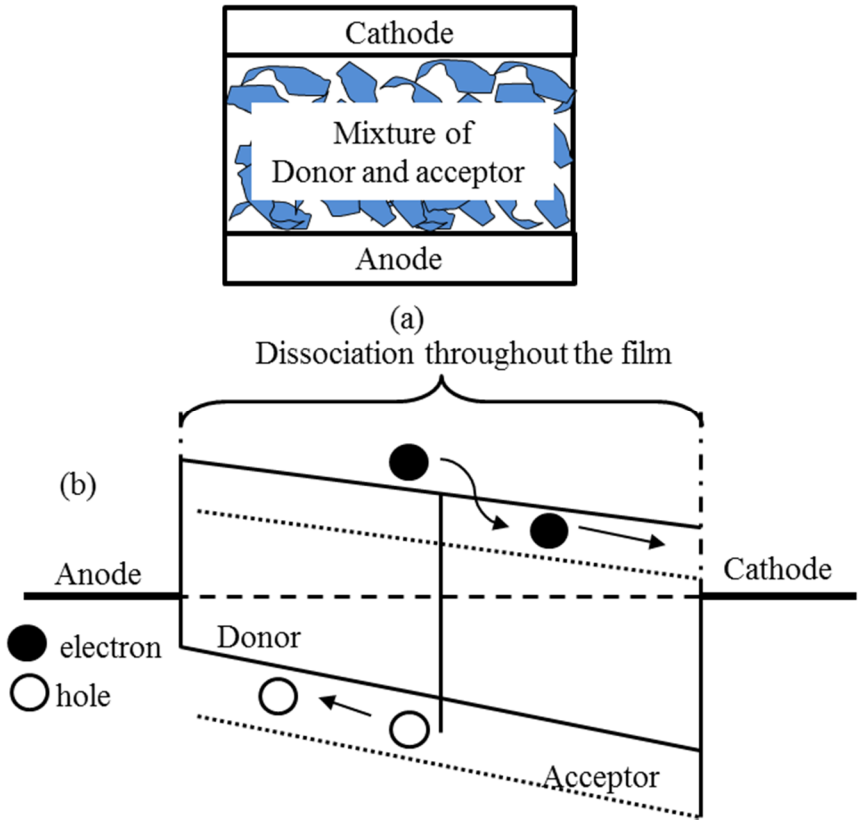

Figure 2.4: (a) Structure of a bulk hetero-junction device (b) Schematic diagram of a bulk hetero-junction device.

2.4 FACTORS GOVERN THE PERFORMANCE OF ORGANIC SOLAR CELLS

The performance of the organic photovoltaic device meets many challenges. Recently, the efficiency of organic photovoltaic device produced around 10.6% for device prepared in the laboratory condition (You *et al.*, 2013) Based on this efficiency, organic photovoltaic cells still cannot yet compete with the latest efficiency in the conventional inorganic-based solar panel of more than 25% (Martin A Green *et al.*, 2012). The efficiency of the photovoltaic device depends on many factors. Some of the factors are the selection of materials and charge carrier transport properties, as to be discussed in the next sub-sections.

2.4.1 Selection of materials

Solution processed materials to be used as an active layer in the fabrication process of organic photovoltaic cells is very attractive due to simplicity and cost effective.

Therefore, organic materials with high solubility in organic solvent can be considered as the most potential candidates for the active layer. Table 2.1 shows some of the organic materials used in organic photovoltaic device and its solvent.

Table 2.1: The energy level of the organic semiconductor materials and its suitable solvent

Material	Suitable solvent	HOMO (eV)	LUMO (eV)	Reference
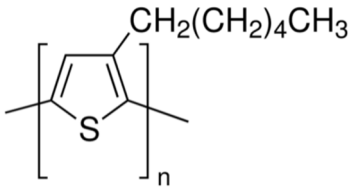 Poly(3-hexylthiophene) (P3HT)	Chloroform, 1,2-dichloroform, chlorobenzene	5.1	3.2	(K. Kim *et al.*, 2011)
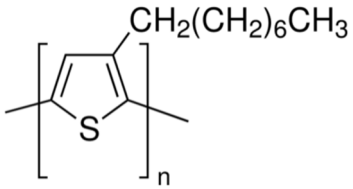 Poly(3-octylthiophene) (P3OT)	Chloroform, 1,2-dichloroform, chlorobenzene	5.1	2.8	(Manoj *et al.*, 2003)
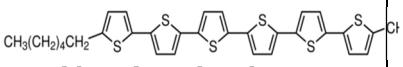 α,ω-dihexylsexithiophene (DH6T)	Chloroform, 1,2-dichlorobenzene	5.2	2.9	(W. Li *et al.*, 2012)

Material	Suitable solvent	HOMO (eV)	LUMO (eV)	Reference
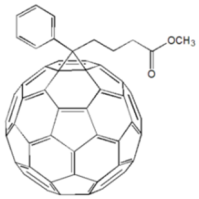 [6,6]-phenyl-C61 butyric acid methyl ester (PCBM)	Chloroform, 1,2-dichlorobenzene	6.0	3.9	(J. Y. Kim *et al.*, 2007)
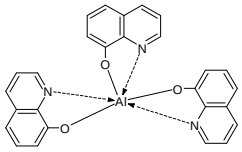 Tris (8-hydroxyquinolinate) aluminium (Alq3)	Chloroform, Dimethylsulfonate	6.3	3.4	(Muhammad *et al.*, 2010)
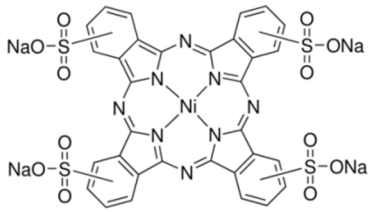 Nickel (II) phthalocyaninetetrasulfonic acid tetrasodium salt (NiTsPc)	Deionized water, DMSO	5.0	2.5	(Fakir *et al.*, 2012)
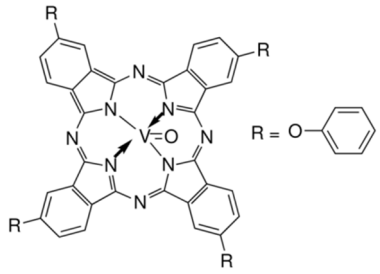 Vanadyl 2,9,16,23-tetraphenoxy-29H,31H-phthalocyanine (VoPcPhO)	Chloroform, 1,2-dichlorobenzene, tetrahydofluoran	5.3	3.3	(Abdullah *et al.*, 2012)

The information on the solubility of an organic material is important as it can be used for surface modification of the deposited film via a solvent treatment. An organic material can be either fully or partially dissolved in their solvents, depending on the functional group linked to the main compound structure or backbone. As an example,

pure fullerene cannot be dissolved in any organic solvent, however become soluble once a phenyl group is introduced to the fullerene molecule.

Besides the ability of the material to dissolve in organic solvent, the energy gap of the material is also a prime important factor in selecting the suitable material. Value of the energy gap in a certain organic material can be calculated by the difference in the HOMO and LUMO level as shown in Table 2.1. Usually, polymer has a wide energy gap and always acts as the insulator. However, polymer type used in organic solar cells is conjugated polymer which has a narrower energy gap. A narrow energy gap makes the charge carrier efficiently transferred between the HOMO and LUMO levels to produce photocurrent.

For a hetero-junction device, the suitable combination of the donor and acceptor as the active layer can be chosen from the combination of HOMO and LUMO level of organic materials. As shown in Figure 2.5(a), the energy profile of is not well-adapted since a high step up potential at the acceptor of the active layer. Electron needs more energy to jump the barrier height. This condition limits the ability of the amount the electron to be transported to the electrode.

A well-adapted energy profile as shown in Figure 2.5(b), indicates an easier process of charge transport. The free charge carrier can be easily transported thus makes a better electrical conduction of the device. Hence this energy profile is preferable in selecting the correct materials for the device. Example of a well-adapted energy profile is P3HT-PCBM, NiTsPc-Alq3, and CuTsPc-Alq3. Therefore, choosing a well-adapted energy profile between the donor and acceptor is very important in fabricating the device.

As mention in the previous section, the light absorption of organic material is limited to cover either UV or visible region. It is a good combination of material if the incorporated thin film can cover both of the regions. Taking Figure 2.6 as an example, most of the light absorbed by the P3HT polymer film (dark blue line) cover from 400-650nm and cadmium sulphide (CdS) (green line) which most absorption occurs at UV

region. Introducing CdS into P3HT film has made the absorption range covers in both UV and visible region (light blue). It is a good improvement to implement film with this absorption property in photovoltaic device since a broader range of light can be absorbed. Another example of materials which have complementing absorption properties are P3HT-PCBM (Hauch *et al.*, 2008) and DH6T-PCBM-P3HT (Muhammad *et al.*, 2011a).

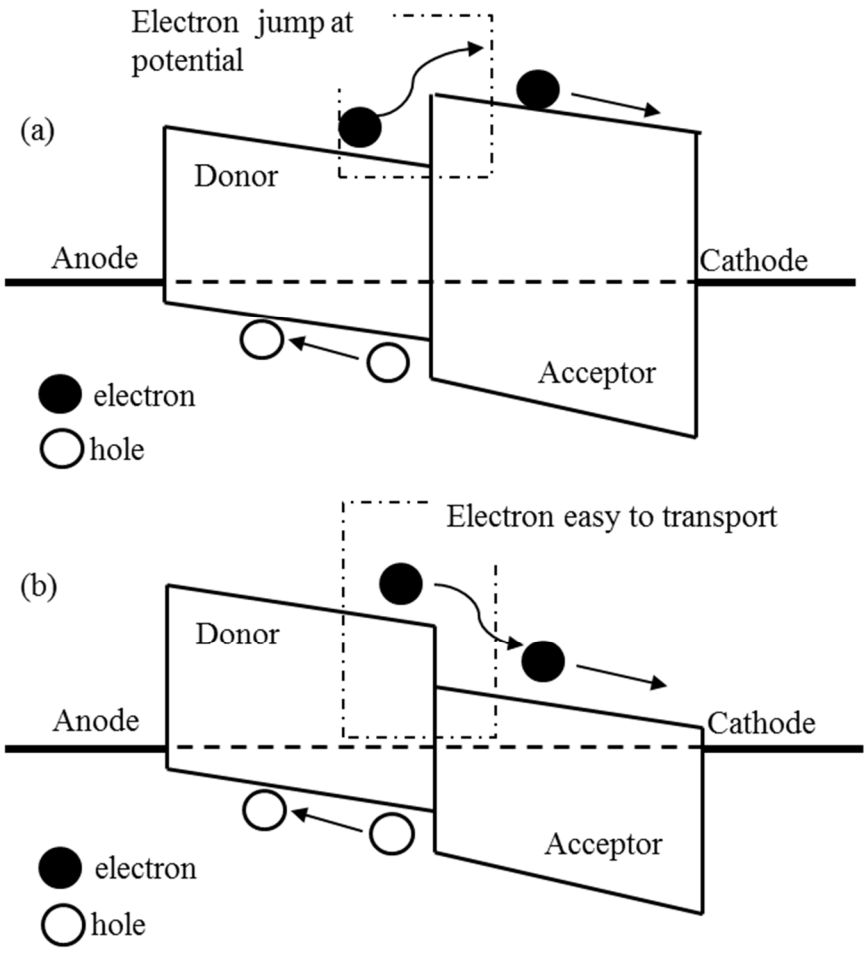

Figure 2.5: The schematic diagrams of charge transport: (a) A high potential at the acceptor of the active layer, (b) a well-adapted energy profile for easier charge transport.

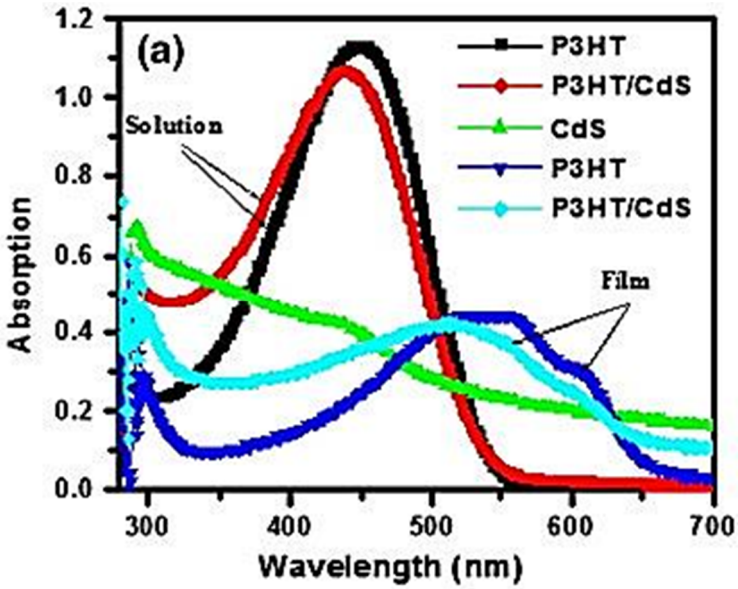

Figure 2.6: Absorption of P3HT, CdS and mixture of P3HT and CdS (Khan *et al.*, 2010).

Recently, researches on low molecular weight materials (oligomers) as an active layer in organic electronics have been developed (Peter Peumans *et al.*, 2003; Stingelin-Stutzmann *et al.*, 2005). One of the focused oligomer materials is phthalocyanine and derivatives. It is known as one of the most promising candidates for optoelectronics devices. Advantageous possesses by phthalocyanines includes chemical stability, excellent film growth, and electronic properties (Schwieger *et al.*, 2002). Phthalocyanine is a p-type, hole conducting material that works as electron donor and characterized by high symmetry, planarity and electron delocalization (Günes *et al.*, 2007). Phthalocyanine also can act as n-type material by modification of the molecule, for example: Copper (II) 1,2,3,4,8,9,10,11,15,16,17,18,22,23,24,25-hexadecafluoro-29H,31H-phthalocyanine (F_{16}CuPc) by adding fluorinated ion to the copper (II) phthalocyanine (CuPc). This addition makes the molecule to have excess electron and act as a good n-type material.

Research on the phthalocyanines with different central atom was done by some researcher mainly on the optoelectronics devices (Kwong *et al.*, 2003; Singh *et al.*, 2006; Singh *et al.*, 2005). Figure 2.7 shows some of the selected phthalocyanines.

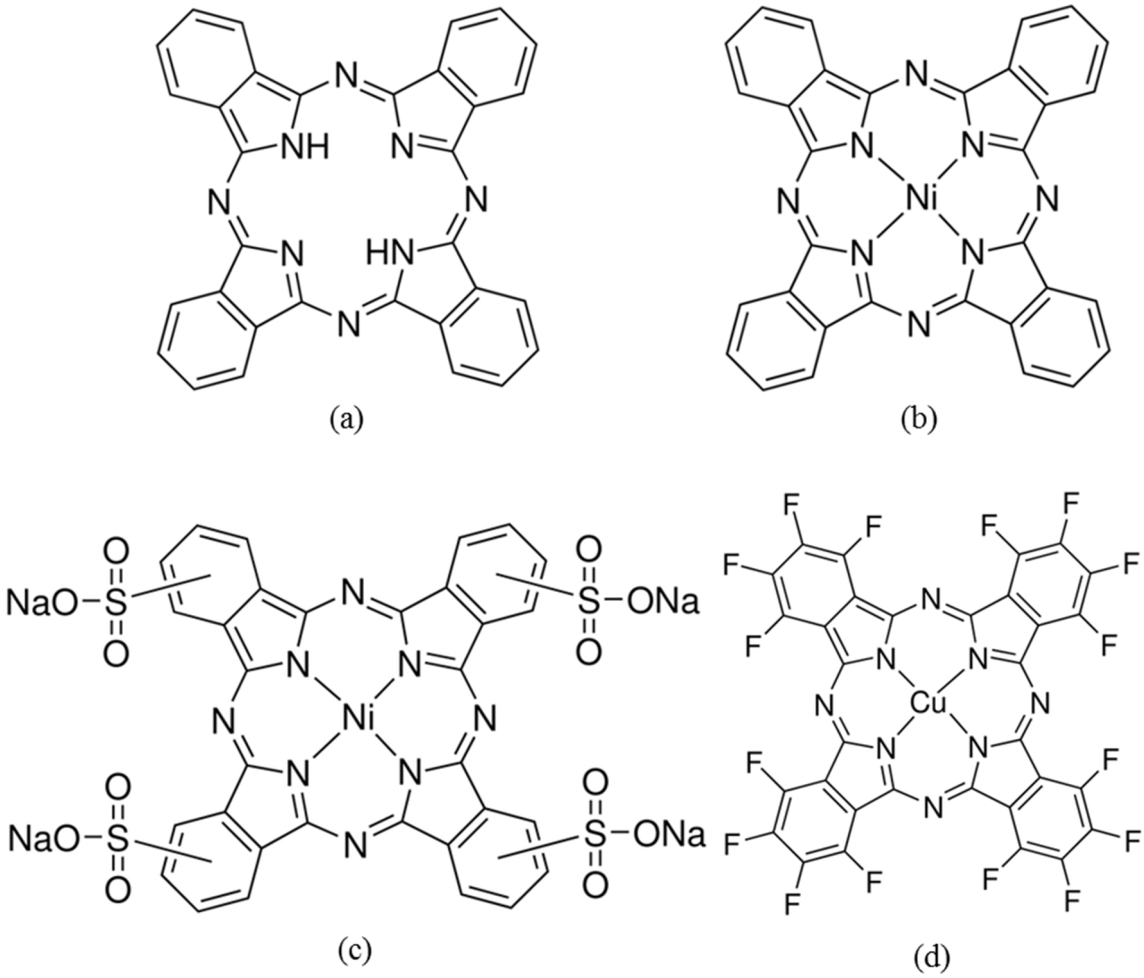

Figure 2.7: (a) Metal free phthalocyanine Pc, (b) Nickel (II) phthalocyanine, NiPc (c) Nickel (II) phthalocyaninetertrasulfonic acid tetrasodium salt, NiTsPc (d)Copper (II) 1,2,3,4,8,9,10,11,15,16,17,18,22,23,24,25-hexadecafluoro-29H,31H-phthalocyanine, $CuF_{16}Pc$.

At the early stage of the research, phthalocyanine film was sublimed in high vacuum systems. Since this method is very intricate and not very cost effective, solution processed phthalocyanine has been introduced. However, most of phthalocynines are insoluble in any organic solvent. Thus, introduction of electron withdrawing substituents such as sodium salt molecules (Sanchez *et al.*, 2001) and tricarbethoxyethyl substituent (Şener *et al.*, 2003), have produce the soluble phthalocyanines.

2.4.2 Charge carrier transport properties

As discussed from the previous section, the free charge carrier transport to its respective electrodes after dissociation process. The movement of the free charge carrier depends on the mobility of the material. Each material has different electron and holes mobility. For a p-type semiconductor, hole mobility is higher than the electron mobility. For example, previous works on a p-type of phthalocyanine with the mobility around 10^{-6} - 10^{-10} $m^2v^{-1}s^{-1}$ (Aimai *et al.*, 1998; Ambily *et al.*, 1999; Gould *et al.*, 2000; Mycielski *et al.*, 1982; Soliman *et al.*, 2003). However, in some cases, the free charge carrier is unable to be efficiently transported to the electrodes due to the existent of impurities in the film (caused by the fabrication process of the device). Any unsuccessful free charge carrier transportation to the electrode will result in charge recombination or trapped. As a result, photocurrent produced by this device is low and do not promise a good organic photovoltaic device. There are numerous methods being employed by researchers to encounter this issue. One of the techniques is to enhance the charge transport at the active layer to the electrode, by increasing the inter-penetrating network as evident by the coarser surface mean roughness of the AFM images. Yusli *et al.* reported that the surface mean roughness of the film become coarser after mixing 1,2-dichlorobenzene and chloroform solvent for P3HT and PCBM and the AFM images are shown in Figure 2.8 (Yusli *et al.*, 2009). Rougher surface yields a greater phase separation and a larger interfacial area for excitons dissociation. Furthermore, this phase separation also develops a continuous pathway for charge carrier to move to its respective electrodes. The same methods was used by Kwong *et al.* for fabrication of organic solar cells device and yielded a higher efficiency (Kwong *et al.*, 2004).

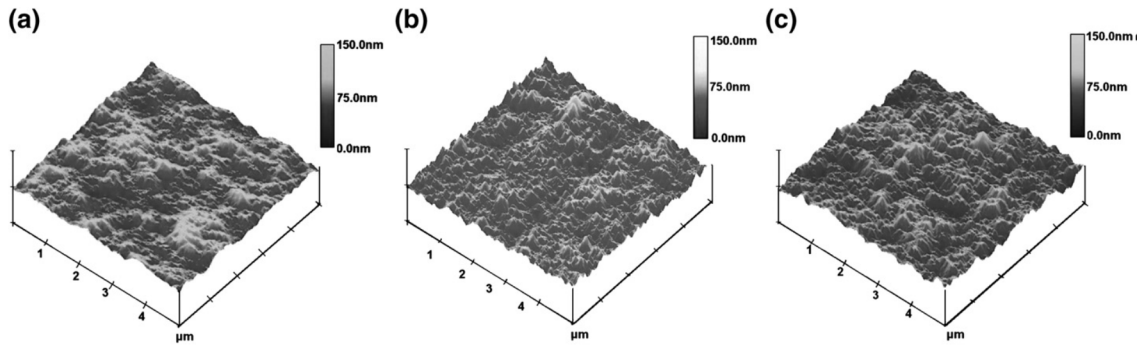

Figure 2.8: 3D atomic force microscopy images of P3HT:PCBM blend films dissolved in (a) pure DCB solvent, (b) CH solvent, and (c) DCB:CH co-solvent yield surface mean roughness 11.062 nm, 12.623 nm and 14.2777 nm respectively .

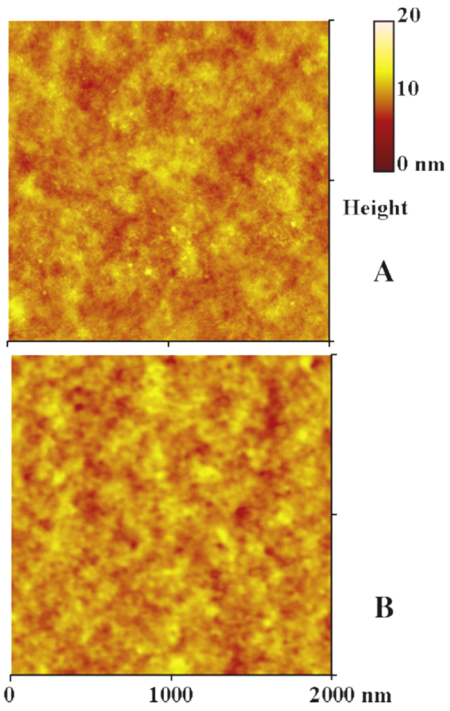

Figure 2.9: Comparison of AFM images of the P3HT: PCBM active layer; (A) fast-thermal-annealing and (B) slow-solvent-vapor-treatment (Chirvase *et al.*, 2004; G. Li *et al.*, 2005; Ma *et al.*, 2005).

For the same reason, slow-solvent-vapor-treatment (SSVT) was done to the organic thin films. The film was place inside a container, filled with saturated vapor of the solvent for a certain time (Y. Zhao *et al.*, 2007). Referring to Figure 2.9, the mean surface roughness was increased after this solvent vapor treatment (Guo *et al.*, 2008). The result suggested that existence of the inter-penetrating between the molecules, which was in good agreement to the other reported findings by other researchers.

2.5 ELECTRICAL ANALYSIS

Figure 2.10 shows a typical current density, *J* against voltage, *V* (*J-V*) graph obtained for the organic solar cell in dark and under light illumination. Exposure of this device to light caused the *J-V* curve to be shifted downward producing a photovoltaic effect. Referring to Figure 2.10 (J_{sc} *a*), no photovoltaic effect occurs and the device act as a normal diode in dark condition. The analysis of this graph is performed by focusing on the two important components in this graph that is open-circuit voltage (V_{oc}) and short-circuits current density (J_{sc}). Maximum square area at the graph corresponds to the maximum power output of the device. The ratio between the maximum power and product J_{sc} and V_{oc} is known as the fill factor. For an ideal photovoltaic cell, the fill factor is equal to one. A higher fill factor indicates a better performance for the photovoltaic device. Equation 2.1 is used to calculate the value of fill factor.

$$Fill\ Factor, FF = \frac{J_{max}V_{max}}{J_{sc}V_{oc}} = \frac{P_{max}}{J_{sc}V_{oc}} \tag{2.1}$$

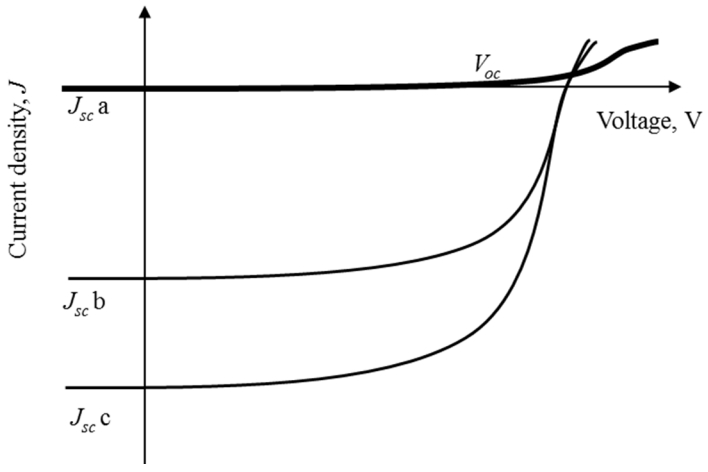

Figure 2.10: Typical *J-V* graph for organic solar cells

The factors that govern the value of V_{oc} are still being debated among the researchers. However, there are some researchers reported that this value depends on the

different of the HOMO and LUMO level of the donor and acceptor (Brovelli *et al.*, 2007; Hoppe *et al.*, 2004; Bernard Kippelen *et al.*, 2009). From the graph, V_{oc} is the maximum potential of the photovoltaic device obtained at zero current (x-intercept) which corresponds to the bias at the p-n junction under light illumination. Therefore, using different materials as donor and acceptor which have different pair of HOMO-LUMO level will result in different V_{oc} value.

The reported experimental result (Jo *et al.*, 2012), as presented in Figure 2.11 shows the variation in *J-V* curves upon exploiting different materials. Table 2.2 tabulates the different V_{oc} values obtained from Figure 2.11.

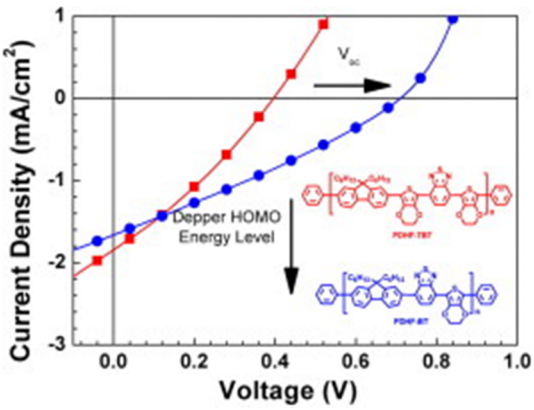

Figure 2.11: The value of shifted to a bigger value when the PCBM incorporated with another material which has different energy level.

Table 2.2: The energy level, energy gap and V_{oc} (Jo *et al.*, 2012)

	HOMO (eV)	**LUMO (eV)**	**Energy gap, E_{gap}**	**V_{oc}**
PDHF-TBT	-5.22	-3.42	1.80	0.40
PDHF-BT	-5.47	-3.45	2.02	0.71

By increasing the difference of HOMO level of a donor, which in this case was poly[{9,9-dihexylfluorene-*alt*-{4-(3,4-ethylenedioxythiesnyl)-2,1,3-benzothiadiazole] (PDHF-BT) and LUMO level of PCBM, hence the V_{oc} value has been significantly improved.

From the graph, the short-circuit current density is the current produced when there is no potential different across the photovoltaic device. It is accepted that the J_{sc} depends on the absorption properties of the films and their charge carrier transport (Muhammad *et al.*, 2011a). From Figure 2.10 (J_{sc}b and J_{sc}c), the different value in J_{sc} corresponds to a better production of current in the device. As discussed in the previous section, the dissociated exciton transport may easier to be collected at the electrodes after treating the organic film by a selected solvent.

Referring to Figure 2.12, the active layer for the device was the treated copper phthalocyanine (CuPc) as the first layer and PCBM as the second layer. Although the CuPc film was treated with different solvents, there was no significant change in the shape of the *J-V* graph and V_{oc}. The result suggested that the solvent treatment did not affect the band structures at the interface, on the other hand has affected the charge carrier transport properties. The modification shows that the current produced was the highest for the film treated with acetone, indicated that the free charge carrier transport ability was higher thus resulted in a higher current.

Besides, the mobility of the free charge carriers can be investigated by analyzing the current produced from the *J-V* graph. By converting the graph into a double log *J-V* graph, the slope of each region can be determined. Each region corresponds to the condition of the charge carrier conduction mechanism. The mechanism was discussed based on the Space charge limited current theory (Murgatroyd, 2002). At the lower bias voltage, the injected charge carriers were very weak and almost the same as the thermally generated intrinsic charge carriers. At this condition, the slope of the graph was almost unity and the device operation based on the Ohm's Law.

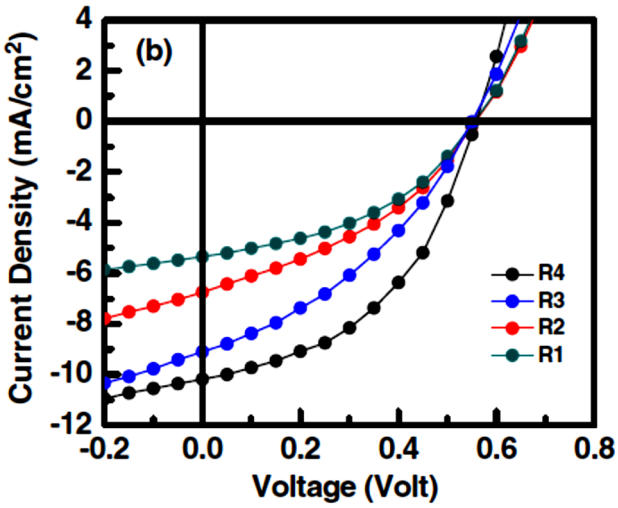

Figure 2.12: Variation of J_{sc} caused by solvent treatment (Karak *et al.*, 2010)

High injected charge carrier resulting a greater magnitude of the electric field as the carriers dominates the voltage bias and become space charge limited (SCLC) (Campbell *et al.*, 1997). The slope at this region is about 2. The mobility can be approximately determined by rearranging Equation 2.2 become Equation 2.4 (Ahmad *et al.*, 2010):

$$Current\ density, J = \frac{9\varepsilon_0\theta\mu V^2}{8d^3} \tag{2.2}$$

$$\theta = \frac{p_0}{p_o+p_t} = \frac{J_1}{J_2} \tag{2.3}$$

$$Mobility, \mu = \frac{8d^3J_2J}{9\,\varepsilon_0V^2J_1} \tag{2.4}$$

J_1 and J_2 is the lower and higher log value of current density at second region. As the value of mobility of the carriers gets higher, hence the carrier is easier to move and collected to the electrodes to generate higher current.

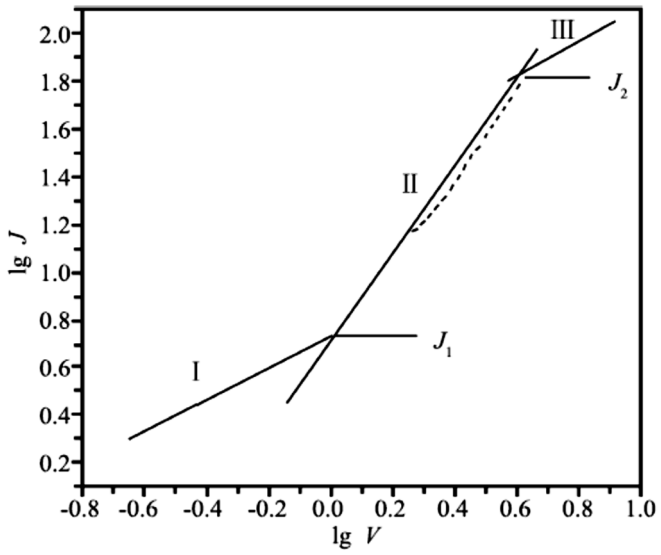

Figure 2.13: A double-log graph constructed from a linear *J-V* graph.

Ahmad et. al investigate the mobility of photovoltaic device with CuPc organic-inorganic. As shown in Figure 2.13, three regions are found (Ahmad *et al.*, 2010). First region was the Ohmic region with slope about to unity from lower voltage until 0.7 V. With slope approximately 2.0, the second region corresponded to the SCLC region. They reported that the calculated mobility was found to be 10^{-6} m^2 $V^{-1}s^{-1}$ for this CuPc-based device. A trap free region occurs with a slope slightly higher than the first region correspond to the trap free region. This region occurs as the space charge is fully filled with free carriers or approaching the trap limit.

CHAPTER 3

EXPERIMENTAL METHODS

3.1 CHAPTER OVERVIEW

In the early part of this chapter, the preparation, deposition and characterization of the thin NiTsPc films are explained, followed by the description on the fabrication and characterization of the photovoltaic device. The preparation process of NiTsPc solution using wet processing method and the deposition technique of the thin film using a thermal evaporator are explained in detail. Afterwards, the treatment process of the NiTsPc thin film via immersion in the selected solvents is elucidated. In this case, the films were treated with solvent that has low solubility with the material to modify the film surface only without destroying the whole film structure.

Morphological and optical characterizations were made to the modified film using Atomic Film Microscopy (AFM), Field Effect Scanning Electron Microscopy (FESEM), KLA Tencor P.6 Surface Profilometer, Jasco V-570 UV/VIS/NIR Spectroscopy, RenishawinVia Raman Microscope and X-ray Diffractrometer D5000. The photovoltaic devices were fabricated using NiTsPc as the p-type to be coupled with an n-type material as the active layer in the sandwiched structure between two electrodes of ITO and Al. Finally, the electrical properties of the devices were measured and characterized using a Keithley 236 source measuring unit and AM 1.5G filter of Oriel Solar stimulator,

3.2 SUBSTRATE PREPARATION

Commercially available glass substrate was purchased and used as the substrate for the deposition of the organic thin film. Glass was chosen as substrate as it possesses high transmission of light within the visible region. Glass substrates were cut to the size of 2.0 cm x 2.3 cm for the measurements of optical properties. The substrates were cleaned by soaking them sequentially with a detergent solution, acetone, isopropyl alcohol and de-

ionized water. A good cleaning process must be done to avoid any contamination that can affect the result of the work. In order to fabricate the photovoltaic device, glass coated-ITO substrates were chosen as the bottom electrode. The commercially available ITO with a sheet resistance 7Ω/square was purchased and cut with size of 2.0 cm x 2.3 cm. Some parts of the ITO were etched to avoid short circuit condition during electrical measurement. Etching process was started by spraying a layer of paint on ITO using commercial spray paint to make a pattern as shown in Figure 3.1(a).

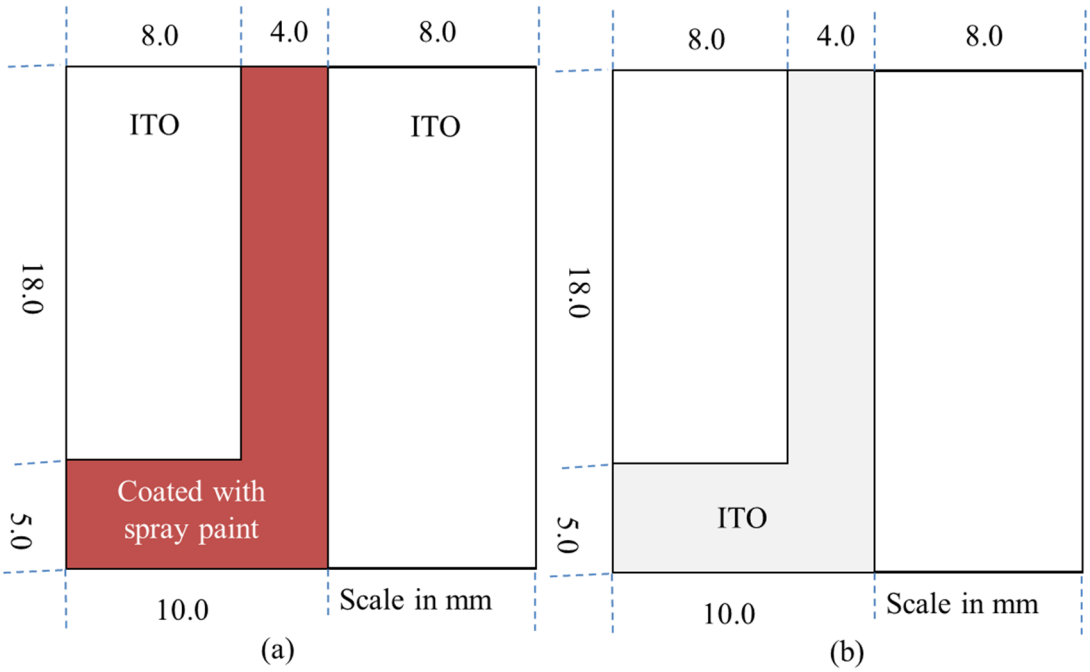

Figure 3.1: (a) Patterned ITO using spray paint. (b) Substrate after etching process.

Once the paint was dried, a diluted hydrochloric acid (HCl: H_2O = 4:6) was used to etched the uncover part of the substrate by heating at 60˚C for about 20 minutes. Then, the ITO substrates were cleaned using similar method of glass substrates; i.e. by soaking them sequentially in a detergent solution, acetone, isopropyl alcohol and de-ionized water. The spray paint was completely removed at the end of the cleaning process. Based on Figure 3.1(b), the un-covered part of the substrate was etched and left the permanent ITO under the spray paint.

3.3 MATERIAL AND PREPARATION OF SOLUTION

In this work, nickel (II) phthalocyaninetetrasulfonic acid tetrasodium salt (NiTsPc) was used as donor material while perylene-3, 4, 9, 10-tetracarboxylic-3, 4, 9, 10-dianhydride (PTCDA) and tris(8-hydroxyquinoline)aluminium (Alq3) was used as the acceptor material. Both of the materials were purchased from Sigma Aldrich and used without further purification. In order to utilize spin-coating method for film deposition, the organic semiconductors must be fully dissolved in organic solvent. All available solvents in the lab of Low Dimensional Material Research Centre (LDMRC) including chloroform, toluene, ethanol and 1, 2-dichlorobenzene were used to dissolve NiTsPc powder. By naked eye, the material solution can be observed to check the solubility. It was found that NiTsPc was fully dissolved in de-ionized water, whereas the other solvents only produced partially dissolved material. Therefore, by weighing and dissolving 15, 20, 25, 30 and 35 mg of NiTsPc in 1 ml of de-ionized water, the solution with concentration of 15, 20, 25, 30 and 35 mg/ml were prepared. The solution was shaken vigorously to help the material to be dissolved. Then, the solution was filtered using 0.2μm^2 filter to remove any contaminant or un-dissolve material.

3.4 DEPOSITION OF THIN FILM

The prepared NiTsPc solution from the previous section was used to deposit the thin film using a spin-coating method before being treated with solvent. In order to fabricate the photovoltaic device, an n-type material was deposited on the treated NiTsPc (p-type) film using a home-built thermal evaporator.

3.4.1 Drop Casting Solution

This technique is a facile method used to produce a thicker thin film around 0.5 – 2.0 µm. Firstly, a cleaned substrate was placed on a leveled surface to make sure that the thickness of each part of the deposited thin film after deposition process was uniformed.

Then, 30µl of NiTsPc solution was dropped on the substrate and it was left to dry in ambient condition for two hours.

3.4.2 Spin Coating Technique

Compared to a drop casting, deposition of thin film using this spin-coating technique can produced a thinner thin film. The value for rotation per minute (rpm) is inversely proportional to the thickness of the thin film. That is means, by increasing the value of rpm, the film thickness of the will decrease. For a film to be used in the fabrication of photovoltaic device, the thickness should be in the range of 100 to 150 nm. However, NiTsPc solution did not show any adherence on the substrate when the rpm was set below 800 rpm and beyond 1000 rpm. Thus the rpm value was limited by the ability of the solution to adhere on the substrate. In this work, the spin speed was set at 1000 rpm to produce an appropriate NiTsPc film thickness. A Laurell P-6000 spin coater was used in this work and Figure 3.2 shows the deposition process diagram using spin coating technique to form NiTsPc film on a solid substrate. The prepared NiTsPc thin films were then annealed in an oven at different temperatures between 80 to 140˚C to remove the residual water content. An optimum temperature was then determined, and discussed in Chapter 4. After this thermal annealing process, the NiTsPc films were ready to be treated with solvent.

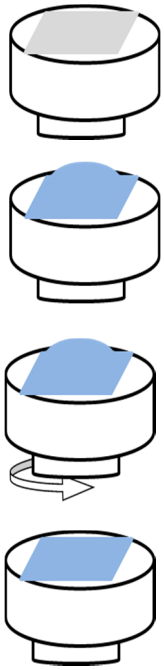

a) A cleaned substrate was placed on the substrate dish.

b) 30µl of NiTsPc solution was dropped on the substrate.

c) Substrate was spun at 1000 rpm for 60 seconds

d) Let the film dry in ambient condition

Figure 3.2: Deposition process using spin coating technique

3.5 SOLVENT TREATMENT

Some researchers (Zhi-Hui *et al.*, 2010) used slow solvent vapor treatment and solvent ratio to modify the film morphology. However, a so-called solvent treatment was applied; the prepared and annealed NiTsPc thin films from the previous section were immersed in its poor solvent to modify the surface morphology, hence would lead to the change in the organic material energy gap. Poor solvent define as the solvent which has low solubility to the NiTsPc material.

Previously, as mentioned in section 3.3, the NiTsPc powder was dissolved in several of solvents in order to distinguish the suitable solvent to be used throughout the work. It was found that de-ionized water was the best solvent. In addition, from that part of the work, it was also known that chloroform ($CHCl_3$) and toluene show very low solubility to NiTsPc powder. As a result, these two solvents were selected to be used in the solvent treatment process as the poor solvent for NiTsPc thin films. This process started by immersing the prepared film in its poor solvent in 20, 40, 60, 80, 100 and 120 minutes. Immersion process was stopped after immersing the film for 120 minutes since

the film was started to etch (which can be observed by naked eyes). After immersion time was achieved, the film was taken out from the solvent and placed on a leveled surface to let the film dry in ambient condition. The whole process was done in a fume cupboard to avoid contaminant.

In order to find a better solvent for surface treatment, an experiment was done to distinguish which solvent (either chloroform or toluene). NiTsPc films were immersed in each solvent for same immersion time of 20 minutes. Next, the photovoltaic devices were fabricated by depositing PTCDA as n-type material on top of the solvent treated NiTsPc film. The electrical properties of the device were measured. From the result, the device using NiTsPc film treated with chloroform give a better electrical performance compared to NiTsPc treated with toluene. Thus, chloroform was used as the poor solvent throughout this work.

3.6 DEVICE FABRICATION

The double layer photovoltaic devices with arrangement of ITO/NiTsPc/n-type material/Al were fabricated. In this case, the second layer of n-type material cannot be deposited onto the first p-type layer using a spin-coating technique because such wet process will destroy the first layer. Thus, n-type material was deposited on the solvent treated NiTsPc, using a home-built thermal evaporator. The typical diagram of a home-built thermal evaporator is shown in Figure 3.3(a). Initially, the treated NiTsPc film was placed on the substrate mask before it was inserted into the thermal evaporator. About 20 mg of the n-type material were placed inside a quartz boat and the thermal evaporator was then pumped down to achieve a pressure of 10^{-4}mbar. Next, the quartz boat was heated by supplying current gradually from 10 to 30 A through a tungsten wire. As a result, the n-type material in the quartz boat was also heated and started to sublime inside the chamber. A shuttle was opened to allow the material to sublime to the treated NiTsPc through a shadow mask for a certain time depending on the desired thickness. In this case, the

deposition time for Alq3 and PTCDA is 60 s and 45 s respectively to produce a 60 nm film thickness.

The final process of device fabrication was the top aluminium electrode deposition. A commercial Auto Edward 306 deposition system (Figure 3.3(b)) was used to deposit the top electrode. Some pieces of Al wire with 99.9% purity were attached on a tungsten filament coil and placed inside the deposition chamber. The pressure inside the chamber was about 1.50 x 10^{-5} mbar before the deposition process was started. The tungsten filament was heated up slowly by increasing the current from 10 to 20 A with increment of 1 A per minutes to melt and evaporate the Al. The small increment of current was performed in order to control the deposition rate only in the range of 1 – 2 nm/s, thus the Al penetration in the active layer can be avoided, hence preventing the device being shorted. As the Al vaporized, the shuttle was opened for 90 s to produce a thickness of around 30 nm of Al layer. The schematic diagram of photovoltaic device in this work was shown in Figure 3.4.

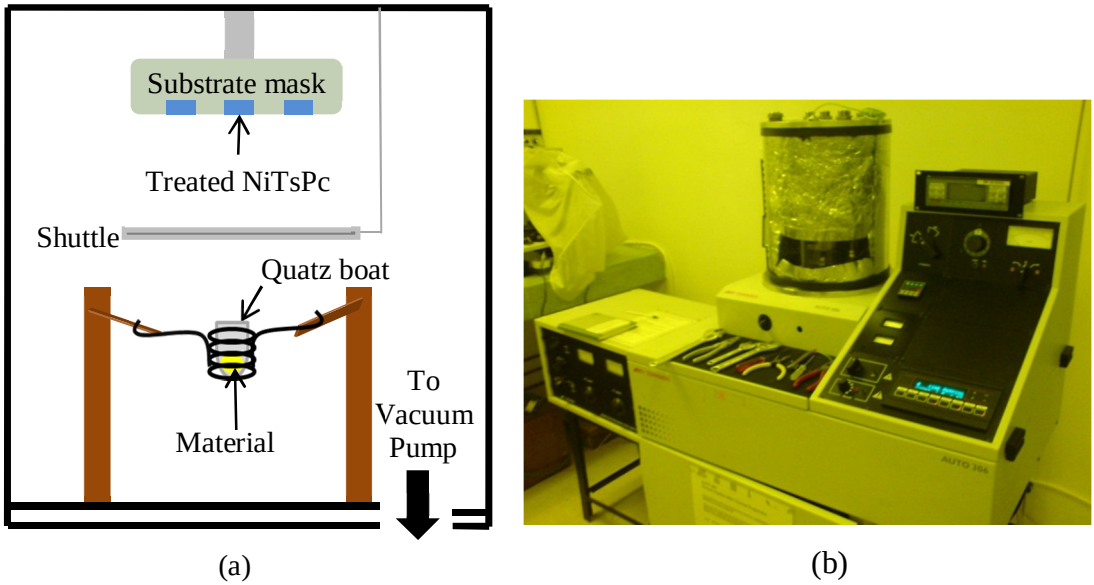

Figure 3.3: (a) Inside view of home built thermal evaporator. (b) Auto Edward 306 deposition system.

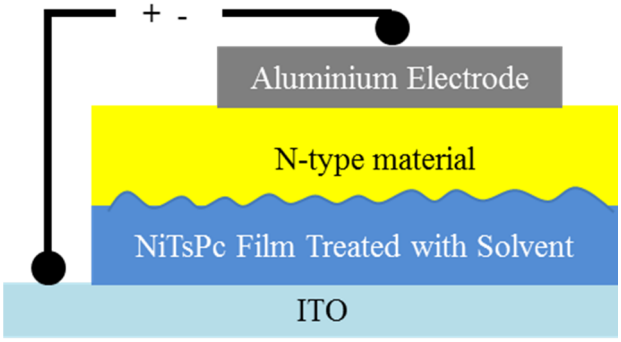

Figure 3.4: Schematic diagram of photovoltaic device with arrangement of ITO/treated NiTsPc/n-type material/Al.

3.7 THICKNESS MEASUREMENT

The thickness of the thin films was measured using a KLA TENCO P-6 surface profilometer. This instrument uses a diamond stylus which moves laterally throughout the surface of the thin film. A scratched line was made on the surface of the film to create the difference height between the substrate and the surface of the film. The surface profile was generated due to the deviation of the diamond stylus as shown in Figure 3.5. In this work, the film was scratched at five different positions and the average value was taken as the thickness of the film.

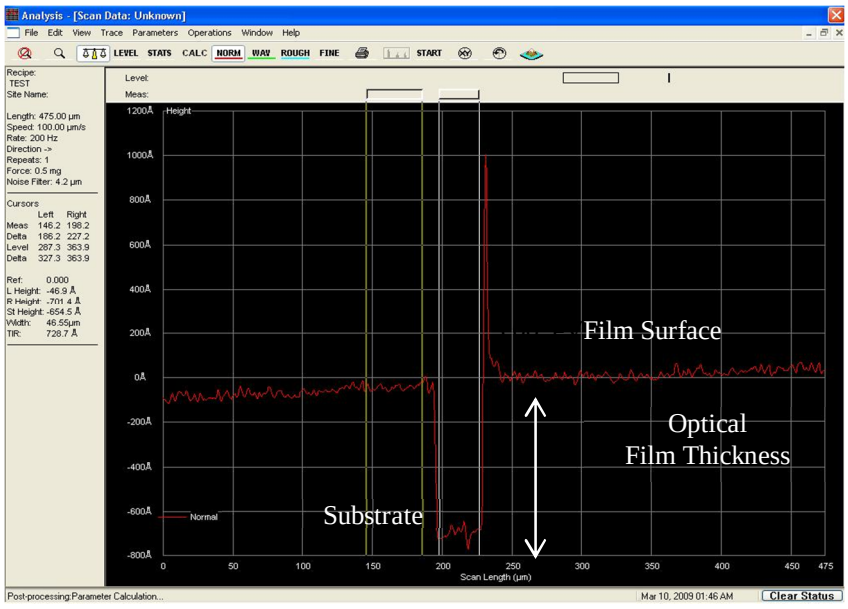

Figure 3.5: Printed screen shot of the surface profilometer, indicates the difference in the height profile of film surface and the substrate to give the film thickness.

3.8 X-RAY DIFFRACTION (XRD)

XRD measurement was performed by a Siemens D5000 Diffractometer in order to determine the structure of the thin films. Using an XRD machine, a thicker film must be used or else it will only give the reading of the substrate. Therefore, film deposited using drop casting method was used since it has thickness up to 2μm which is adequate for this characterization. From the XRD patterns, crystallite size of the sample can be measured by Scherrer equation:

$$Crystallite\ size, Dp = \frac{K\lambda}{B\cos\theta} \quad (3.1)$$

For this XDR machine of Siemens D5000, the Scherrer constant, K = 0.94 and source wavelength, λ = 1.542 Å. B is the full width at half maximum (FWHM). Using an Origin Pro software, the XRD pattern was convoluted at highest intensity peak which corresponds to the main crystallite size at the film to get the value of FWHM to be use in Equation 3.1

3.9 ATOMIC FORCE MICROSCOPY (AFM)

Using a tapping mode of Dimension 3000 AFM, the AFM images of the sample were displayed using the setting parameters as tabulated in Table 3.1. Initially, the AFM machine was started when a sharp tip at a cantilever was probed over a surface area 100 μm^2. Any deflection between the tip and the surface of the sample will trigger the cantilever as a response mechanism. A laser and photodetector was used to detect the deflection. AFM can detect and display the humps and valleys along the surface area of the treated films. Besides, specific software was used to display the 2 and 3 dimensional images of the sample, height, roughness analysis and section analysis. Basic working principle of AFM was shown in Figure 3.6.

Table 3.1: Parameter for the Atomic Force Microscope (AFM) measurement.

Scan size	10.000 µm
Scan rate	2.001 Hz
Image data (for 2 dimension imaging)	Height

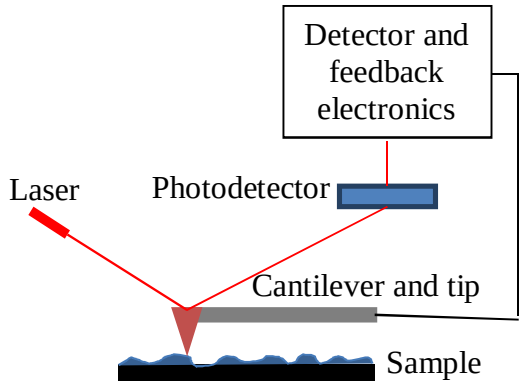

Figure 3.6: Schematic diagram of working principle of AFM.

3.10 FIELD EFFECT SCANNING ELECTRON MICROSCOPY (FESEM)

The surface morphologies of films were investigated by using a field emission scanning electron microscopy (FESEM). A FEI Quanta 200 field emission scanning electron microscopy (FESEM) used in this work is shown in Figure 3.7. The surface images of the films obtained from this FESEM are very important to study the structure of the films surface after the solvent treatment.

The FESEM scanning was carried out in the high vacuum condition. Electrons liberated from field emission source and accelerated in a field gradient. These electrons which are called primary electrons pass through electromagnetic lenses and deflect to produce a narrow scan beam that bombard the sample. This bombardment causes different types of electrons to be emitted from the sample. Only secondary electrons are captured by the detector and images are constructed relative to the scanning primary electron beam. These signals are amplified and transformed to a video scan-image that can be seen on a monitor.

Figure 3.7: Picture of FEI Quanta 200 field emission scanning electron microscope (FESEM).

3.11 ULTRAVIOLET-VISIBLE-NEAR INFRARED (UV-VIS-NIR) SPECTROSCOPY

Light incident towards any medium such as thin film will be either reflected, absorbed or transmitted. In organic solar cells, the ability for a thin film to absorb light is one of the important factors for a device to be optimized. Using a Jasco V-570 UV/VIS/NIR Spectroscopy (Figure 3.8), the absorption of the film can be measured. In brief, two glass slides which will act as the reference was inserted in the sample holder. To produce light with wavelength range 190 nm to 350 nm and 340 nm to 2500 nm, a deuterium discharge tube and a tungsten iodine lamp were used. The light passed through a grating in the monochromater and split into two light path by sector mirror. First light path will pass through the first glass slide and the second light path will go through the second glass slide. The transmitted light was detected by photodiodes. The transmitted light from both sides were collected at the photomultiplier before transferred to the amplifier and decoded to electrical signal. Using software, the signal was then display into spectrum. Besides, overall operation also operated using this software. Basic working principle of the instrument was displayed in Figure 3.9. Since glass was inserted in both sample holders,

thereby no changes had been observed to the transmitted intensity. Thus, a baseline was formed which was used as the reference point for other film deposited on glass slide.

In this work, after the baseline was measured, one of the glass slides was replaced by NiTsPc film. Consequently, it was scanned in range 200 nm to 800 nm which known as the greatest region of the light absorption for organic material. From the absorption spectrum, the value of the optical energy gap can be calculated using Tauc's relationship (Muhammad *et al.*, 2011b):

$$\alpha hv = \alpha_o (hv - E_g)^n \quad (3.2)$$

α is the absorption coefficient and E_g is the energy gap. Value of n depend on the type of transition in which $n = 1/2$ for direct transition, $n = 2$ for indirect allowed transition and $n = 3/2$ for forbidden transition (M. El-Nahass *et al.*, 2003).

Besides, the wavelength of the absorption gives the information regarding the absorption of certain chemical structure. In addition, the electronic transition of the electron can also be elucidating from the absorption spectra. Figure 3.10 shows the possible transition of electron in a thin film. Each transition needs an amount of energy. Higher energy is needed to transit an electron from σ to σ* and n to σ*. Absorption at the shorter wavelength (< 200 nm) will have more energy compared to higher wavelength. Obviously, the absorption at lower wavelength is due to these electronic transitions. For organic material, most of the absorption occurs due to the transition between n to π* and π to π*. These transitions correspond to the absorption spectrum lies in wavelength within 200 – 700 nm which have lower energy.

Figure 3.8: Photograph of Jasco V-570 UV/VIS/NIR Spectroscopy

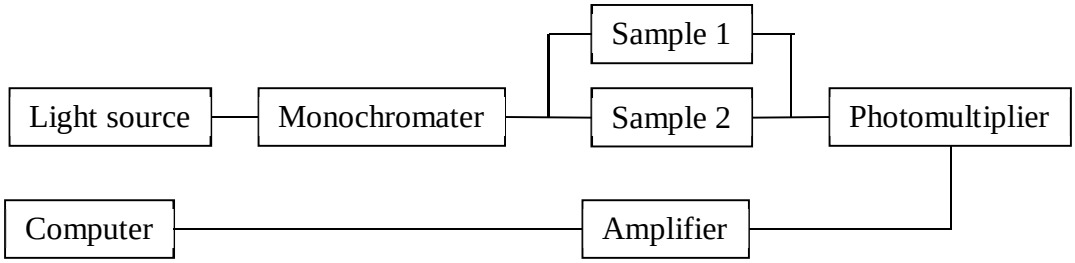

Figure 3.9: Schematic diagram of working principle of UV-Vis-NIR Spectroscopy

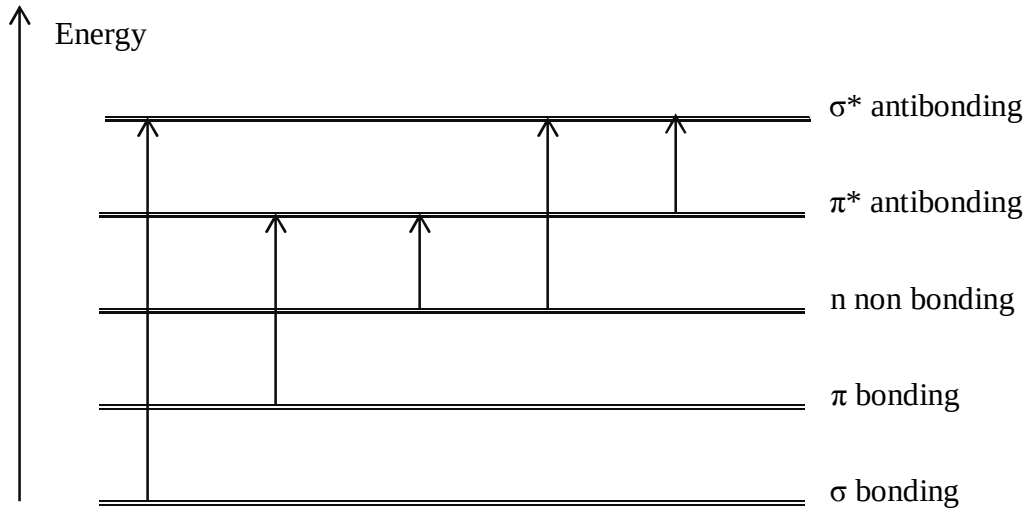

Figure 3.10: Possible electronic transition of electron

3.12 RAMAN SPECTROSCOPY

In order to determine the vibrational, rotational and other low frequency transitions in molecules, RenishawinVia Raman Microscope was used. Referring to Figure 3.11, if a single wavelength of light is shone on a material, most of the light is scattered without color change. This scattering process is called Rayleigh scattering. Nevertheless, there is a tiny fraction of light energy is converted to vibrational energy in material and scattered with different wavelength of light. Difference in energy between the incident light and scattered light is plotted in term of frequency which called the Raman Effect. Selection of laser is very important in Raman spectroscopy because each laser will have different penetration depth.

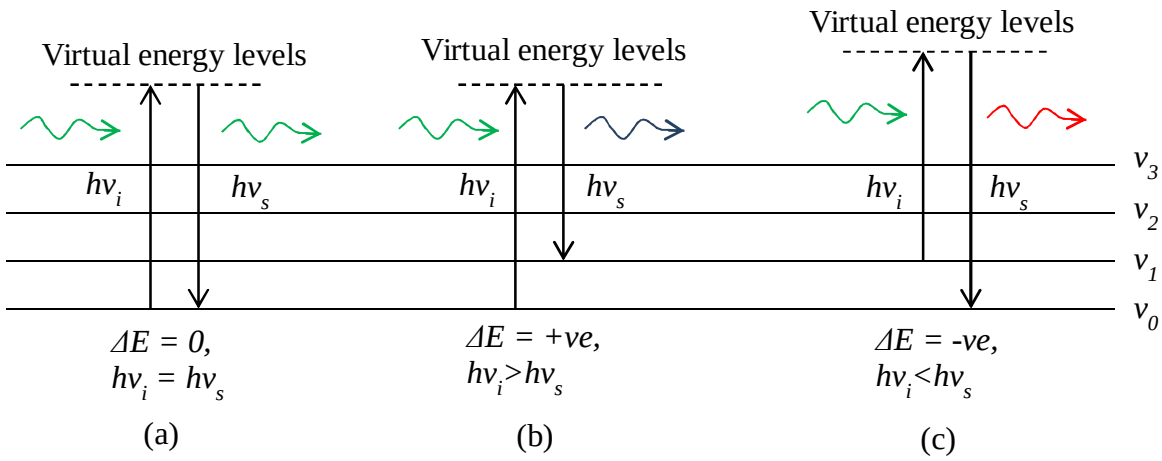

Figure 3.11: The electronic transition of (a) Rayleigh scattering, (b) and (c) Raman scattering

According to (Parr *et al.*, 2001), penetration depth is given by the following equation:

$$Penetration\ depth, d = \frac{2.3}{2\alpha} \quad (3.3)$$

α is the absorption coefficient. If ultraviolet laser (325 nm) laser is used, the absorption coefficient gained from the value of α at 325 nm in α against λ graph. Wrong selection of laser will cause some of the parts of the film could not be characterized. Parameter used in

characterizing the film using RenishawinVia Raman spectroscopy in this work is shown in Table 3.2.

Table 3.2: Set up parameter for Raman spectroscopy.

Scan range	200 – 2000 cm^{-1}
Laser power	10%
Exposure time	10 s
Laser	514 nm (green laser)

3.13 PHOTOLUMINESCENCE SPECTROSCOPY

PL is a process where an incident light is absorbed by an electron at the lower energy state and supplying them with energy to excite to higher energy level as shown in Figure 3.12.

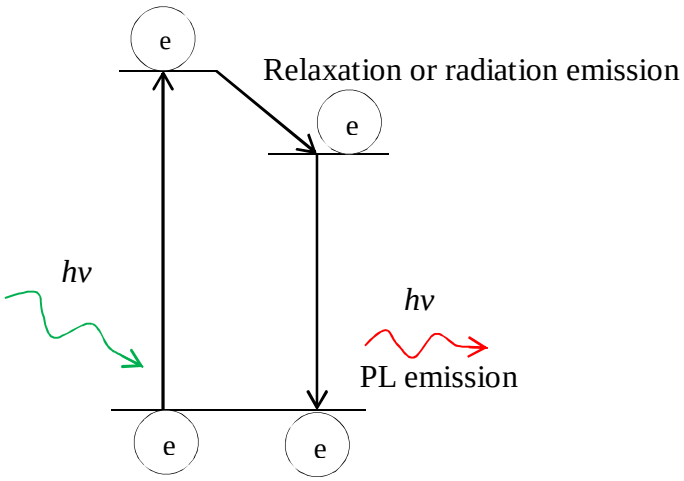

Figure 3.12: Electronic transitions in PL.

However, this process only can occur if the energy supplied to the electron is equal or larger than the energy gap. Prior to starting the PL measurement using RenishawinVia Raman Microscope, a laser source must be properly chosen, in order to produce enough energy for electron excitation. In this study, the laser wavelength was chosen based on the position of the highest absorption coefficient peak of the thin film. Parameter used in characterizing the film for PL measurement is shown in Table 3.3.

Table 3.3: Set up parameter for PL measurement.

Scan range	400 – 1000 nm
Laser power	0.5%
Exposure time	10 s
Laser	325 nm (UV laser)

3.14 ELECTRICAL MEASUREMENT

Fabricated devices from previous section with arrangement ITO/NiTsPc/n-type material/Al were measured using Keithly 236 Source Measurement Unit (SMU) in a controlled environment. A black box was used to place the sample holder, the electrical probe and the light source; hence the background light was eliminated. Characterization under light illumination was done under an Oriel solar stimulator – model 67005 with Air Mass 1.5 filter by standard conditions with a white light irradiation at 100mW/cm^2 to stimulate the irradiation of light from the sun. Overall measurement was controlled by a personal computer, equipped with a LabVIEW system design software.

ITO and Al electrodes were respectively connected to anode and cathode at the SMU before starting the measurement. The voltage was set to be at range -1.0 to 1.5V in order to detect the photovoltaic effect which occurred at the 4th quadrant of the current-voltage curve. The response time was set to 1 µs so that it matched to the typical mobility of electron in organic material. The software gives the value of current and voltage of the device. The value of current was converted to current density by dividing the measured current to effective area of the photovoltaic device. Figure 3.13 shows the effective area of the fabricated photovoltaic device, which is defined as the overlapping area of three parts i.e ITO, organic layer and aluminium. Graph of current density against voltage (*J-V)* was then plotted and analyzed. Information about the short-circuit current density and open-circuit voltage can be gathered from this graph. Equation 3.4 is used to calculate the fill factor of the device from the *J-V* graph

$$Fill\ Factor, FF = \frac{J_{max}V_{max}}{J_{sc}V_{oc}} = \frac{P_{max}}{J_{sc}V_{oc}} \quad (3.4)$$

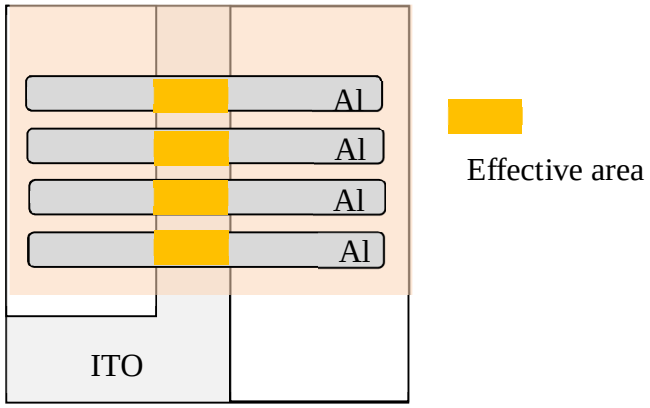

Figure 3.13: The top view of photovoltaic device where effective area is shown.

CHAPTER 4

RESULTS AND DISCUSSIONS

4.1 CHAPTER OVERVIEW

This chapter presents the results of the measurements made throughout the research duration. This chapter is divided into two parts. The first part of the work discusses the selection of parameters in obtaining good physical properties of NiTsPc film. The optimum parameters are obtained from the analysis of the absorption properties, morphology properties of the NiTsPc thin films. Selection of the best concentration of NiTsPc solution to form good thin film is described in the early part of this chapter. Furthermore, the choice of suitable solvent in order to modify the surface morphology of NiTsPc film is also discussed. Then, the optimum annealing temperature of the spin-coated NiTsPc film as well as the selection of the acceptor material to be used in the fabrication of the photovoltaic device, are also described in the first part of this chapter. At the end of the first part, the electrical measurement is described based on the fabricated device consists of NiTsPc film.

In the second part of this chapter, the effect of solvent treatment on the NiTsPc films on their surface morphology is discussed. The variation in surface morphology and optical properties of the NiTsPc films with different immersion times is described in great length. Then, this later part illustrates the electrical properties obtained from the fabricated photovoltaic devices consist of the solvent treated NiTsPc films. Correlation between surface modification and the performance of photovoltaic devices is explained in the second part of this chapter. The characteristics of the untreated and treated films were investigate and analyzed by X-ray diffraction (XRD), Atomic Force Microscopy (AFM), Field Effect Scanning Electron Microscopy (FESEM), Ultraviolet-Visible-Near Infrared (UV-Vis-NIR) Spectroscopy, Raman Spectroscopy and Photoluminescence Spectroscopy

(PL). The electrical properties of the photovoltaic device were measured using Keithley 236 Source Measurement Unit (SMU) in a black box to avoid influence of other light sources on the device.

4.2 PART I: SELECTION OF PARAMETERS

4.2.1 Concentration of NiTsPc solution

There has been reported that the suitable thickness of the donor/acceptor layer to fabricate the organic solar photovoltaic devices is below 200 nm (Moulé *et al.*, 2006). In this work, the donor layer of the spin-coated NiTsPc has the thickness of around 150 nm. Usually, the film thickness can be controlled by adjusting the spin rate of the spin coater. Higher spin rate produces a thinner thin film. A suitable film thickness is very crucial in this study because the deposited film will be used in solvent treatment process. If a film with 100nm, then some upper parts of the film will be etched during the solvent treatment process. Therefore a film with thickness around 150 nm is required in this work, so that the thickness of the donor layer will be in the range of 80-100 nm upon the solvent treatment. Hence the total thickness of donor plus acceptor layers will be around the optimum thickness of 200 nm for organic solar cell.

In some cases, the organic solution cannot stick on the glass substrate during spin-coating process. Therefore, the correct parameters must be used to obtain a good film with a uniform layer. In this research work, a good uniform NiTsPc film can be obtained from the NiTsPc solution by spin coating at a spin rate of in the range 800 rotations per minutes (rpm) to 1000 rpm. As the spin rate of the spin coater cannot be fully utilized to produce different thickness, hence the concentration of the NiTsPc solution can also be manipulated. The NiTsPc solution with a higher concentration of solution produced a thicker film compared to NiTsPc solution with lower concentration using same spin rate of spin coater. Therefore, in this work, the NiTsPc concentrations were varied to fulfill the condition of the film thickness production around 150 nm within the selected spin rate

range of 800 to 1000 rpm. The variation of solution concentrations of 15, 20, 25 and 35 mg/ml on the film thickness is tabulated in Table 4.1. The influence of solution concentration on the film deposition on glass substrates, is also presented in the form of photographs in this Table 4.1.

Table 4.1: Variation of thickness and the corresponding photographs of NiTsPc films, produced from different solution concentrations.

Solution Concentration (mg/ml)	Film thickness (nm)	Photographs of NiTsPc films
15	~35	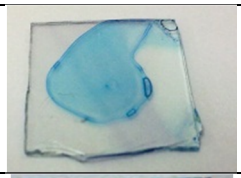
20	~60	
25	~77	
35	~120	

In the case of the concentration of 15 mg/ml, the produced film was very rough and not uniform on the glass substrate as can be viewed in the photograph. As the solution concentration increases up to 25 mg/ml, the NiTsPc film of 75 nm can be obtained with almost uniform layer. However, the uniform film with desired thickness of above 100 nm can only be obtained from the solution concentration of 35 mg/ml. Beware of the material consumption is also one of the factors to be taken into account in selecting the optimum concentration for the film formation. Besides, the influence of solution concentration on the light absorption of NiTsPc films is presented in Figure 4.1**.** For concentration of 15 mg/ml, the absorption coefficient of the film is the highest nevertheless the film is too thin.

Hence, the optimum thickness of 120 nm is selected for the concentration of 35 mg/ml to form a uniform NiTsPc film on glass substrate.

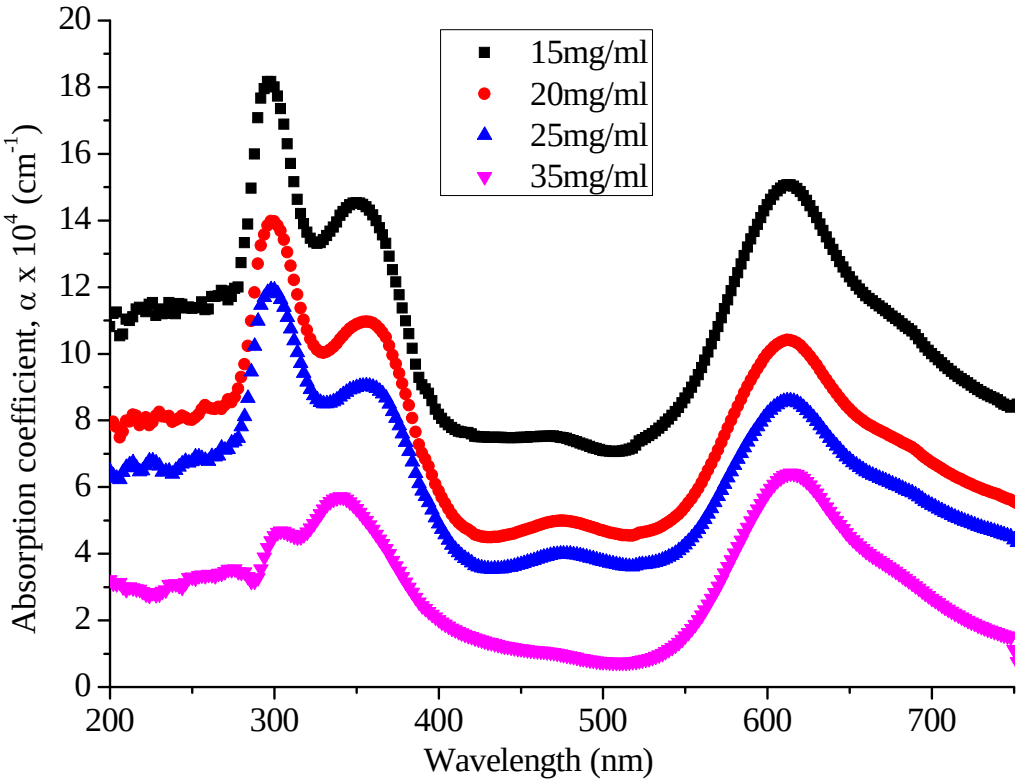

Figure 4.1: The effect of NiTsPc solution concentration on the absorption spectra of the respective film.

4.2.2 Optimum Temperature in Thermal Treatment Process

Light absorption of a thin film is one of the main factors for a good photovoltaic device. Therefore, a thermal treatment was applied to the NiTsPc film so that the morphology of the film can be modified, leading to the improvement in the absorption properties. Similar research work was utilized by some researchers to enhance the absorption capability of the thin films (Karan *et al.*, 2007; Schuster *et al.*, 2010). Furthermore, annealing process was also done to remove the residual water content from the NiTsPc films.

Figure 4.2(a) shows the variation of absorption spectra with the temperature of thermal treatment on the TsNiPc films. The light absorption coefficient is increased as the

annealing temperature increases, however it drops beyond 140˚C. The magnifications of the absorption spectra graphs in the UV region (275 and 375 nm) and visible region (575 and 675 nm) are presented in Figure 4.2(b) and 4.2(c), respectively. Referring to these figures, the absorption coefficient can be increased up to 50% compared to the pristine film, upon thermal annealing at 140˚C. Hence 140˚C is selected as the optimum annealing temperature by producing the highest ability of TsNiPc film to absorb light in the UV as well as in visible regions. The details of the absorption peaks will be explained in section 4.3.3.

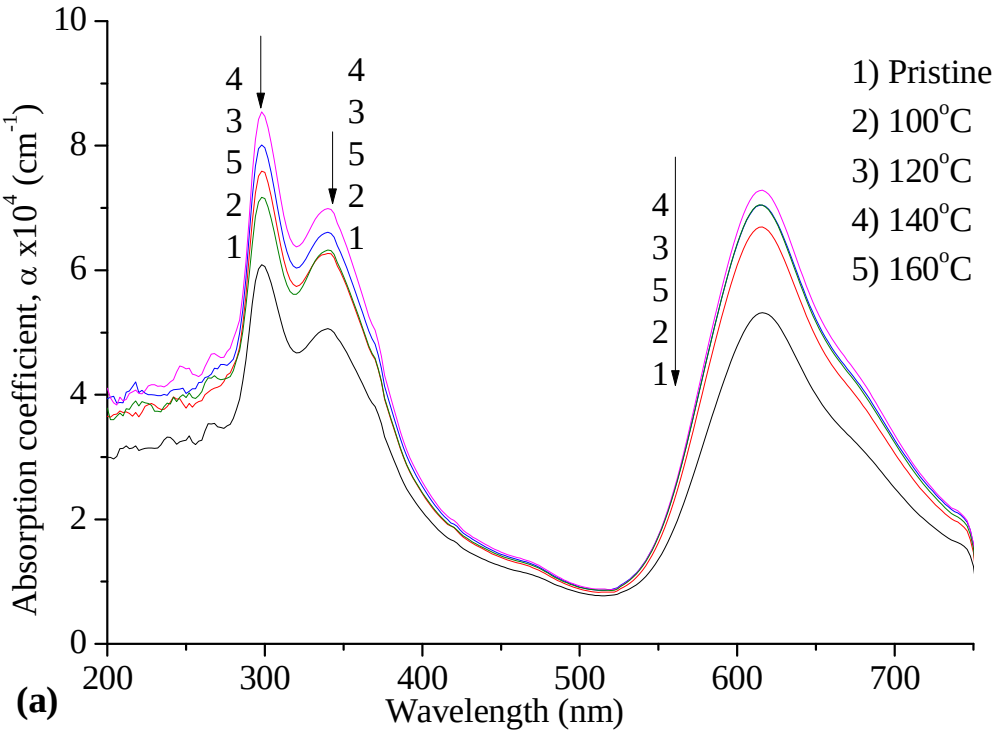

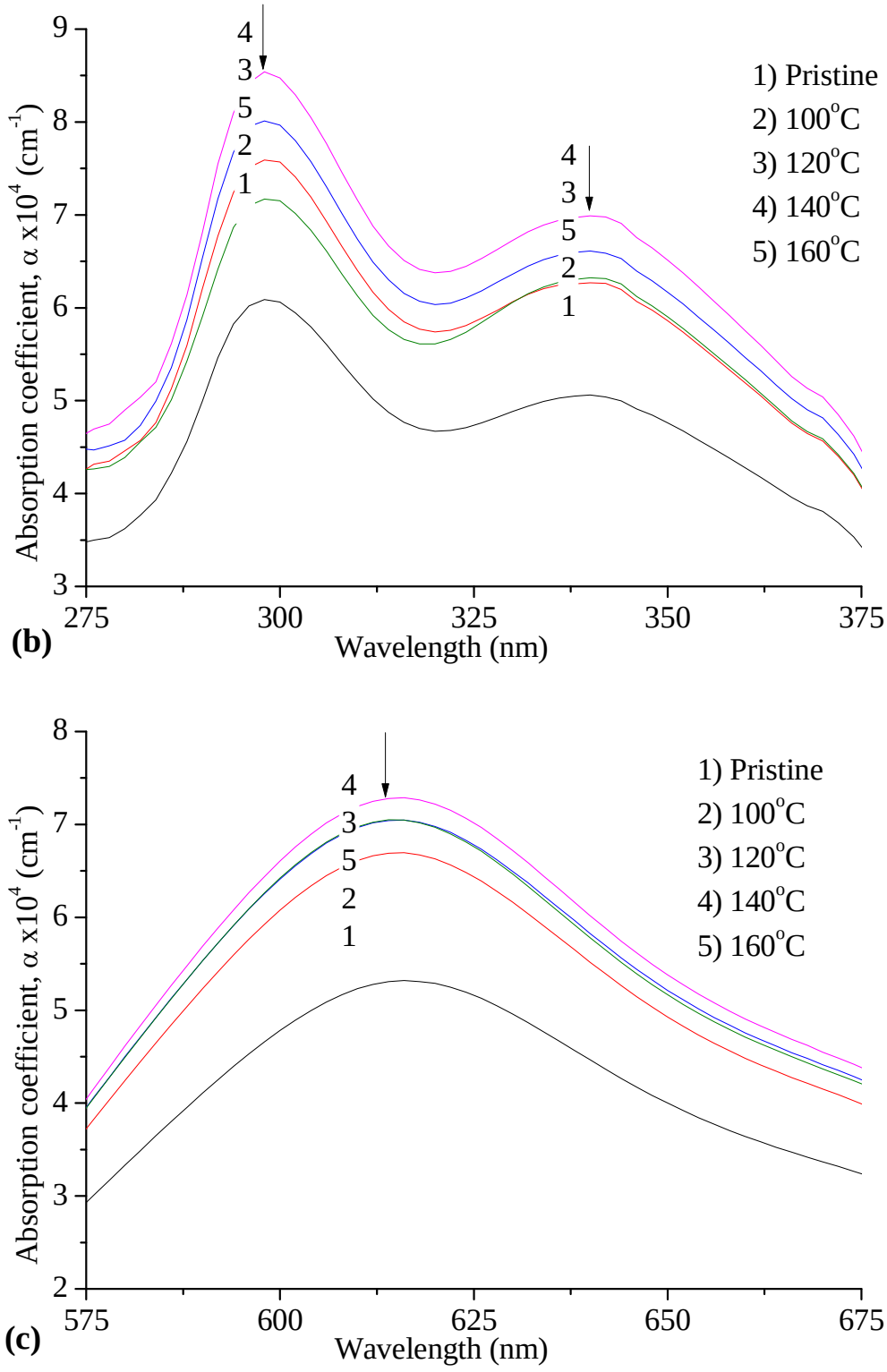

Figure 4.2: (a) The absorption spectra of NiTsPc,(b) Magnification of the absorption spectra at the B band (UV region) and (c) Magnification of the absorption spectra at the Q band (visible region).

4.2.3 Selection of suitable solvent for the film surface treatment

All of the solvents available in the laboratory of the Low Dimensional Materials Research Center (LDMRC) were tested to find the suitable solvent for the NiTsPc film surface treatment. In this case, a suitable solvent is the solvent that has low solubility to NiTsPc. The solution of NiTsPc powder in the respective solvents can be distinguished by naked eyes. From all the tested solvent, only chloroform and toluene have shown the lowest solubility to NiTsPc. In order to find more suitable solvents for NiTsPc, a preliminary experiment on surface modification was done to the NiTsPc film using both solvents with the same immersion time. During the immersion process, the solvent molecules were absorbed into the thin film layer, and then evaporated during the drying process. It is expected that the modification of the film surface was not occur during the immersion process. The film has started to aggregate and align during the evaporation of solvent or the drying process (Yang *et al.*, 2011). If a vapor pressure of a solvent is low, then a longer time is needed for the solvent to evaporate from the film surface. The vapor pressure of toluene and chloroform is 22mmHg and 159mmHg, respectively. Thus, the evaporation rate of toluene is much slower as compared to that of chloroform. Therefore, the film treated with toluene need more time to dry which in turn provides a longer time for the film to aggregate. Based on the results obtained at this stage, the film treated with toluene is expected to form a better surface morphology compared to the chloroform treated film.

The observation of the surface morphology of the treated NiTsPc films was determined by Atomic Force Microscopy images as shown in Figure 4.3. It is found that the roughness mean square (rms) of the untreated pristine, chloroform treated and toluene treated films is approximately 41 nm, 16 nm and 8 nm, respectively. As can be clearly seen from Figure 4.3, without solvent treatment, the NiTsPc film surface has bigger granular structure size corresponds to higher surface roughness. As the film treated with solvent, some part of the bigger structure has been etched by the suitable solvent. Then

such immersion process has produced the smaller granular structure size before the drying process. During the drying process, the smaller structures were aggregated and aligned. In Figure 4.3(b) and 4.3(c), the structures at the film treated with toluene formed are packed and formed only on the surface of the film but rather less packed for the chloroform treated film as observed with larger dark spots in the AFM images.

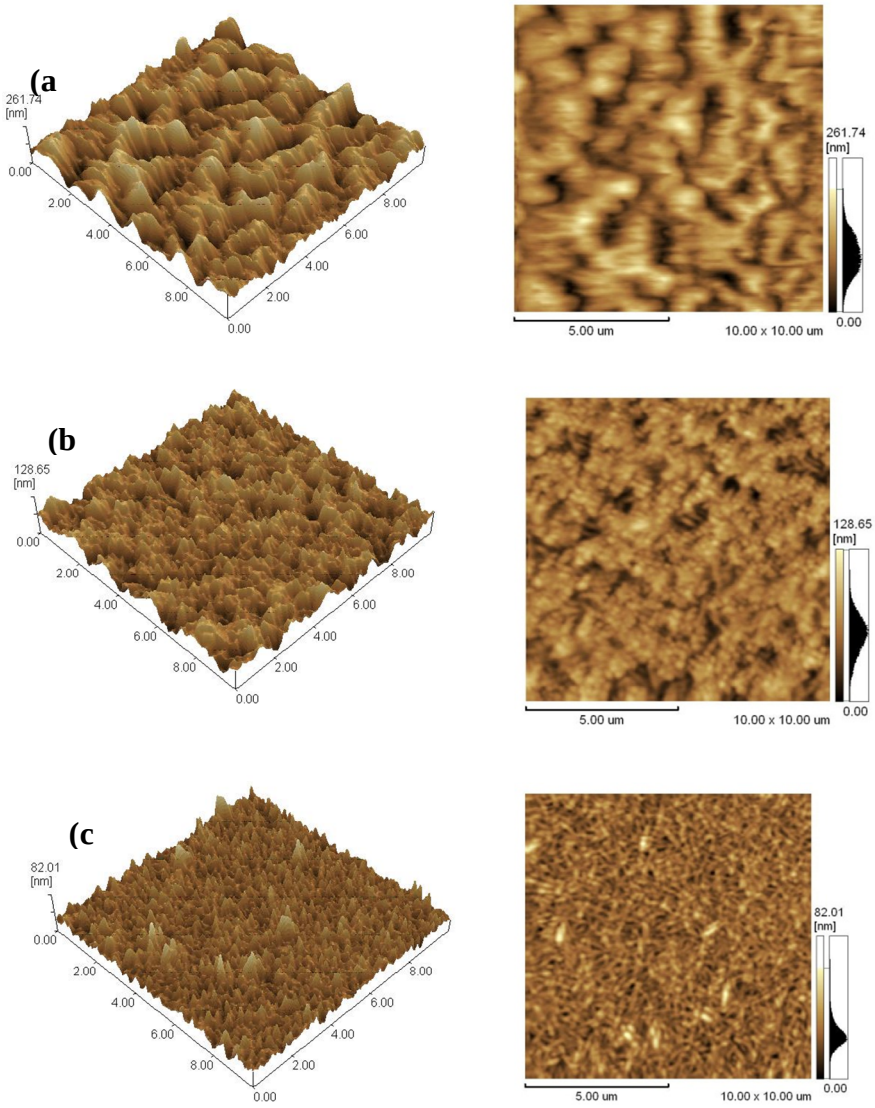

Figure 4.3: AFM images of NiTsPc films in 3-D (on the left) and in 2-D (on the right) for (a) the untreated, (b) treated with chloroform, and (c) treated with toluene.

Comparing the size of the molecule for both solvent, the molecular size of toluene is bigger compared to chloroform due to the presence of the aromatic ring in toluene moiety as shown in Figure 4.4.

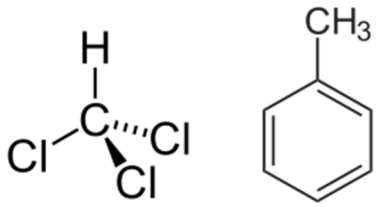

Figure 4.4: The chemical structure of chloroform (left) and toluene (right).

Therefore, as the NiTsPc film immersed in each solvent, the chloroform molecule was easier to be absorbed by the film and can penetrate into the underlying part of NiTsPc film and etched the surface as well as the underlying portion area of the film. The modification for film treated with chloroform involved the underlying part of the film surface. As a result, the film treated with chloroform has larger surface area caused by formation of granular structure. Thus, it is anticipated that chloroform can be the most suitable solvent for solvent treatment of NiTsPc layer as the donor layer of the photovoltaic device. Such granular underlying structures would provide a percolation path for the free charge carrier to be transported to its respective electrodes.

Nevertheless, it is very hard to distinguish which solvent is better in modifying the film surface based on the analysis of AFM images alone. Therefore, further characterization was performed by measuring the electrical properties of the organic solar cell devices. In this work, the NiTsPc was used as a p-type material, to be coupled with an n-type material to form bilayer organic solar cell.

There are two types of small molecule organic semiconductors were used as an electron donor (n-type) to be deposited on top of the NiTsPc film. Perylene-3, 4, 9, 10-tetracarboxylic-3, 4, 9, 10-dianhydride (PTCDA) was chosen due to its good electron mobility (2 x 10^{-4} cm^2/Vs) (Forrest *et al.*, 1994). The other n-type material was tris (8-

hydroxyquinolinate) aluminium (Alq3) due to its high thermal stability, adequate electron transport, and luminescent properties (L. Li *et al.*, 2008; Shukla *et al.*, 2010). The final device constructions consist of ITO/treated-NiTsPc/PTCDA/Al and ITO/treated NiTsPc/Alq3/Al. The electrical properties in terms of the graph of current density, *J* against voltage, *V* was plotted. The short-circuit current density; J_{sc} is the current passes through the solar cells when the voltage is zero. This current was depends on the absorption properties of the films and their charge carrier transport (Muhammad & Sulaiman, 2011a).

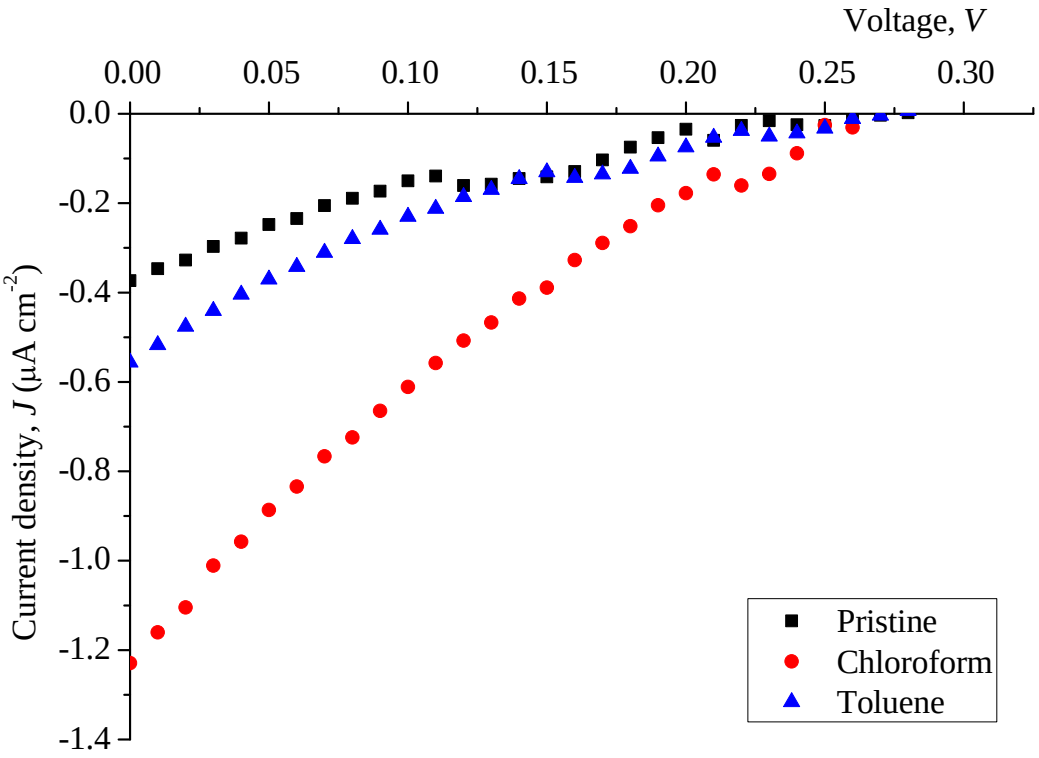

Figure 4.5: Influence of NiTsPc film being treated with different solvent on the current density – voltage (*J-V*) characteristics of the ITO/treated NiTsPc/PTCDA/Al devices. The devices were tested in air under light illumination 100 mW/cm^2.

Figure 4.5 shows the electrical photovoltaic performance of the solar cells using either toluene or chloroform treated NiTsPc films, incorporated with PTCDA as the second active layer. The *J-V* characteristic of the pristine layer in the ITO/untreated NiTsPc/PTCDA/Al device is also shown as a reference device. The values of the J_{sc} for devices consist of the toluene and chloroform treated active layer are increased half and

two times compared to the untreated NiTsPc film, respectively. Previously, it has been mentioned that the formation of the granular structures at the underlying part of the chloroform treated film may provide a percolation path for a better free charge carrier transport to its respective electrodes. In fact, a better charge transport to electrodes generates the higher value of J_{sc} has been generated from the chloroform treated NiTsPc film. The dependency of J_{sc} on the photo induced charge carriers transport between the donor and acceptor layer, suggests that in this current work, the charge transfer process at the NiTsPc/PTCDA interface has been enhanced.

However, the value of the open-circuit voltage, V_{oc} has not been changed upon replacing the pristine with the solvent treated NiTsPc. V_{oc} is the voltage produced when no current being generated in the device. V_{oc} value can be defined either as the difference in the electrodes work function or the difference between the Highest Occupied Molecular Orbital (HOMO) of the donor and the Lowest Unoccupied Molecular Orbital (LUMO) of the acceptor (Muhammad *et al.*, 2011a). In addition in Figure 4.5, it is observed that there is a very small change in the open-circuit voltage (V_{oc}), i.e. around 0.25 to 0.28 V upon immersion NiTsPc films in either toluene or chloroform. Such unchanged voltage value can be explained as no alteration of the HOMO-LUMO level of the active layer upon solvent treatment. Nevertheless, it will be shown that the solvent treatment process with different immersion time has produced a significant change in open circuit voltage as well as photocurrent, later.

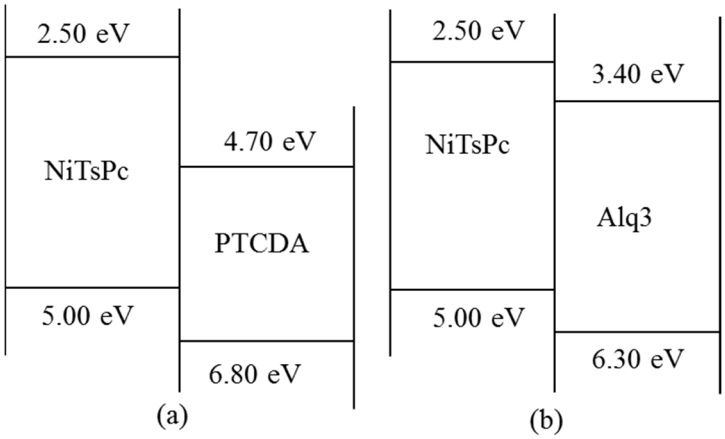

Figure 4.6: The energy level diagrams; (a) NiTsPc film incorporated with PTCDA (Brovelli *et al.*, 2007) and (b) NiTsPc film incorporated with Alq3 (Muhammad *et al.*, 2010).

A larger value of V_{oc} can be generated by increasing the difference in HOMO-LUMO level of the donor and acceptor. In this work, Alq3 was used to replace the PTCDA as an acceptor. Figure 4.6 shows the schematic diagram of the energy levels between the donor and acceptor layer. It can clearly observed in these energy levels that the gap between HOMO-LUMO level of NiTsPc and Alq3 is bigger compared to the difference in HOMO-LUMO level of NiTsPc and PTCDA. Hence, it can be inferred that larger gap between HOMO-LUMO levels of NiTsPc/Alq3 has generated larger open circuit voltage as shown in Figure 4.7.

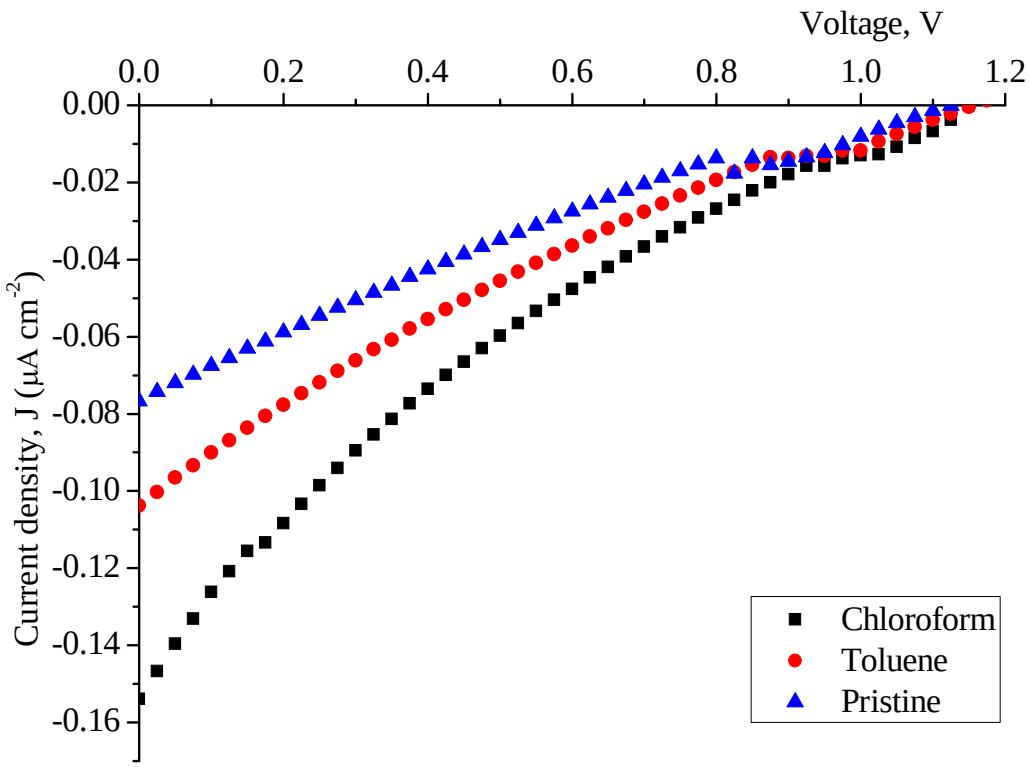

Figure 4.7: The current density – voltage (*J-V*) characteristics of ITO/NiTsPc/Alq3/Al and ITO/treated NiTsPc/Alq3/Al devices. The devices were tested in air under light illumination 100 mW/cm^2.

Chloroform treated devices for both PTCDA-based (see Figure 4.6) and Alq3-based (see Figure 4.7), generate larger values of J_{sc} as compared to that of the toluene treated devices. This finding reveals that more photocurrent can be produced by applying the chloroform solvent treatment. This behavior can be described as the improved charge transport ability due to the enhancement in surface morphology of the chloroform treated NiTsPc layer. In addition, chloroform treated device for both Alq3 and PTCDA has a higher J_{sc} compared to the toluene treated device. Therefore, it can be safely said that chloroform is a good and suitable solvent for surface treatment in order to improve the morphological characteristic, leading to an enhancement in the photocurrent generation.

4.3 PART II: EFFECTS OF SOLVENT TREATMENT TIME TO MORPHOLOGICAL, STRUCTURAL, OPTICAL AND ELECTRICAL PROPERTIES

4.3.1 Morphological properties

The influence of thermal treatment process on the surface morphology of the chloroform treated NiTsPc films is depicted by the FESEM images in Figure 4.8. In this case the images were obtained from the pristine and thermally treated films, but without underwent the solvent treatment process. Figure 4.8(a) and 4.8(b) show the images of the pristine NiTsPc film with 10k and 30k magnification. As can be clearly seen from these figures, nanostructure feature cannot be observed in the film before the thermal treatment process although the image has been enlarged with a higher magnification (see Figure 4.8(b)). On the other hand, a striking different in FESEM image can be clearly seen in Figure 4.8(c) for the film being applied of a thermal treatment at 140°C. There are many nano-structures with a diameter below 200 nm appear in the image. Karan et al and B.-E. Schuster *et al.* reported almost the same FESEM images due to the thermal treatment process in NiTsPc films (Karan *et al.*, 2007; Schuster *et al.*, 2010).

Nano-structures with random orientation as the ramiform structures are called nanofibers since it shape more like a fiber. It is believed that the thermal treatment can initiate the formation of nanofibers as observed in the images of Figure 4.8. Therefore, the surface of the NiTsPc film can be modified via a thermal treatment process. Then, the formation of nanofibers can be further enhanced via a solvent treatment process, as will be discussed later. Furthermore, FESEM images in Figure 4.8 shows the presence of white dots on the surface of the NiTsPc films. These white dots represent the insoluble NiTsPc powder. As discussed earlier, the NiTsPc powder was dissolved in deionized water, then spin-coated onto glass substrates to form thin films. The size of the insoluble NiTsPc particles is around 200 nm. Nevertheless, these insoluble particles disappear as a response to the solvent treatment process, as will be described in next paragraph.

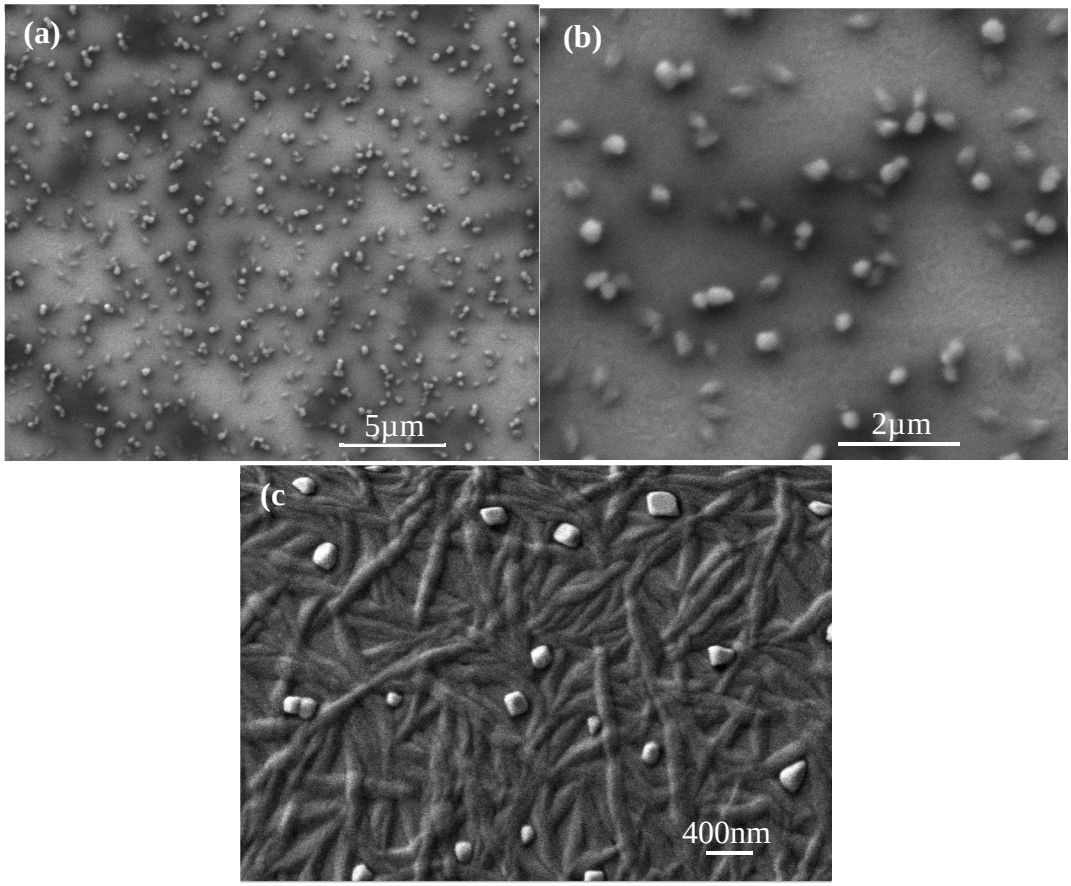

Figure 4.8: The FESEM images of the NiTsPc thin film (a) before thermal annealing with 10k magnification (b) before thermal annealing with 30k magnification (c) after thermal annealing with 20k magnification.

In the second process of solvent treatment, the thermally annealed NiTsPc films were immersed in chloroform with different soaking times. The films were then left under ambient condition to allow evaporation of the solvent until the films were completely dried. As discussed earlier in the first part of the chapter, the film starts to aggregate and align during evaporation process. For a longer immersion time in the solvent treatment process, the chloroform molecules were allowed to absorb deeper into the NiTsPc thin film layer. Therefore, the time needed to dry the thin film become longer. Variation surface morphology of the NiTsPc films upon different immersion time can be observed in the FESEM images as shown in Figure 4.9. The size of the nanofibers was calculated by measuring the diameter of nanofibers at five different parts and the average values were recorded. The influence of immersion time at 0, 40, 80 and 120 minutes on the nanofiber diameter size is presented in the bar graphs on the right hand side correspond to the time,

respectively. The number of nanofibers with diameter in the range of 81-120 nm is greater than the nanofiber with diameter of 41-80 nm can be seen in the untreated film as compared to the film being immersed in a suitable solvent for 40 minutes. However, as the treatment time increases beyond 40 minutes, the number of nanofibers with smaller diameter has increased. Therefore, longer time of immersion allows the chloroform molecule to etch the exposed surface of the films. This condition suggests that the chloroform molecule has partly modified the larger size nanofiber, hence the smaller nanofibers are produced. Comparison between the untreated film and the 40 minutes treatment time, it can be observed that the number of nanofiber with diameter 41-80 nm has increased by 1.5 times. As the immersion time increased to 80 minutes, then the number of nanofiber with a smaller diameter decreased (see the bar graph in Figures 4.9(c)), corresponds to the effect of solvent molecules in the film modification. From this experiment, it is found that if the film being treated beyond a certain time, then number of smaller nanofibers drops. Herein, the immersion times of 40 and 60 minutes can be considered to produce a better number of smaller size nano-fibers in NiTsPc films.

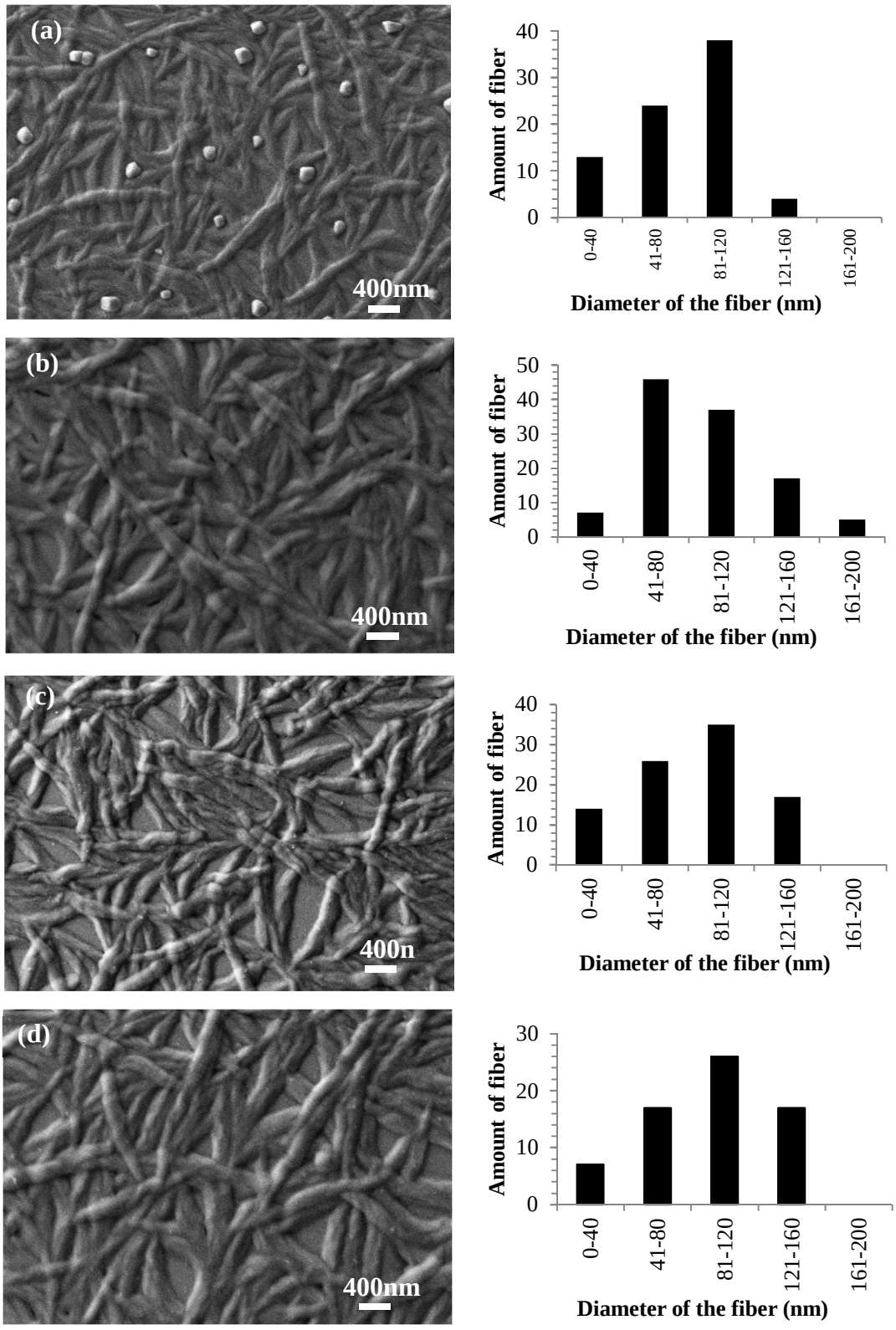

Figure 4.9: FESEM images comparing the morphology of NiTsPc films upon different treatment times. (a) untreated, (b) 40 minutes, (c) 80 minutes and (d) 120 minutes.

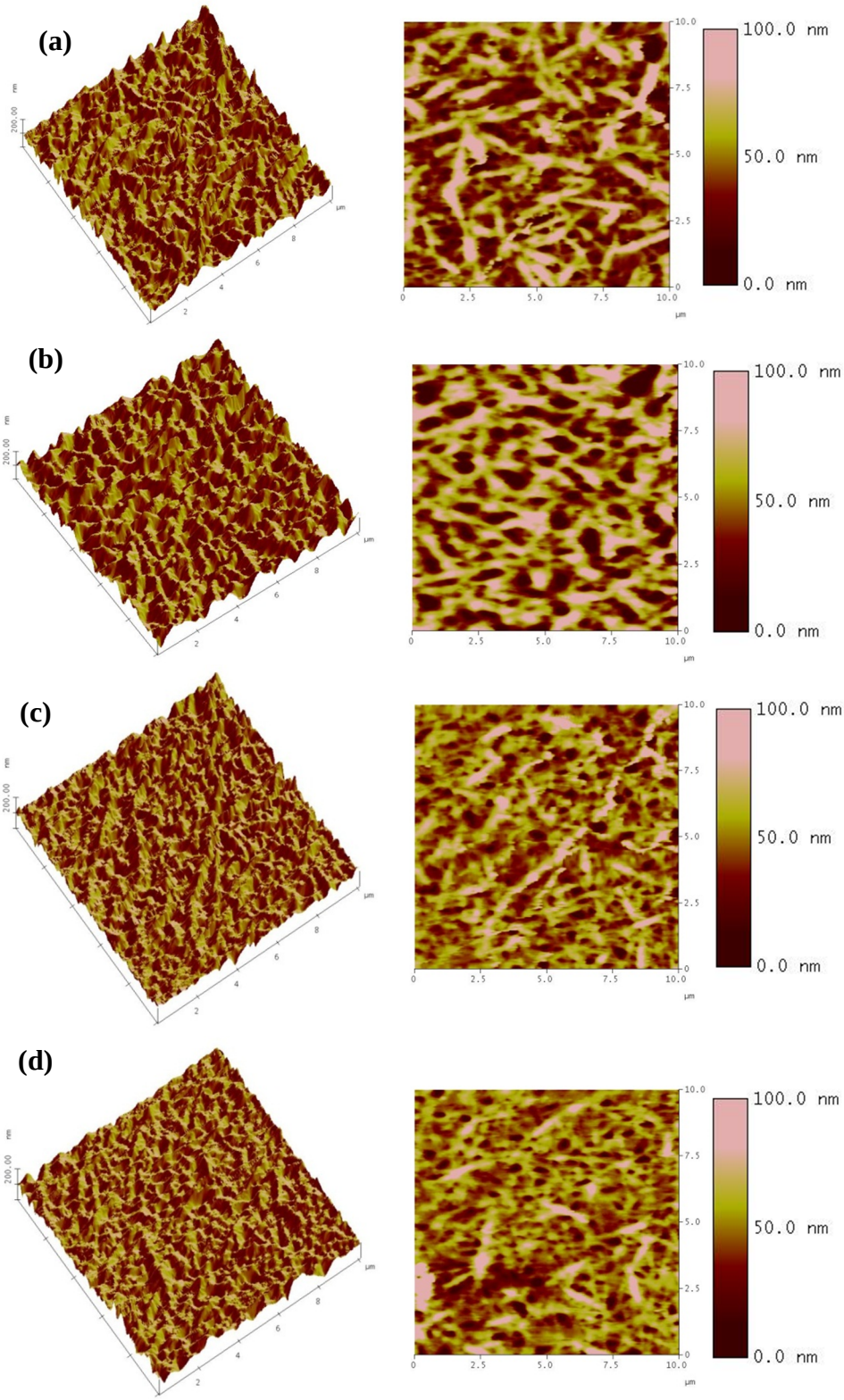

Figure 4.10: AFM images comparing the morphology of NiTsPc films upon different treatment times. (a) untreated, (b) 40 minutes, (c) 80 minutes and (d) 120 minutes.

Further analysis of the influence different annealing time on the surface of NiTsPc films was carried out by AFM images, as shown in Figure 4.10. The untreated film image shows that inter-planar distance between the nanofibers is far from each other. After solvent treatment, the nanofiber structure has been interconnected and separated by a closer distance. As previously discussed, the nano-fibers were formed during the solvent evaporation process upon film aggregation as reported by J.L. Yang *et al* (Yang *et al.*, 2011). For the film being treated at 40 minutes, the interval region between the grains became smaller as more nanofibers are formed in the film, as shown in Figure 4.10(b). However, referring to Figure 4.10(c), some part of the exposed surface of the film has been etched for the film being solvent treated at 80 minutes. Therefore, increasing the immersion times beyond 80 minutes allows the solvent molecules to be absorbed and penetrates deeper into the NiTsPc film, causing upper layer of the film being etched away. Such film is certainly not appropriate for further solar cell fabrication, as it would lead to a short-circuit device.

Table 4.2: The rms roughness value of solvent treated thin films, obtained from the AFM images.

Treatment time, t (minutes)	Root mean square roughness, rms (nm)
0 (untreated)	~ 22
40	~ 28
80	~ 17
120	~ 14

Table 4.2 provides a list of the root mean square roughness (rms) of each NiTsPc film upon different treatment time. The film surface becomes rougher with 25% increment of rms from untreated to 40 minutes treated film with chloroform. This result indicates that the coarser nanofibers being formed by a larger amount of humps and valleys along the thin film surface, are influenced by the film treatment in suitable solvent. Same as described previously in the FESEM images, the nanofibers shown in the AFM images have been etched away after achieving the maximum immersion time. Therefore, the drop

values in rms (from AFM images) for 80 minutes and 120 minutes of solvent treatment, is related to the smaller number of nanofibers on the film surface (from FESEM images).

As a summary, the morphological properties of the NiTsPc thin film surface can be modified by a solvent treatment. Enhanced number of nanostructure has been obtained upon immersing the thin film in a suitable solvent (which in this case is chloroform). The results in Figure 4.9 and 4.10 suggest that the formation of the nanofibers on the surface of NiTsPc films, is controlled by the immersion time.

4.3.2 Structural properties

The structural characterization was made by X-ray diffraction traces from the deposited NiTsPc thin film on glass substrate in the range of 2θ between 5° to 80°. Figure 4.11 shows the X-ray diffraction traces of the films. The untreated NiTsPc film is amorphous, as indicated by a broad XRD feature without any peak. After being treated with chloroform between 40 to 120 minutes, the NiTsPc film shows a semicrystalline feature to certain extent with a protruding peak as can be observed at 2θ = 32°. The crystallite size of the NiTsPc can be obtained by convoluting this peak using an Origin Pro 8.0 software and inserting the value of its full width at half maximum (FWHM) into Equation 4.1:

$$L = \frac{K\lambda}{\beta \cos\theta} \qquad (4.1)$$

From this equation, L is the mean crystallite size, K is the Scherrer constant with value 0.94, λ= 1.542 Angstroms is the X-ray source wavelength and β is the FWHM value. The crystallite size of NiTsPc has been determined to be in the range of 70-100 nm. This finding reasonably agrees with the reported values of 20-100 nm for the other type of phthalocyanine by other researchers (Boudjema *et al.*, 1984; M. M. El-Nahass *et al.*, 2005).

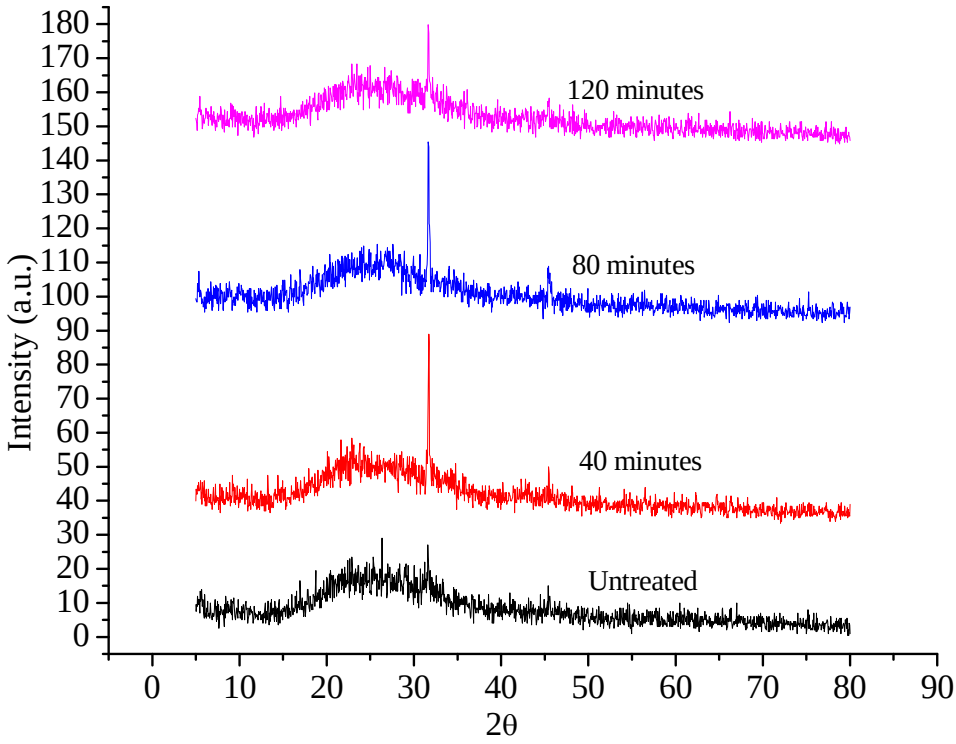

Figure 4.11: XRD diffraction pattern for the NiTsPc film with different treatment time.

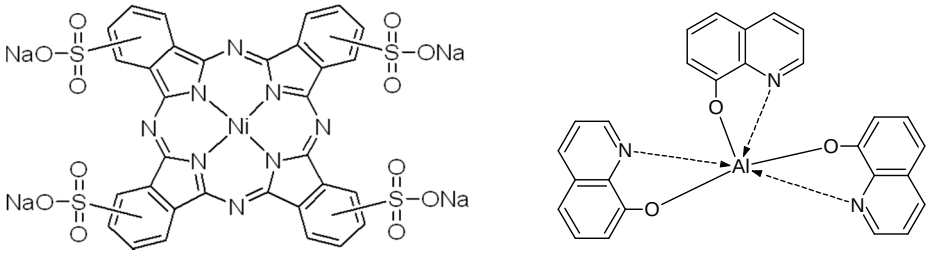

Figure 4.12: Chemical structure of NiTsPc (left) and Alq3 (right)

Furthermore, the structural characterization can also be done by analyzing the spectrum of NiTsPc thin film on glass substrate using the Renishawin Via Raman Microscope. NiTsPc structure is defined as a planar molecule consists of 57 atoms based on the chemical structure in Figure 4.12. Therefore, the characterization of the vibration of the molecule is based on the square planar molecule (point group D_{4h}). For this characterization, the vibration, Γ_{vib} of NiTsPc molecule is represented by Equation 4.2 (Bała *et al.*, 2006):

$$\Gamma_{vib} = 14A_{1g} + 13A_{2g} + 14B_{1g} + 14B_{2g} + 13E_g + 6A_{1u} + 8A_{2u} + 7B_{1u}$$
$$+7B_{2u} + 28E_u \qquad (4.2)$$

This equation consists of the translational and internal vibrations of the NiTsPc molecule. However, only the internal vibration, E_g is out of plane vibration while A_{1g}, B_{1g}, B_{2g} are in plane vibrations and taken into consideration here. Referring to Figure 4.12, the symmetrical atomic shifts in case B_{1g} vibrational mode is correspond to C'_2 axis folds, an axis of vibration through the central atom and benzene ring. On the other hand, B_{2g} vibrational mode is corresponding to the C''_2 axis folds, an axis of vibration through the nitrogen atoms (Bała *et al.*, 2006; Szybowicz *et al.*, 2004). The Raman shifts for each peaks in the untreated NiTsPc film (see Figure 4.13) are in good agreement to those reported results by other researchers for ruthenium phtalocyanine (X. Li *et al.*, 2004), copper phthalocyanine (Szybowicz *et al.*, 2004) and cobalt phthalocyanine (Szybowicz *et al.*, 2010) , even though the central atoms are different to the material used in this study.

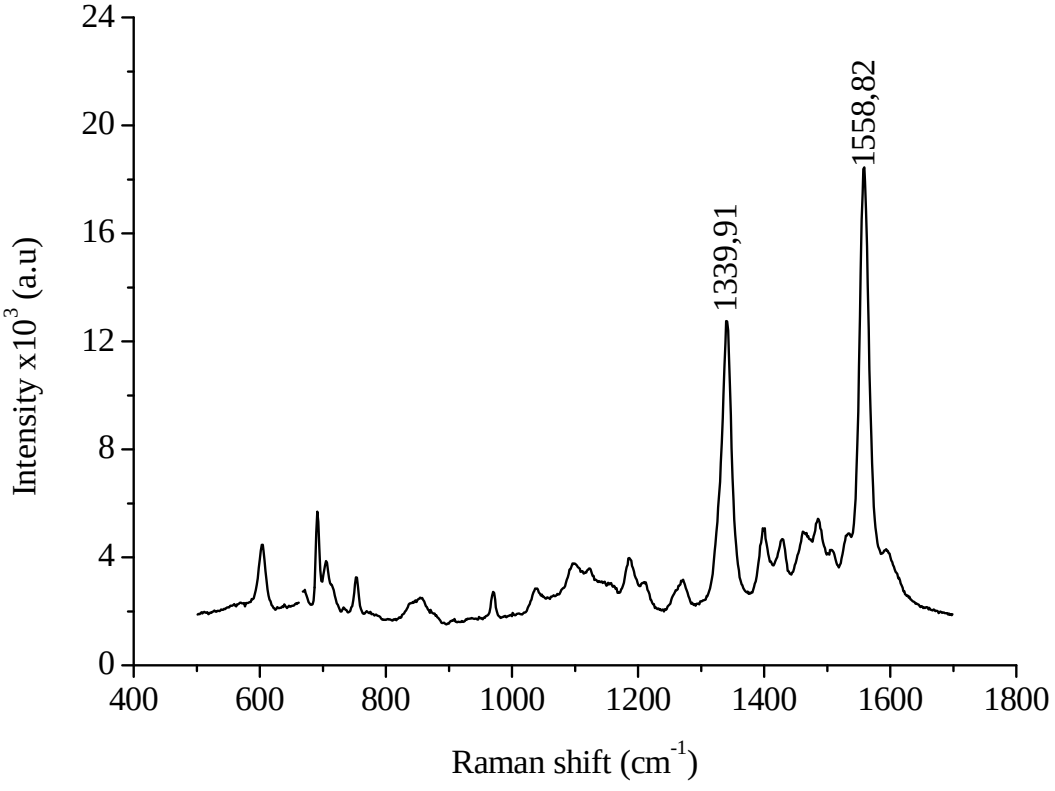

Figure 4.13: Raman spectra for the untreated NiTsPc film.

Interestingly, there are two protruding peaks occur at 1350 and 1580 cm^{-1}, correspond to the D and G peaks (Chu *et al.*, 2006). The appearance of the D peak in the spectra is an indication of the presence of six-fold aromatic ring in the film. On the other hand, the existence of G peak indicates the presence of both six-fold aromatic ring and chain (Ferrari *et al.*, 2000). Tentative band assignment of vibration (Saini *et al.*, 2011) for each Raman active mode is tabulated in Table 4.3.

Comparison of the Raman shift upon varying the treatment time on the NiTsPc films can be observed in Figure 4.14. Focusing only at the D and G peak, there is no shift in the peak positions in Raman spectra but the intensity of these two peaks is not similar. Therefore, the analysis of the structural properties can be done based on the variation in intensity. Figure 4.15 shows the magnification of the D and G peak of each film. The intensity has been altered by immersing the film in chloroform at different treatment time.

Table 4.3: Tentative band assignment of Raman active modes of NiTsPc film.

Band position (cm^{-1})	Band assignment	Raman active modes
604 - 690	C-N, Ni-N,C=N	A_{1g}
1035 - 1094	C-N, C=N, C=C-C	B_{2g}
1181 - 1339	C=C-C	A_{1g}
1550 - 1558	C-N, C-N=C-C=C	B_{1g}

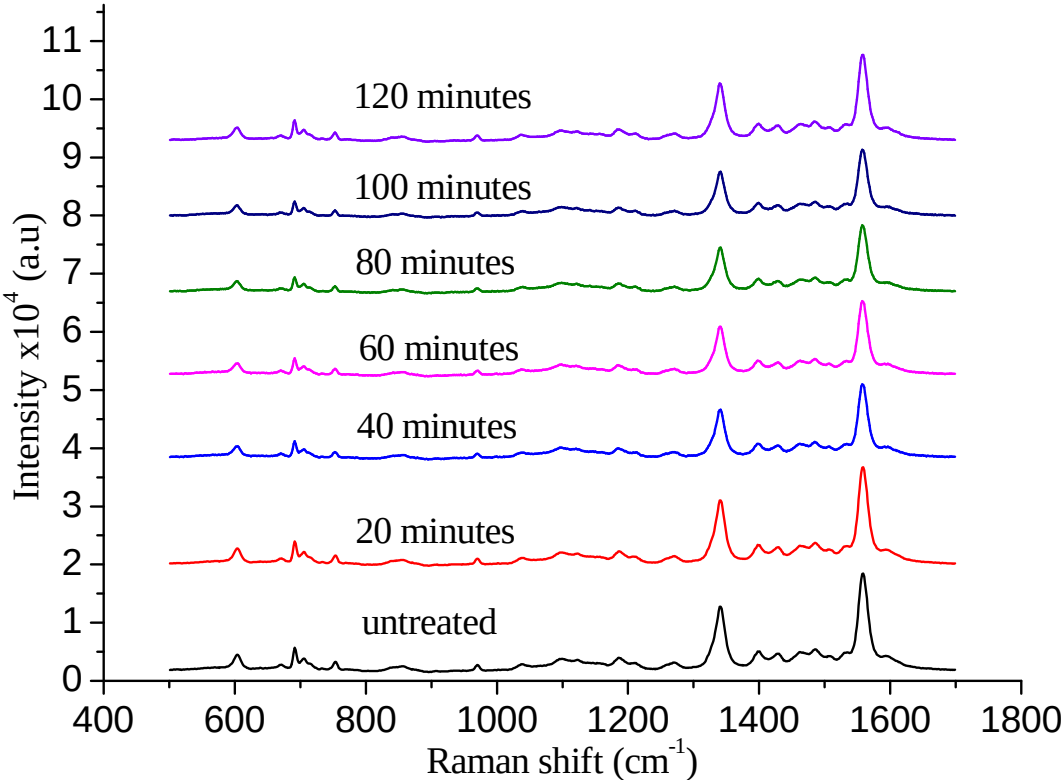

Figure 4.14: Stacks of Raman spectra for the untreated and treated NiTsPc films with different immersion time in a suitable solvent.

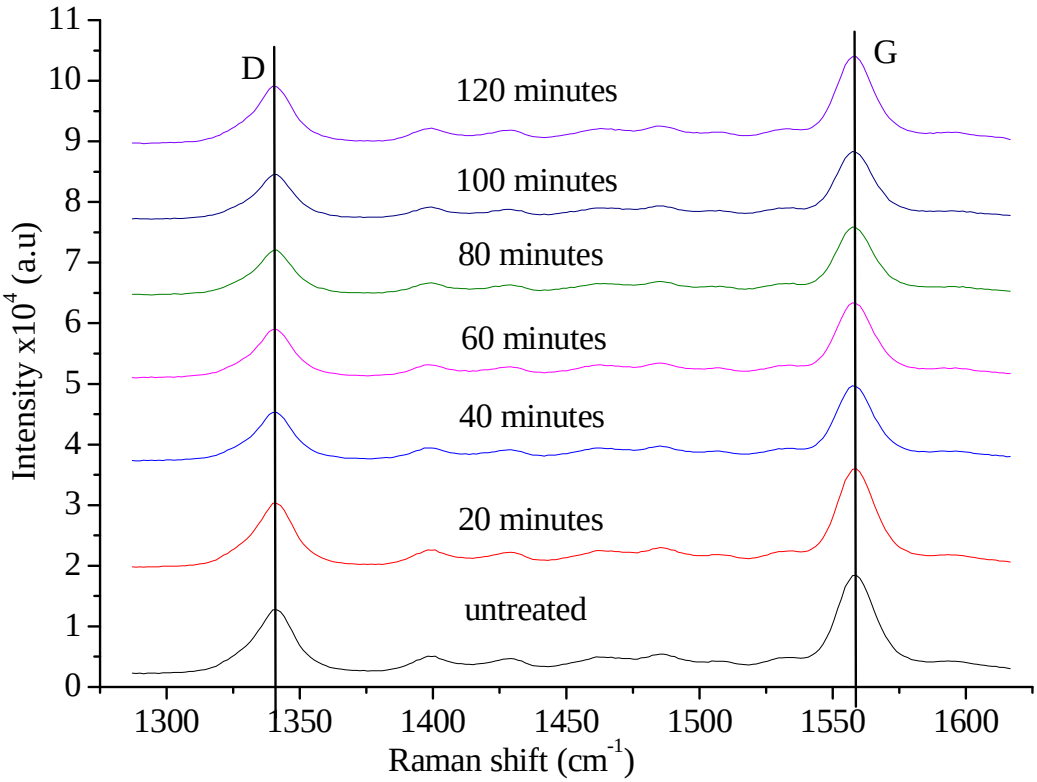

Figure 4.15: The D and G peak of Raman Spectra around 1350 and 1580 cm^{-1} (The plot is magnified from Figure 4.14)

In order to explain the behavior of both peaks upon varying the treatment time, the intensity ratio of both peaks is evaluated by convoluting them to fit the theoretical Lorentz curve. The relationship between the intensity ratio of D and G peaks with the presence of six-fold ring and chain can be presented in the following relation:

$$\frac{I_D}{I_G} \propto \frac{I_R}{I_C + I_R} \tag{4.3}$$

The ratio of I_D and I_G is inversely proportional to $I_C + I_R$. If the intensity ratio for D and G peaks is unity, it suggests that the presence of six-fold aromatic rings and no presence of chains are detected. For the case of deviation of the ratio from unity may be attributed to the defects in the materials. Such defects may be originated from the distortion of six-fold aromatic ring in the NiTsPc molecule.

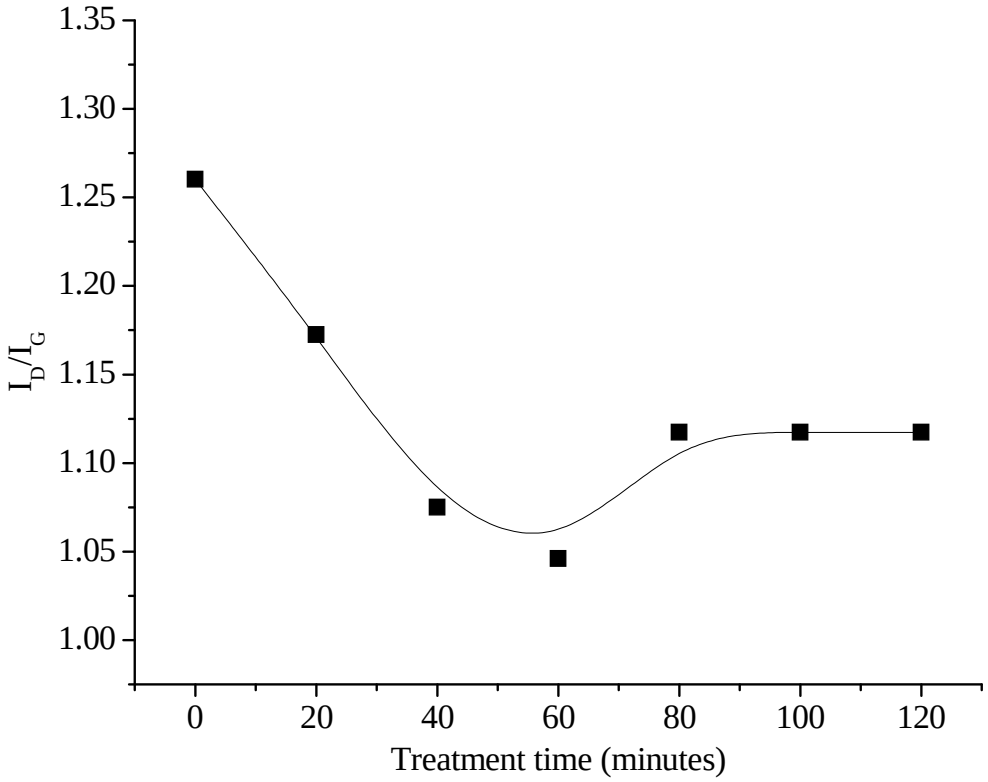

Figure 4.16: Intensity ratio of D and G peak for different treatment time.

Figure 4.16 shows the influence of treatment time on the ratio of I_D and I_G. For the untreated film, the value of $I_C + I_R$, is minimum whereas the ratio I_D/I_G is maximum since the ratio of I_D and I_G is inversely proportional to $I_C + I_R$. From this figure, the value of the I_D/I_G ratio is greater than one for all the films, hence it may be attributed to the presence of chain as the sixfold aromatic is distorted. On the contrary, for film being treated for 60 minutes, the I_D/I_G ratio found as the minimum, suggesting that the presence of chain in the film via the increment of $I_C + I_R$. In Table 4.3, it is can be found that the G peak is triggered from the vibration of C-N and C-N=C-C=C. The latter vibration shows that the six-fold aromatic ring has been distorted and then initiates the opening of the six-fold aromatic ring from the structure of NiTsPc and forming some sort of defects in the molecule. As the treatment time increases, more defects are formed at the film. These defects may influence the optical energy gap which will be explained in next section.

4.3.3 Optical properties

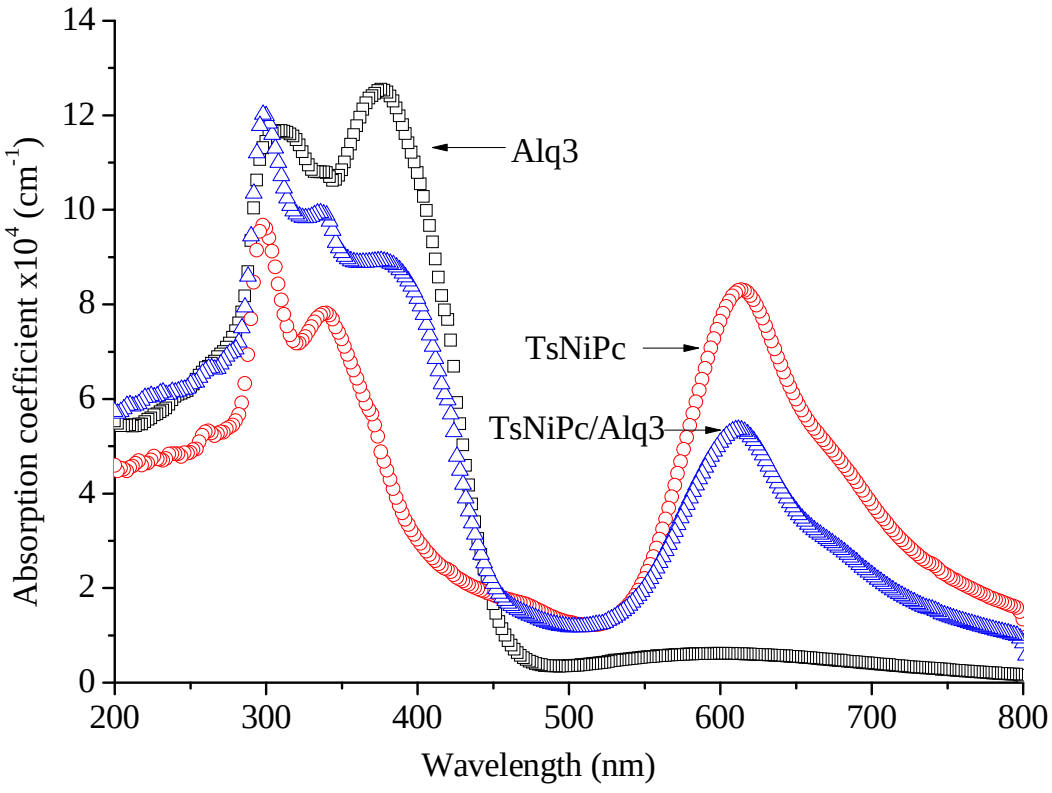

Figure 4.17: Absorption properties of NiTsPc, Alq3 and NiTsPc/Alq3 double layer films.

Absorption spectra of the NiTsPc and Alq3 films are shown in Figure 4.17. The absorption spectrum of the NiTsPc film exhibits two peaks in both B and Q bands. In Q band, an intense absorption peak at 630 nm is due to the transition between the bonding and antibonding (π-π^*) at the dimer part of the phthalocyanine (Pc) molecule. In addition, a shoulder peak occurs with low absorption intensity in the Q band region at 670 nm. This shoulder corresponds to the absorption at the monomer part of the molecule from second π-π^* transition or as excitation peak or as a vibrational interval (Farag, 2007). The central atom (Nickel) of the phthalocyanine molecule is associated with the d–band (Farag, 2007). On the other hand, a strong absorption peak at 288 nm and a shoulder at 350nm within the UV region of the spectrum, are attributed to π-d and partially occupied d-π^* transitions, respectively (M. El-Nahass *et al.*, 2004). The absorption features of this spin-coated phthalocyanine derivative film is similar to the reported thermally evaporated phthalocyanine films (Karan *et al.*, 2007; G. Park *et al.*, 2011). The result indicates that the simple spin-coating method can be utilized to obtain similar light absorption properties of a soluble phthalocyanine, as provided by the complicated thermal evaporation technique. A simple superposition of bilayer NiTsPc/Alq3 thin film shows that a broad light absorption at the UV region. When this layer is applied as the active layer in the photovoltaic device, it can increase the absorption ability of the device.

Upon chloroform treatment, all the absorption peaks of the NiTsPc film still exist as shown in Figure 4.18(a). It can be observed clearly from Figure 4.18(b) and 4.18(c) that the solvent treatment does not cause any shift of the peaks in neither B nor Q bands. The treatment time only affects the absorption intensity. As the treatment time increases from 20 to 60 minutes, the absorption intensity of the treated films is higher as compared to the untreated sample. However, the absorption intensity starts to decrease for the films being treated longer than 60 minutes. Besides, the absorption spectrum became wider for this film so that light with wider range of wavelength can be absorbed. Hence, the optimum treatment time is found 60 minutes.

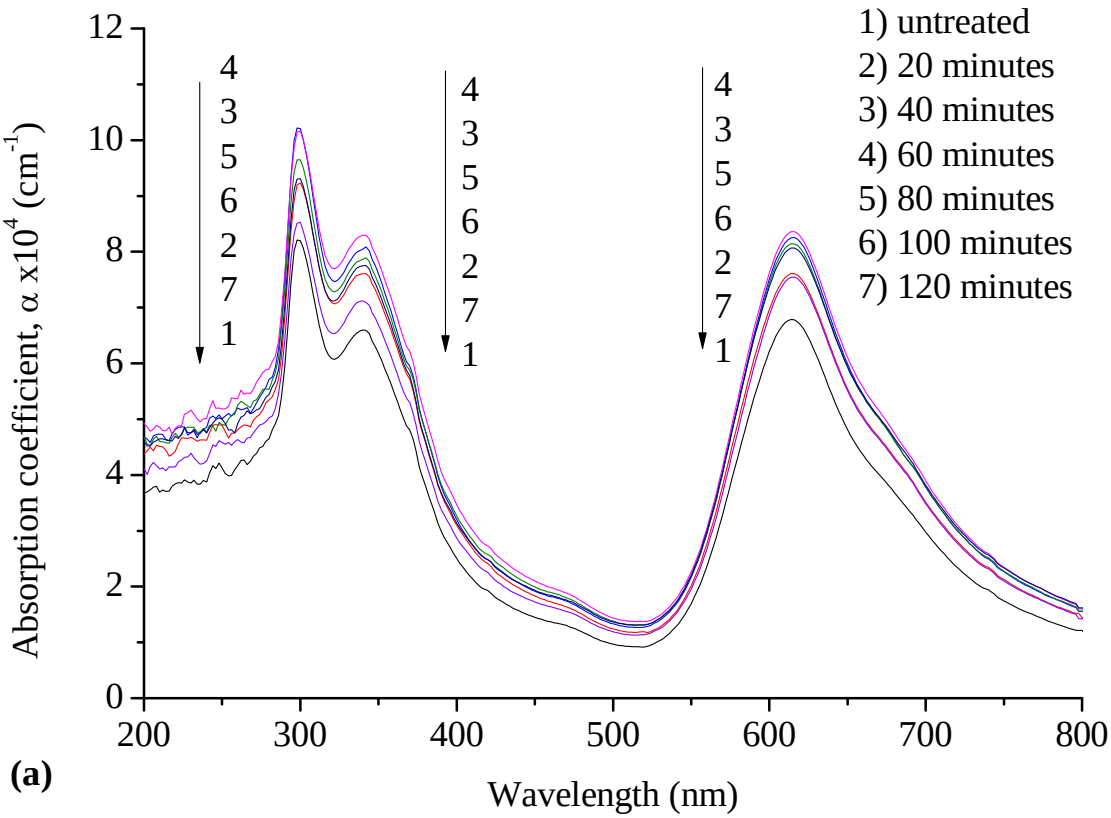
1) untreated
2) 20 minutes
3) 40 minutes
4) 60 minutes
5) 80 minutes
6) 100 minutes
7) 120 minutes
Absorption coefficient, α x10^4 (cm^-1)
Wavelength (nm)
0
2
4
6
8
10
12
200
300
400
500
600
700
800

(a)

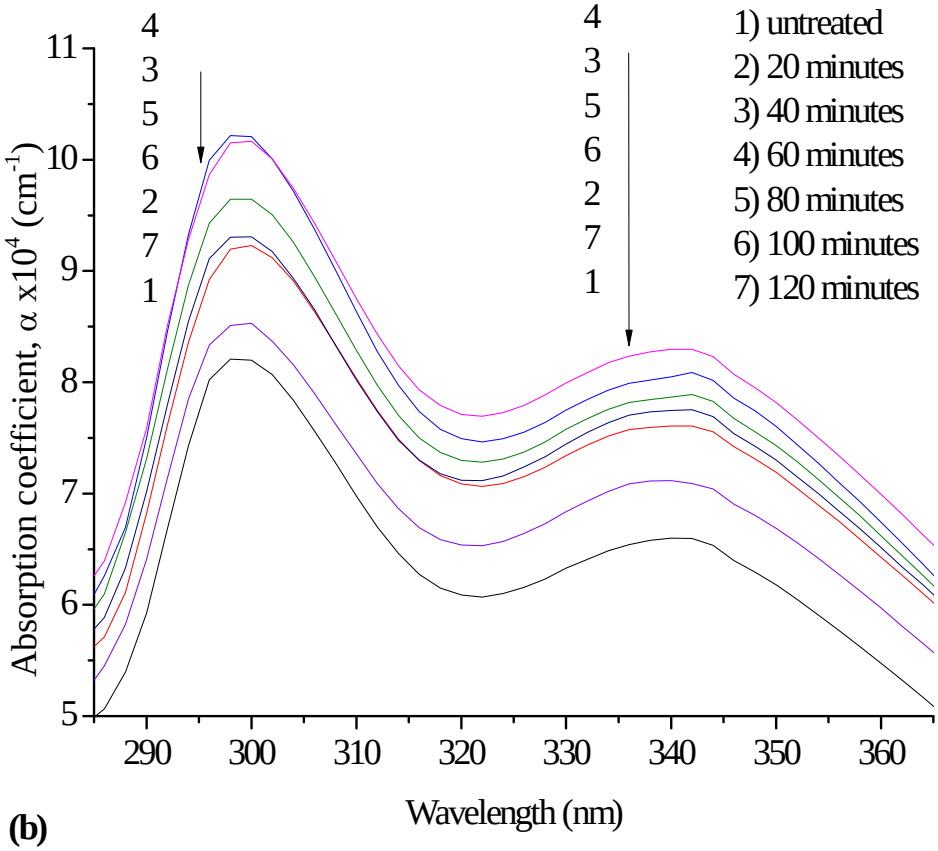
1) untreated
2) 20 minutes
3) 40 minutes
4) 60 minutes
5) 80 minutes
6) 100 minutes
7) 120 minutes
Absorption coefficient, α x10^4 (cm^-1)
Wavelength (nm)
5
6
7
8
9
10
11
290
300
310
320
330
340
350
360

(b)

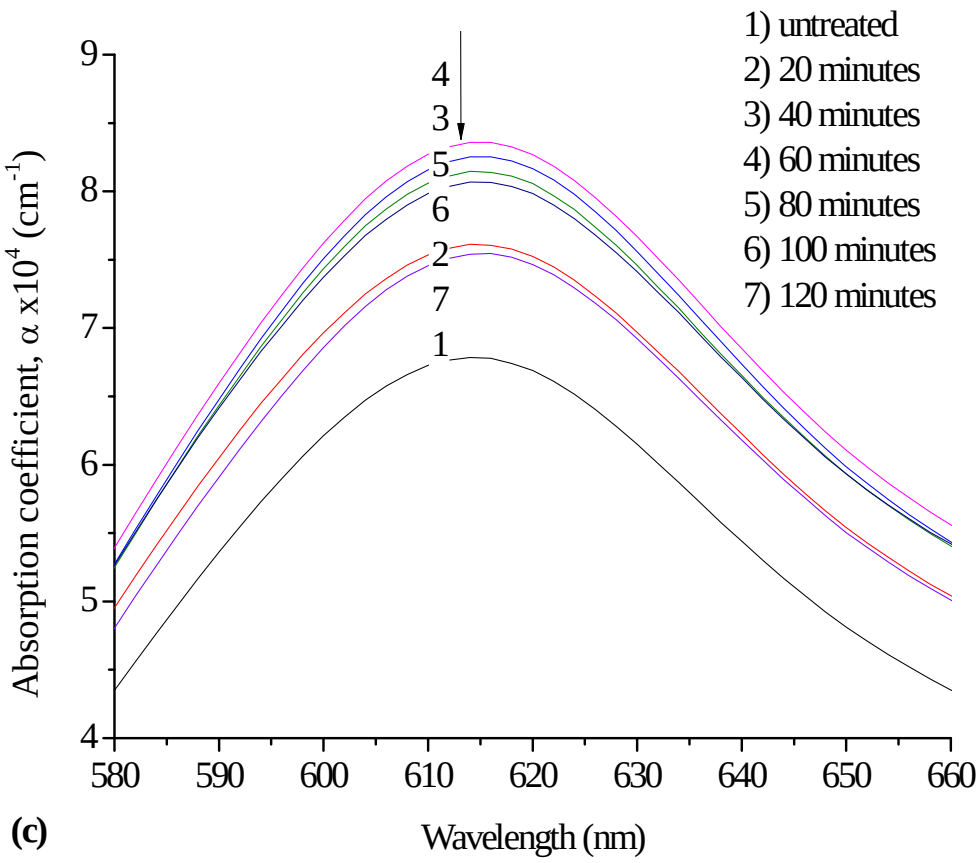

Figure 4.18: (a) The absorption spectra for untreated and treated NiTsPc with chloroform (b) Magnification of the absorption intensity at B band (c) Magnification of the absorption intensity at Q band.

Two absorption edges in the absorption spectra suggest the existence of two different energy gaps for the NiTsPc film. Further investigation on the optical energy gap has been performed by plotting the a Tauc's plot (Muhammad & Sulaiman, 2011b) as shown in Figure 4.19. The Tauc's relation can be written as: .

$$\alpha h\nu = \alpha_o (h\nu - E_g)^n \qquad (4.4)$$

where, α_o is the energy dependent constant and E_g is the optical energy gap. The value of n represents the type of the absorption transition. The Tauc plot in Figure 4.19(a) shows the two regions; the region with higher energy is called fundamental energy gap and the region with lower energy gap is called the onset energy gap. The tail of the graph shows an

exponential behavior indicating the presence of localized state, which can be correlated with an indirect transition (M. El-Nahass *et al.*, 2004). Hence, the value of $n = 2$ is used, assuming an indirect transition. This indirect transition with $n = 2$ also reported by other researchers for NiPc (M. El-Nahass *et al.*, 2004; Kumar *et al.*, 2000).

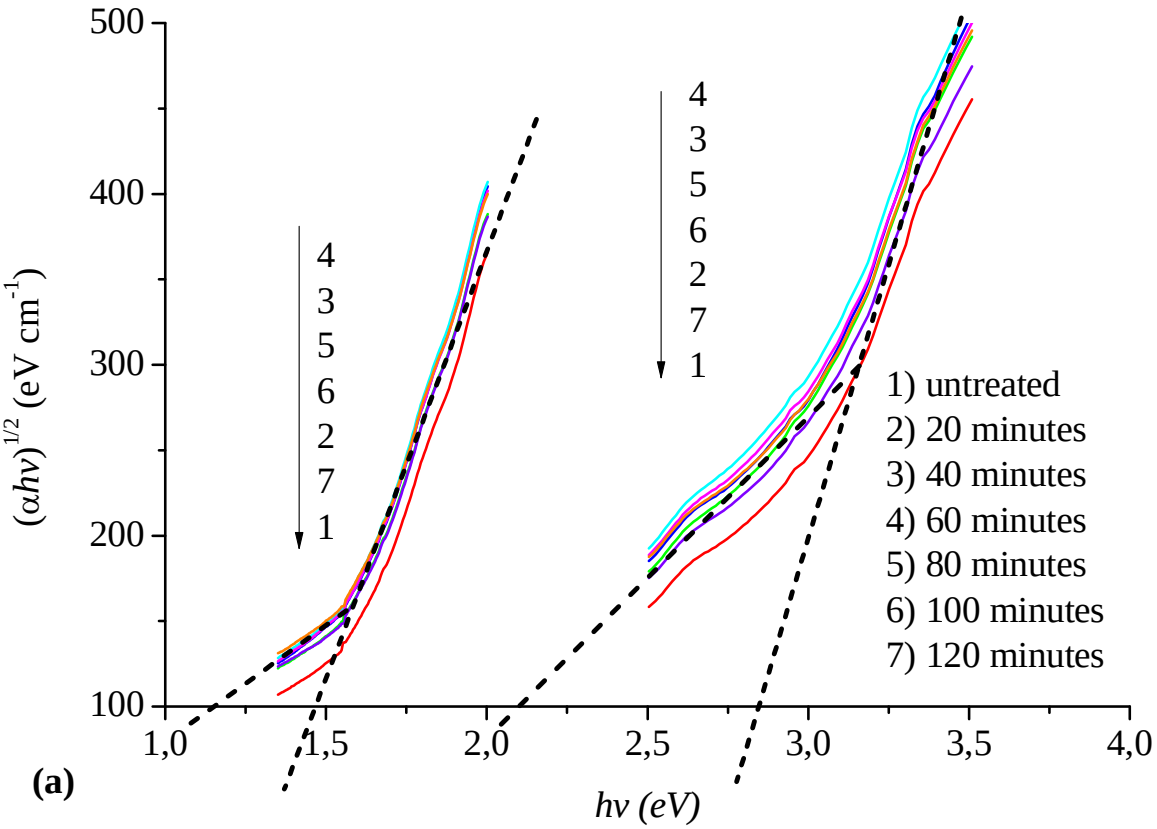

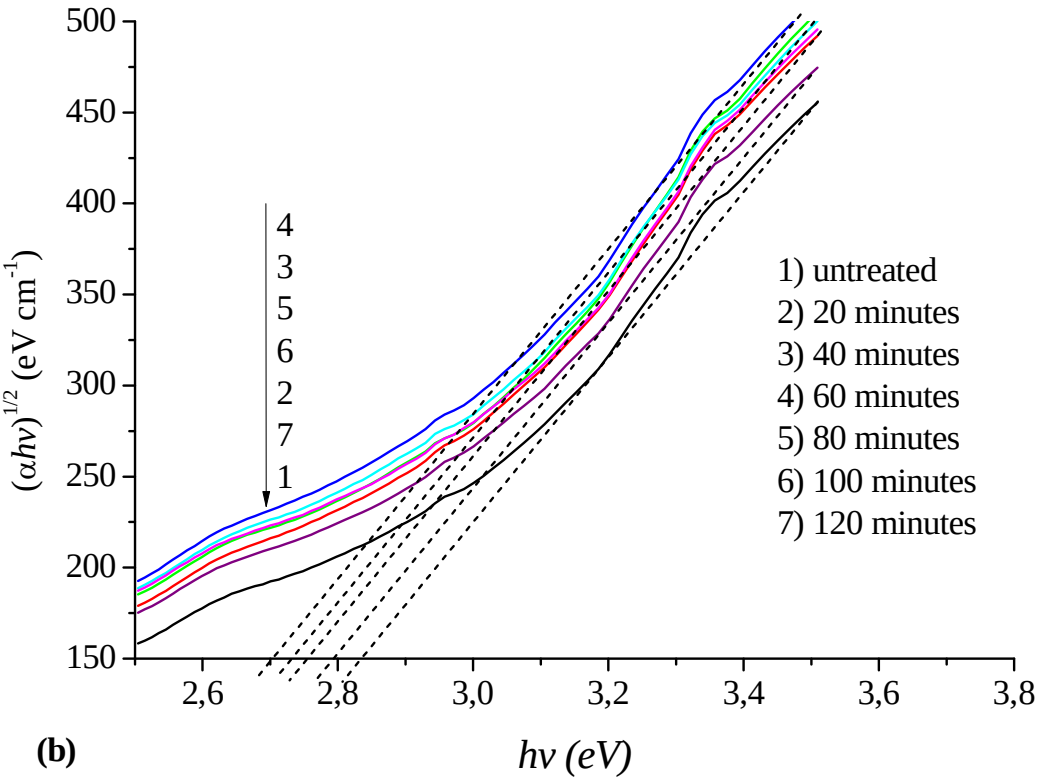

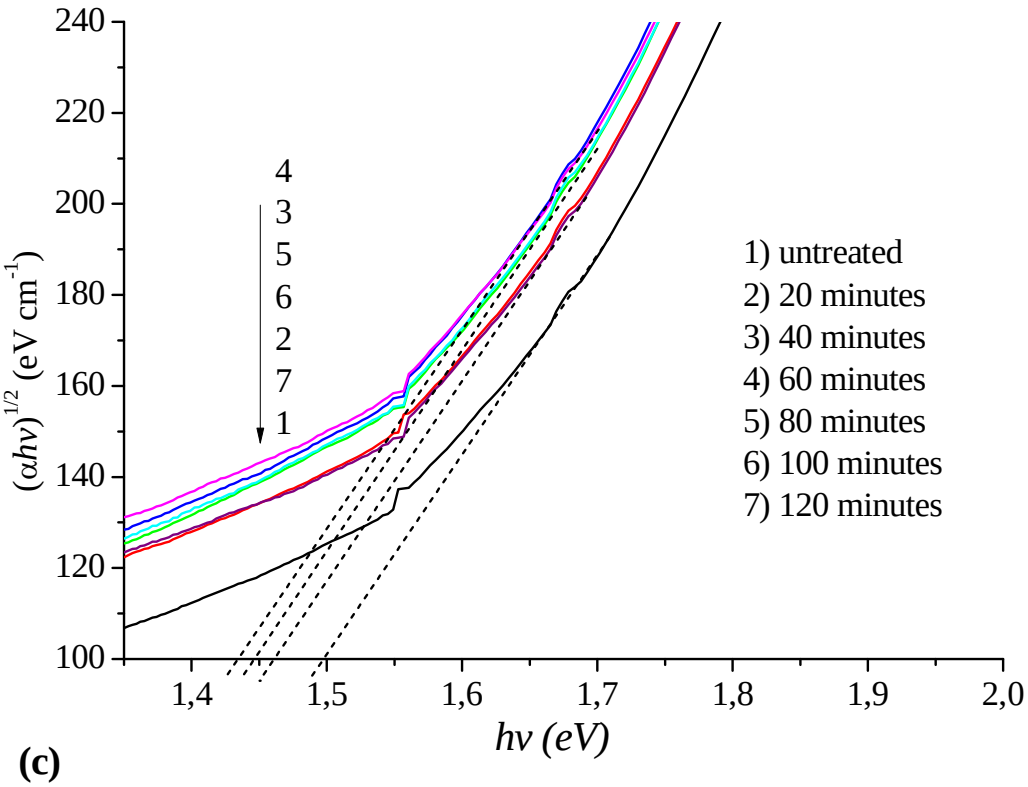

Figure 4.19: (a) The Tauc's Plot of the untreated and treated NiTsPc films with different treatment time, (b) Enlargement of the fundamental energy gap region, and (c) Enlargement of the onset energy gap region. Optical energy gap was obtained by extrapolating line from 1.7 and 3.5 eV.

Table 4.4: List of the optical energy gaps for the untreated and treated NiTsPc films with different treatment time.

Treatment time (minutes)	Fundamental energy gap, E_{g1} (eV)	Onset energy gap, E_{g2} (eV)
0 (untreated)	2.85	1.50
20	2.75	1.46
40	2.73	1.43
60	2.70	1.43
80	2.73	1.45
100	2.75	1.45
120	2.79	1.46

Table 4.4 shows the value of the energy gap, both at the fundamental and onset by extrapolating the straight linear lines from the fix points at 1.7 eV and 3.5 eV (correspond to the peaks in the NiTsPc absorption spectrum). It is noted that the value of energy gap in NiTsPc is influenced by the treatment time. The minimum fundamental energy gap is obtained for the film treated up to 60 minutes. The fundamental energy gap of 2.70 eV of the untreated NiTsPc obtained from the Tauc's plot is in agreement to those reported in other phthalocyanines (B. Kippelen *et al.*; Krebs, 2009; P. Peumans *et al.*, 2003). The result of the energy gap can be related by the result in the structural properties section. Previously discussed in the morphological properties, more defects have been formed in the NiTsPc film as the treatment time increases. These defects create the density of states of energy level and produce a narrower energy gap (Broqvist *et al.*, 2009; Mensing *et al.*, 2002). Hence, the formation of the defects after the film being treated by solvent, has altered the energy gap of the NiTsPc film.

An n-type material of Alq3 was thermally evaporated on top of the treated NiTsPc film, to be used as the active layer in the photovoltaic device. The charge transfer behavior of the donor and acceptor (D/A) heterojunction between layer and Alq3 layer, is examined by the photoluminescence (PL) spectroscopy measurements. The pristine sample of the untreated NiTsPc/Alq3 is used as reference. The effect of treatment time of the NiTsPc film on the PL spectra of the NiTsPc/Alq3 bilayer is shown in Figure 4.20. The PL

intensity of the film is reduced to some extend as the NiTsPc is treated from 20 to 60 minutes compared to the pristine sample, while the intensity increased as the film being treated from 80 to 120 minutes. High PL intensity does not favor the photovoltaic properties. Hence, the reduction in PL intensity, known as PL quenching is more beneficial here. In this study, a small PL quenching phenomenon can be seen for the bilayer films particularly the 60 minutes treated film. Such PL quenching represents an efficient charge transfer at the D/A interface (Xu *et al.*, 1993).

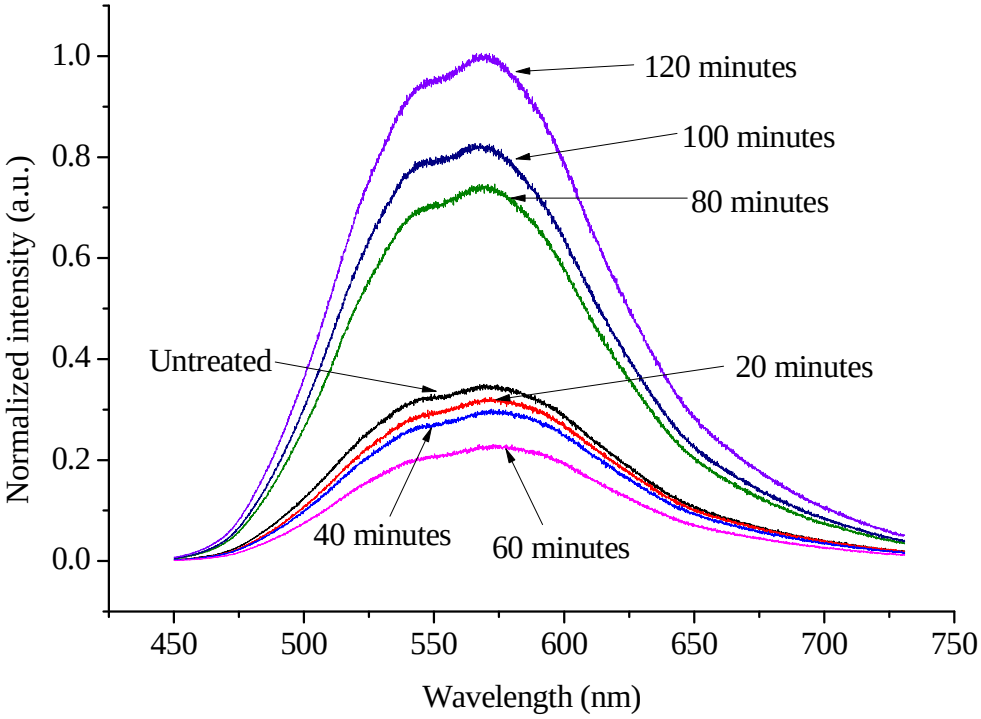

Figure 4.20: Photoluminescence spectra of untreated and treated NiTsPc films.

4.3.4 Electrical properties

NiTsPc/Alq3 bilayer film was sandwiched between ITO and Al electrodes to form ITO/NiTsPc/Alq3/Al photovoltaic devices. The photovoltaic effects can be observed in the fourth quadrant of the *J-V* curve, when the ITO/NiTsPc/Alq3/Al devices were illuminated by a standard 100 mW/cm^2 light in air. The variation in the J-V curves upon solvent treatment time is presented in Figure 4.21, showing different values of short-circuit current, J_{sc} and open-circuit voltage, V_{oc}.In this study, if a higher voltage than 6V, then it

causes the breakdown in the devices. It is well accepted that the value J_{sc} of a photovoltaic device, depends on the absorption property of the active layer and it charge carrier transport.

However, the open-circuit voltage, V_{oc} is still in debate whether it is caused by the difference in the electrodes' work function or by the difference in the Highest Occupied Molecular Orbital (HOMO) of the donor and the Lowest Unoccupied Molecular Orbital (LUMO) of the acceptor (Muhammad *et al.*, 2010). The difference in electrodes work function is about 0.8 V (Greenham *et al.*, 1996). In this study, the value of V_{oc} for the devices falls within the range of 1.3 V to 1.4 V. Hence, it can be said that the V_{oc} is attributed to the difference in HOMO of NiTsPc (5.0 eV) and LUMO of Alq3 (3.4 eV). This small variation in V_{oc} suggests that the HOMO and LUMO molecular energy levels are insignificant by the solvent treatment as described in the previous section. The exact value of the HOMO-LUMO of NiTsPc, Alq3 and PTCDA was not determined in this work. In general, HOMO-LUMO values of those organic layer on metal electrodes can be measured from a combination of X-ray and ultraviolet photoemission (XPS,UPS). Nevertheless, both UPS and XPS are not available at University of Malaya.

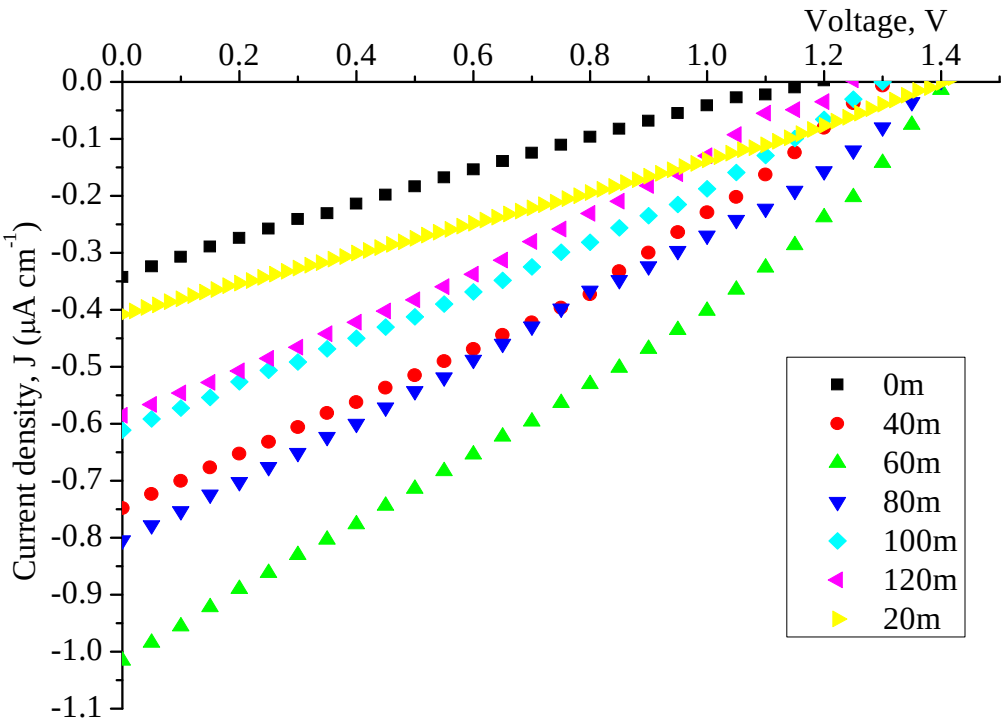

Figure 4.21: The current density – voltage (*J-V*) characteristics of the photovoltaic devices consist of untreated and treated NiTsPc film for different immersion time. The devices were tested in air under light illumination 100 mW/cm^2.

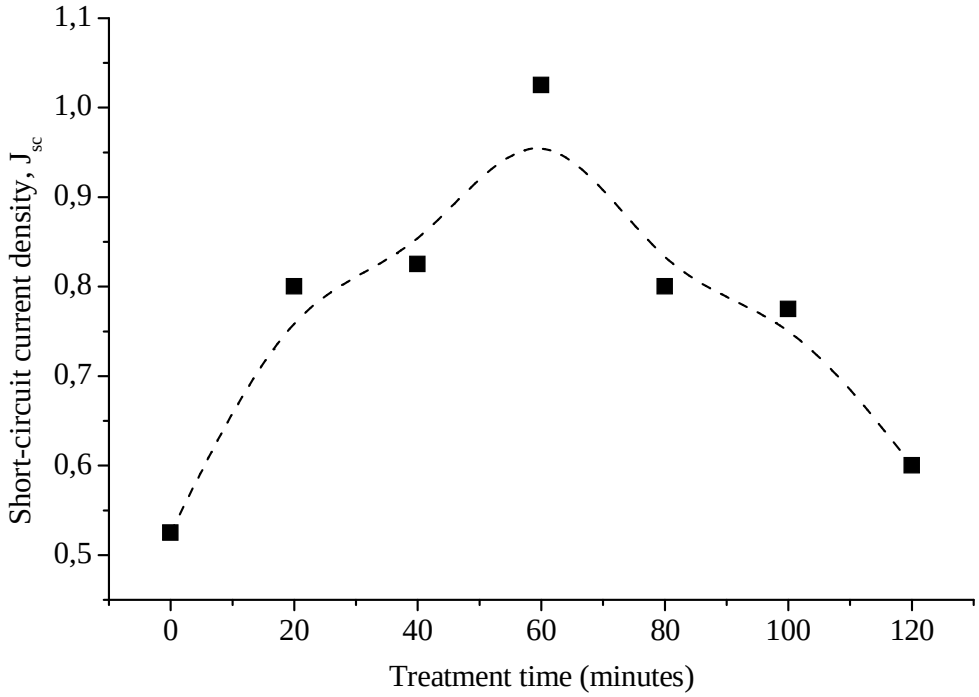

Figure 4.22: The short-circuit current density (J_{sc}) of the photovoltaic device.

The effect of treatment time on the J_{sc} value (obtained from Figure 4.21) is then presented by a graph in Figure 4.22. Initially, the current increases with treatment time approaching

a maximum value at 60 minutes then drops for 80 to 120 minutes. The variation of J_{sc} value can be explained by referring to the ability of the NiTsPc films to absorb light as shown in Figure 4.18. In this figure, the intensity of the light absorbed has been increased and the absorption range becomes wider upon solvent treatment on the film. These conditions allow the photovoltaic device containing treated NiTsPc layer, to generate more excitons upon light illumination. Furthermore, it is expected that the photoinduced charge carriers' transport through the the donor/acceptor interface can be enhanced upon increasing the treatment time. Such a longer treatment period provides a larger interface area as indicated by the larger number of nano fibers in the FESEM images. Hence, the film being treated with chloroform for 60 minutes, is selected as the optimum time in this study producing the highest J_{sc} = 1.0 μA/cm^2 as presented in Figure 4.22. This current value is approximately double the value of the untreated device when incorporated with Alq3. Hence, the charge transport behaviour is more efficient between the treated NiTsPc layer (as donor) and the second layer of Alq3 (as acceptor) compared to the device consists of the untreated NiTsPc/Alq3 film. Furthermore, the FF of the device treated with solvent shows an increased nearly double from the untreated device. The value of fill factor for each device is calculated using equation 4.5 and shows in Table 4.5.

$$Fill\ factor, FF = \frac{J_{max}V_{max}}{J_{sc}V_{oc}} = \frac{P_{max}}{J_{sc}V_{oc}} \qquad (4.5)$$

Table 4.5: The value of P_{max}, J_{sc}, V_{oc} and fill factor (FF).

	Maximum power, P_{max}	**Short-circuit current density, J_{sc} (μA/cm^2)**	**Open-circuit voltage, V_{oc} (V)**	**Fill factor, FF**
Untreated film	0.09	0.52	1.30	0.14
20 minutes	0.16	0.80	1.36	0.15
40 minutes	0.30	0.82	1.36	0.27
60 minutes	0.43	1.02	1.40	0.30
80 minutes	0.31	0.80	1.30	0.29
100 minutes	0.23	0.77	1.26	0.23
120 minutes	0.20	0.60	1.20	0.28

Overall J_{sc} and fill factor values produced from the ITO/NiTsPc/Alq3/Al devices are very small compared to those reported in literatures for organic solar cells (Karak *et al.*, 2010). There are many factors contribute to this small value including un-encapsulated device and electrical behavior being measured in air. These processes have certainly reduced the solar cell performance through device degradation. Furthermore, the aluminium atoms from the top electrode may diffuse to the organic layer of Gaq3 leading to formation of oxidized sub-layer (Jørgensen *et al.*, 2008). Several suggestions to increase the solar cell performance are described in Chapter 5.

CHAPTER 5

CONCLUSIONS AND FUTURE WORKS

5.1 Conclusions

Phthalocyanine and its derivatives have shown a good physical properties and promising materials to be used as active layer in organic solar cells. Nevertheless, most phthalocynines thin films can only be deposited on to solid substrates via a thermal evaporation technique. Herein, a simple solution processed of spin-coating technique was demonstrated to deposit a nickel (II) phthalocyaninetetrasulfonic acid tetrasodium salt (NiTsPc) thin films. Several parameters including spin rate of the spin-coater and the solution concentration are among the most important factors to produce a homogenous and good NiTsPc films, with the desired thickness on the cleaned glass substrates. In this study, the spin rate was fixed to be around 800-1000 rpm to avoid the non-adhering problem of the thin film on the substrate. Even though the lowest spin rate of 800 rpm was used, the spin-coated film was not at the optimum film desired. Hence, the concentration of NiTsPc solution was varied. As a result, the desired homogenous NiTsPc film with 120 nm can be produced using a solution concentration of 35mg/ml and the spin rate of 800 to 1000 rpm.

In order to enhance the absorption properties of the film, a thermal treatment was done to the deposited NiTsPc thin films. The results reveal that the shape of the absorption plot of the thermally annealed NiTsPc film, remain the same compared to the pristine sample. Such behavior indicates that there is no change in the conjugated bond of NiTsPc compound. However, there was a small variation in the absorption intensity upon thermal annealing treatment. From the experiment, the annealing temperature was selected at temperature 140°C, to enhance the absorption coefficient up to 50% compared to the pristine NiTsPc film.

Surface modification of the NiTsPc thin films was done by immersing the film in its suitable solvent with different immersion times. Immersion process allows the solvent molecule to absorb and penetrate into the film and it is believed that the modification of the film occurred during the drying process. In this research work, two types of solvents were chosen for surface modification namely chloroform and toluene, due to their low solubility to NiTsPc film. The surface morphology of the solvent treated NiTsPc films was initially analyzed using the AFM images. The AFM results have shown that the roughness mean square (rms) values of the chloroform and toluene treated thin film are 16 nm and 9 nm respectively which is smaller compared to pristine film of 41 nm. Hence, the treated film forming a smaller granular structure as a result of the etching process by the solvent. Furthermore, the toluene treated NiTsPc film has formed more packed structures compared to that of the chloroform treated film. Such observation is attributed to the lower vapor pressure of toluene (22 mmHg) compared to chloroform (159.8 mmHg), in which toluene needs more time to evaporate from the film, allowing more time for molecular re-arrangement. The value of film roughness mean square increases 25% upon solvent treated from the untreated film. This result indicates that the coarser nanofibers being formed by a larger amount of humps and valleys along the thin film surface are influenced by the film treatment in its suitable solvent.

Further characterization was performed by measuring the electrical properties of the solar cells using either toluene or chloroform treated NiTsPc film as the first layer, incorporated with PTCDA as the second active layer. The solar cells with sandwiched structure of ITO/NiTsPc/PCTDA/Al were illuminated with a standard 100 mW/cm^2 light source through the ITO electrode and the *J-V* characteristics were measured. J_{sc} of the solar device consisting chloroform treated NiTsPc film was measured to be twice higher compared to the device with untreated NiTsPc film. Besides, the toluene treated device only a slight increment of photocurrent. Therefore, chloroform was chosen to for the next part of study; variation in immersion time of the solvent treatment process.

Prior to solvent treatment, the NiTsPc films were thermally treated at 140°C. The FESEM images show that the nano fibers were formed after thermal treatment. Such nanofibers cannot be observed in the FESEM image of the pristine sample of non-annealing NiTsPc film, even at higher magnification. Then, the solvent treatment with different immersion times of 40, 80 and 120 minutes on the NiTsPc films was performed in chloroform. A significant variation in the surface morphological properties has been generated upon different soaking times in this suitable chloroform solvent. The results revealed that the nano fibers with diameter below 200 nm appeared in the untreated NiTsPc film. By immersing the film in chloroform, a part of the exposed surface has been etched and modified to produce larger diameter nano-fibers compared to the pristine sample. As the immersion time increases beyond 40 minutes, the number of nano fibers with smaller diameter was increased 1.5 times. From the FESEM images of the film with longer immersion time (80 and 120 minutes), the nano fiber has been interconnected and separated by closer distance. Both FESEM and AFM results show that the films were etched by the suitable solvent after achieving the optimum time.

For the structural characterization, the NiTsPc film has a semi-crystalline feature as evident from a protruding peak at $2\theta = 32°$ for the film being treated with its suitable solvent. Calculated value of the mean crystallite size for the treated film determined to be in the range of 70-100 nm. Raman spectrum of the NiTsPc film shows two clear peaks at 1350 and 1580 cm^{-1} correspond to the D and G peaks. The Raman spectra for all the untreated and treated film did not show any shift in the peak positions, but rather variation in Raman intensity. The intensity ratio of the D to G peak (I_D/I_G) is greater than unity for all films. The plot of I_D/I_G against treatment time shows that the minimum point occurs for the NiTsPc film being soaked at 60 minutes. This result indicates the formation of defects by opening the six-fold aromatic ring from the NiTsPc molecule becoming a planar chain. As the treatment time increases, more defects are formed in the film, and these defects have influenced the optical energy gap to certain extent.

Optical characterization on the film shows that the absorption of NiTsPc film produce two peaks in B-band and Q-band. Strong absorption at B-band occurs at 288 nm and a shoulder peak at 350 while at Q-band the absorption occurs at 630 nm and a small shoulder peak at 670 nm. No shift on the absorption peaks position was recorded at the absorption spectrum but the intensity increased around 22% and 23% at the strong absorption peaks (B-band and Q-band) for film treated for 60 minutes. Besides the increase of intensity, the absorption spectrum becomes wider for the NiTsPc film with a longer soaking time in chloroform solvent. Therefore, NiTsPc film being treated at 60 minutes in chloroform has the ability to absorb more photons, thus generates more excitons for charge carrier. This result is further supported by the observation in the PL measurement. PL quenching around 80% has been obtained for NiTsPc film being treated with solvent at 60 minutes.

By employing the Tauc's relation, two different energy gaps for the film named fundamental energy gap and onset energy gap based on the high and low energy regions. The fundamental energy gap using Tauc plot of the untreated NiTsPc with the value of 2.85 eV, is in agreement to those reported in other phthalocyanines systems. The lowest energy gap (fundamental and onset) was estimated to be 2.70 eV and 1.43 eV, which is a drop of 5% compared to the untreated film. The change in optical energy gap can be explained in terms of defects formation upon solvent treatment. As the treatment time increases, the NiTsPc film creates the density of states of energy level and produces a narrower energy gap for film treated at 40 minutes. However, both energy gaps for the film increased when the films were immersed beyond 60 minutes. Photoluminescence (PL) characterization was done by incorporating the film with Alq3, an n-type material. Low PL intensity is favorable in the fabrication organic solar cells as it represents an efficient charge transfer at the donor-acceptor interface.

The photovoltaic device was fabricated by sandwiching the untreated and treated NiTsPc/Alq3 bilayer between ITO and Al electrodes to form ITO/NiTsPc/Alq3/Al device.

The current density-voltage *(J-V)* measurement was focused on the short-circuit-current density, J_{sc} since this value represent charge transfer transport behavior. Highest J_{sc} value as well as fill factor are determined for the device consists of NiTsPC film being treated at 60 minutes. At this optimum time of 60 minutes, the value of fill factor reaches 0.30, which is nearly double compared to the untreated device. Charge transport in this device is more efficient thus yield higher J_{sc} value. This result agrees with the explanation in the morphology, structural and optical properties for 60 minutes of the solvent treatment.

However, overall performance based on solution processed NiTsPc film, is still very small compared to those reported organic solar cells. Such low performance is attributed to many factors primarily the fabricated device was not performed in a glove box. This becomes the major problem in the device degradation and oxidation, which reduces the performance of the device. Besides, the electrical measurements were performed in air compared to those reported devices in literatures, being measured under vacuum.

5.2 Closing Remarks

To restate the objectives of this study from Chapter 1 is to investigate the parameter in forming the homogenous NiTsPc film using spin-coated method and modify the surface morphology of NiTsPc films by immersing the films in the selected solvents. By considering the comprehensive results and discussions in Chapter 4, it can be seen that all objectives have been accomplished. This thesis marks a considerable stride towards reduction of energy gap in solution processed organic NiTsPc film for solar photovoltaic devices. Therefore, the performance of OSC can be improved to some extent via thin film surface modification by soaking in a suitable solvent at an optimum time.

5.3 Future Works

From the research work, some of the properties of the treated NiTsPc were determined and can be applied in enhancing the performance of the photovoltaic device. For future works, the condition of the treated not only can be used as the active layer in the photovoltaic device but can also be practiced as the replacement of PEDOT: PSS as the buffer layer. Treated NiTsPc can avoid the contamination caused by the acidity of PEDOT: PSS which can dissolve indium ions from the ITO layer. In addition, it can also assist the free charge carrier to transport to the electrode.

Both X-ray and ultraviolet photoemission (XPS,UPS) can be utilized to obtain the value of HOMO and LUMO of the solvent treated organic films. Information from the XPS and UPS measurements can provide the exact energy levels of the organic films. Furthermore, for future works, the device fabrication should be carried out in a glove box. Besides, the device should be fully encapsulated to the degradation and oxidation processes significantly. Besides, encapsulation of the fabricated device also gives the same advantage as it will be tested under ambient condition.

References

Abdullah, S. M., Ahmad, Z., Aziz, F., & Sulaiman, K. (2012). Investigation of VOPcPhO as an acceptor material for bulk heterojunction solar cells. *Organic Electronics, 13*(11), 2532-2537.

Ahmad, Z., Sayyad, M. H., & Karimov, K. S. (2010). CuPc based organic-inorganic hetero-junction with Au electrodes. *Journal of Semiconductors, 31*, 074002.

Aimai, N., Gould, R., & Saleh, A. (1998). Space-charge-limited conductivity in evaporated α-form metal-free phthalocyanine thin films. *Vacuum, 50*(1), 53-56.

Ambily, S., & Menon, C. S. (1999). The effect of growth parameters on the electrical, optical and structural properties of copper phthalocyanine thin films. *Thin Solid Films, 347*(1–2), 284-288.

Aziz, F., Sayyad, M., Ahmad, Z., Sulaiman, K., Muhammad, M., & Karimov, K. S. (2012). Spectroscopic and microscopic studies of thermally treated Vanadyl 2, 9, 16, 23-tetraphenoxy-29H, 31H-phthalocyanine thin films. *Physica E: Low-dimensional Systems and Nanostructures, 44*(9), 1815–1819.

Bała, W., Grodzicki, A., Piszczek, P., Wojdyła, M., Bratkowski, A., Szybowicz, M., Runka, T., & Drozdowski, M. (2006). Temperature dependence of FT-IR absorption and Raman scattering of copper phthalocyanine thin layers deposited on silicon substrate. *Journal of Molecular Structure, 782*(2–3), 177-182.

Boudjema, B., Guillaud, G., Gamoudi, M., Maitrot, M., Andre, J., x, Jacques, Martin, M., & Simon, J. (1984). Characterization of metallophthalocyanine‐metal contacts: Electrical properties in a large frequency range. *Journal of Applied Physics, 56*(8), 2323-2329.

Broqvist, P., Alkauskas, A., Godet, J., & Pasquarello, A. (2009). First principles investigation of defect energy levels at semiconductor-oxide interfaces: Oxygen vacancies and hydrogen interstitials in the Si–SiO 2–HfO 2 stack. *Journal of Applied Physics, 105*(6), 061603-061603-061605.

Brovelli, F., Rivas, B. L., Bernède, J. C., del Valle, M. A., Díaz, F. R., & Berredjem, Y. (2007). Electrochemical and optical studies of 1,4-diaminoanthraquinone for solar cell applications. *Polymer Bulletin, 58*(3), 521-527.

Campbell, A., Bradley, D., & Lidzey, D. (1997). Space-charge limited conduction with traps in poly (phenylene vinylene) light emitting diodes. *Journal of Applied Physics, 82*(12), 6326-6342.

Chen, H.-Y., Hou, J., Zhang, S., Liang, Y., Yang, G., Yang, Y., Yu, L., Wu, Y., & Li, G. (2009). Polymer solar cells with enhanced open-circuit voltage and efficiency. *Nat Photon, 3*(11), 649-653.

Chirvase, D., Parisi, J., Hummelen, J., & Dyakonov, V. (2004). Influence of nanomorphology on the photovoltaic action of polymer–fullerene composites. *Nanotechnology, 15*(9), 1317.

Chu, P. K., & Li, L. (2006). Characterization of amorphous and nanocrystalline carbon films. *Materials Chemistry and Physics, 96*(2), 253-277.

Chunder, A., Pal, T., Khondaker, S. I., & Zhai, L. (2010). Reduced graphene oxide/copper phthalocyanine composite and its optoelectrical properties. *The Journal of Physical Chemistry C, 114*(35), 15129–15135.

Dennler, G., & Sariciftci, N. S. (2005). Flexible Conjugated Polymer-Based Plastic Solar Cells: From Basics to Applications. *Proceedings of the IEEE, 93*(8), 1429-1439.

El-Nahass, M., Abd-El-Rahman, K., Farag, A., & Darwish, A. (2004). Optical characterisation of thermally evaporated nickel phthalocyanine thin films. *International Journal of Modern Physics B, 18*(3), 421-434.

El-Nahass, M., El-Gohary, Z., & Soliman, H. (2003). Structural and optical studies of thermally evaporated CoPc thin films. *Optics & Laser Technology, 35*(7), 523-531.

El-Nahass, M. M., Farag, A. M., Abd El-Rahman, K. F., & Darwish, A. A. A. (2005). Dispersion studies and electronic transitions in nickel phthalocyanine thin films. *Optics & Laser Technology, 37*(7), 513-523.

Fakir, M. S., Ahmad, Z., & Sulaiman, K. (2012). Modification of Optical Band Gap and Surface Morphology of NiTsPc Thin Films. *Chinese physics letters, 29*(12), 126802.

Farag, A. (2007). Optical absorption studies of copper phthalocyanine thin films. *Optics & Laser Technology, 39*(4), 728-732.

Ferrari, A., & Robertson, J. (2000). Interpretation of Raman spectra of disordered and amorphous carbon. *Physical Review B, 61*(20), 14095.

Forrest, S., Burrows, P., Haskal, E., & So, F. (1994). Ultrahigh-vacuum quasiepitaxial growth of model van der Waals thin films. II. Experiment. *Physical Review B, 49*(16), 11309.

Frederik C, K. (2009). Fabrication and processing of polymer solar cells: A review of printing and coating techniques. *Solar Energy Materials and Solar Cells, 93*(4), 394-412.

Gould, R., & Rahman, M. (2000). Power-law currents in some ZnO-Sn composite materials. *Journal of Physics D: Applied Physics, 14*(1), 79.

Green, M. A., Emery, K., Hishikawa, Y., Warta, W., & Dunlop, E. D. (2012). Solar cell efficiency tables (version 39). *Progress in Photovoltaics: Research and Applications, 20*(1), 12-20.

Green, M. A., Emery, K., King, D. L., Igari, S., & Warta, W. (2003). Solar cell efficiency tables (version 22). *Progress in Photovoltaics: Research and Applications, 11*(5), 347-352.

Greenham, N. C., Peng, X., & Alivisatos, A. P. (1996). Charge separation and transport in conjugated-polymer/semiconductor-nanocrystal composites studied by photoluminescence quenching and photoconductivity. *Physical Review B, 54*(24), 17628.

Günes, S., Neugebauer, H., & Sariciftci, N. S. (2007). Conjugated Polymer-Based Organic Solar Cells. *Chemical Reviews, 107*(4), 1324-1338.

Guo, T.-F., Wen, T.-C., L'Vovich Pakhomov, G., Chin, X.-G., Liou, S.-H., Yeh, P.-H., & Yang, C.-H. (2008). Effects of film treatment on the performance of poly(3-hexylthiophene)/soluble fullerene-based organic solar cells. *Thin Solid Films, 516*(10), 3138-3142.

Hauch, J. A., Schilinsky, P., Choulis, S. A., Childers, R., Biele, M., & Brabec, C. J. (2008). Flexible organic P3HT: PCBM bulk-heterojunction modules with more than 1 year outdoor lifetime. *Solar energy materials and solar cells, 92*(7), 727-731.

Hiramoto, M., Fujiwara, H., & Yokoyama, M. (1991). Three-layered organic solar cell with a photoactive interlayer of codeposited pigments. *Applied Physics Letters, 58*(10), 1062-1064.

Hoppe, H., & Sariciftci, N. S. (2004). Organic solar cells: An overview. *Journal of Materials Research, 19*(07), 1924-1945.

Huang, S. Y., Schlichthörl, G., Nozik, A. J., Grätzel, M., & Frank, A. J. (1997). Charge Recombination in Dye-Sensitized Nanocrystalline TiO2 Solar Cells. *The Journal of Physical Chemistry B, 101*(14), 2576-2582.

Jo, M. Y., Park, S. J., Park, T., Won, Y. S., & Kim, J. H. (2012). Relationship between HOMO energy level and open circuit voltage of polymer solar cells. *Organic Electronics, 13*(10), 2185-2191.

Jørgensen, M., Norrman, K., & Krebs, F. C. (2008). Stability/degradation of polymer solar cells. *Solar energy materials and solar cells, 92*(7), 686-714.

Karak, S., Ray, S., & Dhar, A. (2010). Improvement of efficiency in solar cells based on vertically grown copper phthalocyanine nanorods. *Journal of Physics D: Applied Physics, 43*(24), 245101.

Karan, S., & Mallik, B. (2007). Effects of annealing on the morphology and optical property of copper (II) phthalocyanine nanostructured thin films. *Solid State Communications, 143*(6–7), 289-294.

Kearns, D., & Calvin, M. (1958). Photovoltaic effect and photoconductivity in laminated organic systems. *Journal of Chemical Physics, 29*(4), 950-951.

Khan, M. T., Bhargav, R., Kaur, A., Dhawan, S., & Chand, S. (2010). Effect of cadmium sulphide quantum dot processing and post thermal annealing on P3HT/PCBM photovoltaic device. *Thin solid films, 519*(3), 1007-1011.

Kim, J. Y., Lee, K., Coates, N. E., Moses, D., Nguyen, T.-Q., Dante, M., & Heeger, A. J. (2007). Efficient tandem polymer solar cells fabricated by all-solution processing. *Science, 317*(5835), 222-225.

Kim, K., Lee, J. W., Lee, S. H., Lee, Y. B., Cho, E. H., Noh, H.-S., Jo, S. G., & Joo, J. (2011). Nanoscale optical and photoresponsive electrical properties of P3HT and PCBM composite nanowires. *Organic Electronics, 12*(10), 1695-1700.

Kippelen, B., & Bredas, J.-L. (2009). Organic photovoltaics. *Energy & Environmental Science, 2*(3), 251-261.

Kippelen, B., & Brédas, J. L. (2009). Organic photovoltaics. *Energy Environ. Sci., 2*(3), 251-261.

Kodigala, S. R. (2010). Chapter 2 - Growth Process of I-III-VI2 Thin Films. In K. Subba Ramaiah (Ed.), *Thin Films and Nanostructures* (Vol. Volume 35, pp. 21-53): Academic Press.

Krebs, F. C. (2009). Fabrication and processing of polymer solar cells: A review of printing and coating techniques. *Solar Energy Materials and Solar Cells, 93*(4), 394-412.

Kumar, G., Thomas, J., George, N., Kumar, B., Radhakrishnan, P., Nampoori, V., Vallabhan, C., & Unnikrishnan, N. (2000). Optical absorption studies of free (H2Pc) and rare earth (RePc) phthalocyanine doped borate glasses. *Physics and Chemistry of Glasses-European Journal of Glass Science and Technology Part B, 41*(2), 89-93.

Kwong, C., Djurišić, A., Chui, P., Cheng, K., & Chan, W. (2004). Influence of solvent on film morphology and device performance of poly (3-hexylthiophene): TiO< sub> 2</sub> nanocomposite solar cells. *Chemical Physics Letters, 384*(4), 372-375.

Kwong, C., Djurišić, A., Chui, P., Lam, L., & Chan, W. (2003). Improvement of the efficiency of phthalocyanine organic Schottky solar cells with ITO electrode treatment. *Applied Physics A: Materials Science & Processing, 77*(3), 555-560.

Li, G., Shrotriya, V., Huang, J., Yao, Y., Moriarty, T., Emery, K., & Yang, Y. (2005). High-efficiency solution processable polymer photovoltaic cells by self-organization of polymer blends. *Nature materials, 4*(11), 864-868.

Li, L., & Xu, B. (2008). Synthesis and characterization of 5-substituted 8-hydroxyquinoline derivatives and their metal complexes. *Tetrahedron, 64*(49), 10986-10995.

Li, W., & Kwok, H. L. (2012). Charge transport and light emission in bilayer organic field-effect transistors. *Thin solid films, 520*(9), 3600-3604.

Li, X., Xu, W., Wang, X., Jia, H., Zhao, B., Li, B., & Ozaki, Y. (2004). Ultraviolet-visible and surface-enhanced Raman scattering spectroscopy studies on self-assembled films of ruthenium phthalocyanine on organic monolayer-modified silver substrates. *Thin Solid Films, 457*(2), 372-380.

Liu, Y., Hu, W., Qiu, W., Xu, Y., Zhou, S., & Zhu, D. (2001). Organic field-effect transistors based on Langmuir–Blodgett films of substituted phthalocyanines. *Sensors and Actuators B: Chemical, 80*(3), 202-207.

Ma, W., Yang, C., Gong, X., Lee, K., & Heeger, A. J. (2005). Thermally stable, efficient polymer solar cells with nanoscale control of the interpenetrating network morphology. *Advanced Functional Materials, 15*(10), 1617-1622.

Manoj, A. G., & Narayan, K. S. (2003). Photovoltaic properties of polymer p–n junctions made with P3OT/BBL bilayers. *Optical Materials, 21*(1–3), 417-420.

Martin A, G. (2002). Photovoltaic principles. *Physica E: Low-dimensional Systems and Nanostructures, 14*(1-2), 11-17.

Mensing, G., Gilligan, J., Hari, P., Hurt, E., Lüpke, G., Pantelides, S., Tolk, N., & Taylor, P. C. (2002). Defect transition energies and the density of electronic states in hydrogenated amorphous silicon. *Journal of Non-Crystalline Solids, 299–302, Part 1*(0), 621-625.

Moulé, A. J., Bonekamp, J. B., & Meerholz, K. (2006). The effect of active layer thickness and composition on the performance of bulk-heterojunction solar cells. *Journal of Applied Physics, 100*(9), 094503.

Muhammad, F. F., Abdul Hapip, A. I., & Sulaiman, K. (2010). Study of optoelectronic energy bands and molecular energy levels of tris (8-hydroxyquinolinate) gallium and aluminum organometallic materials from their spectroscopic and electrochemical analysis. *Journal of Organometallic Chemistry, 695*(23), 2526-2531.

Muhammad, F. F., & Sulaiman, K. (2011a). Photovoltaic performance of organic solar cells based on DH6T/PCBM thin film active layers. *Thin Solid Films, 519*(15), 5230-5233.

Muhammad, F. F., & Sulaiman, K. (2011b). Utilizing a simple and reliable method to investigate the optical functions of small molecular organic films – Alq3 and Gaq3 as examples. *Measurement, 44*(8), 1468-1474.

Murgatroyd, P. (2002). Theory of space-charge-limited current enhanced by Frenkel effect. *Journal of Physics D: Applied Physics, 3*(2), 151.

Mycielski, W., Ziółkowska, B., & Lipiński, A. (1982). Transient currents in copper phthalocyanine layers. *Thin solid films, 91*(4), 335-338.

Nunzi, J. M. (2002). Organic photovoltaic materials and devices. *Comptes Rendus Physique, 3*(4), 523-542.

Park, G., Heo, I., Ryu, I., & Yim, S. (2011). Study on Electronic Absorption and Surface Morphology of Double Layer Thin Films of Phthalocyanines. *Bull. Korean Chem. Soc, 32*(3), 943.

Park, S. H., Roy, A., Beaupre, S., Cho, S., Coates, N., Moon, J. S., Moses, D., Leclerc, M., Lee, K., & Heeger, A. J. (2009). Bulk heterojunction solar cells with internal quantum efficiency approaching 100%. *Nat Photon, 3*(5), 297-302.

Parr, A. A., Bodart, C., Demonchy, D., & Gardiner, D. J. (2001). Depth profiling variously deposited LPCVD polysilicon films using Raman microscopy. *Semiconductor science and technology, 16*(7), 608.

Peumans, P., & Forrest, S. R. (2004). Organic photosensitive devices: Google Patents
.

Peumans, P., Yakimov, A., & Forrest, S. R. (2003). Small molecular weight organic thin-film photodetectors and solar cells. *Journal of Applied Physics, 93*(7), 3693-3723.

Peumans, P., Yakimov, A., & Forrest, S. R. (2003). Small molecular weight organic thin-film photodetectors and solar cells. *Journal of Applied Physics, 93*, 3693.

Ribeiro, A. O., Tomé, J. P., Neves, M. G., Tomé, A. C., Cavaleiro, J. A., Iamamoto, Y., & Torres, T. (2006). [1, 2, 3, 4-Tetrakis (α/β-d-galactopyranos-6-yl) phthalocyaninato] zinc (II): a water-soluble phthalocyanine. *Tetrahedron letters, 47*(52), 9177-9180.

Saini, G., Dogra, S. D., Sharma, K., Singh, S., Tripathi, S., Sathe, V., & Singh, R. K. (2011). Experimental and density functional theoretical study of the effects of chemical vapours on the vibrational spectra of nickel phthalocyanine thin films. *Vibrational Spectroscopy, 57*(1), 61-71.

Sanchez, M., Fache, E., Bonnet, D., & Meunier, B. (2001). Synthesis of organo-soluble metallophthalocyanines bearing electron-withdrawing substituents. *Journal of Porphyrins and Phthalocyanines, 5*(12), 867-872.

Sariciftci, N., Braun, D., Zhang, C., Srdanov, V., Heeger, A., Stucky, G., & Wudl, F. (1993). Semiconducting polymer-buckminsterfullerene heterojunctions: Diodes, photodiodes, and photovoltaic cells. *Applied Physics Letters, 62*(6), 585-587.

Schmidt-Mende, L., Fechtenkötter, A., Müllen, K., Moons, E., Friend, R., & MacKenzie, J. (2001). Self-organized discotic liquid crystals for high-efficiency organic photovoltaics. *Science, 293*(5532), 1119-1122.

Schumann, S., Hatton, R. A., & Jones, T. (2011). Organic photovoltaic devices based on water-soluble copper phthalocyanine. *The Journal of Physical Chemistry C, 115*(11), 4916–4921.

Schuster, B.-E., Basova, T. V., Plyashkevich, V. A., Peisert, H., & Chassé, T. (2010). Effects of temperature on structural and morphological features of CoPc and CoPcF16 thin films. *Thin Solid Films, 518*(23), 7161-7166.

Schwieger, T., Peisert, H., Golden, M., Knupfer, M., & Fink, J. (2002). Electronic structure of the organic semiconductor copper phthalocyanine and K-CuPc studied using photoemission spectroscopy. *Physical Review B, 66*(15), 155207.

Šebera, J., Nešpůrek, S., Kratochvílová, I., Záliš, S., Chaidogiannos, G., & Glezos, N. (2009). Charge carrier mobility in sulphonated and non-sulphonated Ni phthalocyanines: experiment and quantum chemical calculations. *The European Physical Journal B - Condensed Matter and Complex Systems, 72*(3), 385-395.

Şener, M. K., Gül, A., & Koçak, M. B. (2003). Synthesis of tetra (tricarbethoxy)-and tetra (dicarboxy)-substituted soluble phthalocyanines. *Journal of Porphyrins and Phthalocyanines, 7*(09), 617-622.

Shrotriya, V. (2010). *Polymer Solar Cells: Achieving High Efficiency by Device Engineering and Morphology Control*: LAP Lambert Acad. Publ.

Shukla, V. K., & Kumar, S. (2010). Conversion of a green light emitting zinc-quinolate complex thin film to a stable and highly packed blue emitter film. *Synthetic Metals, 160*(5), 450-454.

Singh, V., Parsarathy, B., Singh, R., Aguilera, A., Anthony, J., & Payne, M. (2006). Characterization of high-photovoltage CuPc-based solar cell structures. *Solar energy materials and solar cells, 90*(6), 798-812.

Singh, V., Singh, R., Parthasarathy, B., Aguilera, A., Anthony, J., & Payne, M. (2005). Copper-phthalocyanine-based organic solar cells with high open-circuit voltage. *Applied Physics Letters, 86*(8), 082106-082106-082103.

Skompska, M. (2010). Hybrid conjugated polymer/semiconductor photovoltaic cells. *Synthetic Metals, 160*(1-2), 1-15.

Smith, W. (1873). The action of light on selenium. *Telegraph Engineers, Journal of the Society of, 2*(4), 31-33.

Soliman, H., El Nahass, M., Farid, A., Farag, A., & El Shazly, A. (2003). Structural and transport properties of evaporated iron phthalocyanine (FePc) thin films. *The European Physical Journal- Applied Physics, 21*(3), 187-193.

Spanggaard, H., & Krebs, F. C. (2004). A brief history of the development of organic and polymeric photovoltaics. *Solar energy materials and solar cells, 83*(2–3), 125-146.

Stingelin-Stutzmann, N., Smits, E., Wondergem, H., Tanase, C., Blom, P., Smith, P., & de Leeuw, D. (2005). Organic thin-film electronics from vitreous solution-processed rubrene hypereutectics. *Nature materials, 4*(8), 601-606.

Szybowicz, M., Bała, W., Fabisiak, K., Paprocki, K., & Drozdowski, M. (2010). Micro-Raman spectroscopic investigations of cobalt phthalocyanine thin films deposited on quartz and diamond substrates. *Crystal Research and Technology, 45*(12), 1265-1271.

Szybowicz, M., Runka, T., Drozdowski, M., Bała, W., Grodzicki, A., Piszczek, P., & Bratkowski, A. (2004). High temperature study of FT-IR and Raman scattering spectra of vacuum deposited CuPc thin films. *Journal of Molecular Structure, 704*(1–3), 107-113.

Tang, C. W. (1986). Two-layer organic photovoltaic cell. *Applied Physics Letters, 48*, 183-185.

Triyana, K., Yasuda, T., Fujita, K., & Tsutsui, T. (2005). Tandem-type organic solar cells by stacking different heterojunction materials. *Thin Solid Films, 477*(1-2), 198-202.

Winder, C., & Sariciftci, N. S. (2004). Low bandgap polymers for photon harvesting in bulk heterojunction solar cells. *Journal of Materials Chemistry, 14*(7), 1077-1086.

Xu, B., & Holdcroft, S. (1993). Molecular control of luminescence from poly (3-hexylthiophenes). *Macromolecules, 26*(17), 4457-4460.

Yang, J. L., Schumann, S., & Jones, T. S. (2011). Tuning the morphology and molecular orientation of copper hexadecafluorophthalocyanine thin films by solvent annealing. *Thin Solid Films, 519*(11), 3709-3715.

You, J., Dou, L., Yoshimura, K., Kato, T., Ohya, K., Moriarty, T., Emery, K., Chen, C.-C., Gao, J., & Li, G. (2013). A polymer tandem solar cell with 10.6% power conversion efficiency. *Nature Communications, 4*, 1446.

Yusli, M. N., Way Yun, T., & Sulaiman, K. (2009). Solvent effect on the thin film formation of polymeric solar cells. *Materials Letters, 63*(30), 2691-2694.

Zhao, D. W., Tan, S. T., Ke, L., Liu, P., Kyaw, A. K. K., Sun, X. W., Lo, G. Q., & Kwong, D. L. (2010). Optimization of an inverted organic solar cell. *Solar Energy Materials and Solar Cells, 94*(6), 985-991.

Zhao, Y., Xie, Z., Qu, Y., Geng, Y., & Wang, L. (2007). Solvent-vapor treatment induced performance enhancement of poly (3-hexylthiophene): methanofullerene bulk-heterojunction photovoltaic cells. *Applied physics letters, 90*(4), 043504-043504-043503.

Zhi-Hui, F., Yan-Bing, H., Quan-Min, S., Xiao-Jun, L., & Feng, T. (2010). Effect of slow-solvent-vapour treatment on performance of polymer photovoltaic devices. *Chinese Physics B, 19*(9), 098601.